

POLITECNICO DI TORINO

**Corso di Laurea Magistrale
in Ingegneria Civile**

Tesi di Laurea Magistrale

**STRUCTURAL BEHAVIOR OF PRESTRESSED BRIDGES
UNDER CORROSION DAMAGE**



Relatori:

Francesco Tondolo

Donato Sabia

Candidato:

Francesca Maria Pavone

A.A. 2017/2018

ABSTRACT

Prestressed bridges constitute the main infrastructures' typology. Elements built with this technology are particularly subjected to corrosion, because of the simultaneous presence of high stress levels in the tendons and aggressive agents from the outside environment. The in-service structural behavior of prestressed concrete structures is difficult to accurately define because of multiple parameters that must be considered. For this reason, not much has been done in terms of studies. In this work, the Corso Grosseto's bridge, in Turin, Italy, has been defined. The aim has been to provide a mono dimensional model capable to seize the multiple properties of a pretensioned prestressed beam through the use of the bending moment-curvature diagrams, such as a variable prestress force along the transfer length that varies the resisting stress-strain relation. Which means, essentially, to provide a simple model capable to catch the element behavior. Then, 7 corrosion scenarios have been defined and analyzed. Results show that the theoretical corrosion level is critical especially if analyzed at the ultimate limit state. A security level Δ has been determined as the difference between ULS actions and resistance. The Δ parameter permits to better compare the different scenarios. Moreover, from visual inspections, many beams exhibit a corrosion state that could be greater than the analytical one. For these reasons, it can be said that, in the Corso Grosseto's flyover, the Δ security parameter is almost null for a corrosion percentage that should be the real one.

CONTENTS

ABSTRACTi
INTRODUCTION	1
CHAPTER 1: CORROSION	5
GENERAL ASPECTS	5
ELECTROCHEMICAL ASPECTS	5
DEGRADATION EVOLUTION	8
CORROSION TYPES	10
CARBONATION	11
CHLORIDE ATTACK.....	14
CRITICAL CHLORIDE CONTENT	16
STRESS CORROSION CRACKING	17
CORROSION SPEED	18
CORROSION CONSEQUENCES	21
EFFECTS ON STEEL.....	22
UNIFORM CORROSION	22
LOCALIZED CORROSION.....	23
DUCTILITY.....	26
STEEL MECHANICAL PROPERTIES.....	26
EFFECTS ON CONCRETE.....	27
STEEL-CONCRETE BOND	30
PRESTRESS FORCE	33
CHAPTER 2: CASE STUDY	35
CHAPTER 3: ANALYTICAL ANALYSIS	39
MATERIALS	41
GEOMETRY	43
DATA ON PRESTRESSING	49
TRANSFER OF PRESTRESS	50
ANCHORAGE LENGTH.....	54
TRAFFIC LOAD.....	55
TENSIONAL ANALYSIS.....	59
RHEOLOGICAL LOSSES	65
SHRINKAGE.....	65
CREEP	66
RELAXATION	67

CORROSION	67
CHAPTER 4: MODELLING.....	69
EXCEL PROGRAM	71
FIRST IMPROVEMENT: DIFFERENT constitutive law FOR THE SUPERIOR AND INFERIOR TENDONS.....	73
SECOND IMPROVEMENT: DIFFERENT TENSION STATE FOR TENDONS WHICH PROVOKES REINFORCEMENT DESIGN CHANGES	74
ADINA MODEL	76
CHAPTER 5: NUMERICAL ANALYSIS	79
TRAFFIC LOAD MOVEMENT.....	79
CORROSION VARIATION	82
SCENARIO1	82
SCENARIO2	85
SCENARIO3	87
SCENARIO4	91
SCENARIO5	96
SCENARIO6	100
SCENARIO7	103
CHAPTER 6: CONSIDERATIONS ABOUT THE REAL CORROSION STATE TRHOOUGH PICTURES.....	109
CONCLUSIONS	115
BIBLIOGRAPHY	117
FIGURE INDEX.....	121

INTRODUCTION

Prestressed concrete members have been largely used, in the past decades, especially to build strategic importance structures such as highways, bridges, viaducts, etc. These structures are particularly sensitive to steel corrosion because they are subjected to long-term exposure in an aggressive environment caused by de-icing salts. Among several others, the factors that affect the performance of prestressed concrete elements are mainly the loss of the tendon's resisting area, loss of bond between tendons and concrete, and the modification of the σ - ϵ diagram, which cause a reduction of the effective prestressing force and the shear capacity close to the supports. Since these properties are very difficult to measure in situ with non-destructive methods, accurate analytical methods are required. In other words, prestressed elements have tremendously time-dependent properties because concrete creeps and shrinks and the prestressing steel relaxes; these phenomena in combination with repeated loading may introduce cracking and accelerate the corrosion process.

Even so, studies regarding the structural response of prestressed structures affected by corrosion are limited if compared to the literature about corroded reinforced concrete elements, probably because of the problem's complexity due to the large number of parameters that must be taken into account. In fact, the in-service structural properties of prestressed concrete structures are difficult to accurately define, especially when the members have been in the field for an extended period.

In the past few years, some effort has been made, for example by (D.Coronelli, 2009), to study the structural response of post-tensioned beams with bonded wires experimentally and through a nonlinear finite element model that simulates the effect of stress corrosion failure, development of anchorage of the wires on each side of the fracture and the residual structural performance. The same authors have

been interested even to deteriorating unbonded post-tensioned beams (D.Coronelli, 2011). Those tests have been made on beams casted for the study and artificially corroded. Tests on elements that have been in service were even performed, for example, by Parry Osborn et al., that tested seven bridge girders to investigate the effective prestress force and shear capacity of 42-year-old prestressed girder bridge (G. Parry Osborn, 2012). Furthermore, two 40-year-old inverted T-beam, from the prestressed concrete ATH-144-0844 bridge, were tested to destruction by J.T.Halsey and R.Miller (J.T. Halsey, 1996); they compared the estimated losses evaluated through the AASHTO Code with the measured values and they found a good correlation between the two values.

Corrosion of prestressed tendons is a great concern because it is the most widely diffused cause of degradation. In prestressed concrete structures, high-performance concrete and high-strength steel are used and they are loaded at very high-tension levels. In other words, in these kinds of structures, because of the high stress level in the tendons, the steel corrosion process is modified. Stress corrosion is characterized by both the conventional corrosion, due to pitting attacks in chloride environment, and the steel microcracking, induced by the high stress level and hydrogen embrittlement. Since the cracking load is mainly determined by the effective pretension of the tendons, it decreases with the increasing corrosion levels, throughout the tendon's cross section loss. Steel microcracking can lead to the brittle failure of the prestressing steel for a very low corrosion level and under normal service loading. Stress corrosion is more critical than traditional corrosion because it leads to abrupt, brittle failure of tendons without any striction or clear warning signal and without sufficient ultimate elongation (J. Woodtli, 2000). The mechanism of SCC (stress corrosion cracking) is due to the simultaneous action of stress, corrosive media and material properties. This makes the damage mechanism very complex as it depends on the particular material and damaging medium (Toribio, 1997). Because one important parameter of SCC is the

mechanical loading, the damage diffuses preferentially at notches or cracks where stress becomes concentrated (J. Woodtli, 2000).

As a case study, the Corso Grosseto's flyover, in Turin, Italy, is considered. This bridge has been an important hub for the city for almost 50 years. The demolition process started nearly one year ago to permit the construction of a underpass tunnel and it is not over yet. The bridge has been subjected to different kinds of corrosion which even includes the chloride attack due to the use of antifreeze salts during the winter season.

For the analysis, dimensions, materials and loads of the bridge, have been studied. First of all, an analytical analysis has been realized to help the numerical modelling and to compare the results from the historic executive report with the ones defined with the modern methods. Then, it is proposed a mono dimensional model made with the finite element program Adina.

Different corrosion scenarios, coming from both analytical evaluations and visual observations, have been taken into account. As an input for the model, corrosion scenarios have been modeled as a loss of the prestressing force, due to a reduction of the tendons resisting area loss, and a reduction of the concrete-tendons bond, proportional to the cross-section loss. The bond degradation provokes essentially a variation of the transfer length.

CHAPTER 1: CORROSION

Corrosion is the main cause of structural damage. This phenomenon affects, above all, reinforcements either in ordinary reinforced concrete than in prestressed elements. In general, reinforcements embedded in concrete are protected by the environment's alkalinity which ensure a PH>15 and makes an oxide cover which upholsters the bars. So, concrete protects the steel bars or tendons either chemically than mechanically. This process is the well-known steel passivation and it blocks the corrosion initialization; but, this protection, in contrast, does not last in time.

Structural durability depends on corrosion initialization because it is defined as the property that permits the preservation of structural characteristics (mechanical and physical) and materials performances in time, making just ordinary maintenance. So, durability is an essential attribute to maintain unchanged security levels along the entire structural life time.

GENERAL ASPECTS

ELECTROCHEMICAL ASPECTS

To activate corrosion initialization, it is necessary to establish an electrochemical circuit for which it is necessary the presence of three elements: cathode, electrolyte and anode. If one constituent is removed or the circuit in the galvanic cell is interrupted, then corrosion stops. In other words, if there is an electrolyte which put into contact a cathode and an anode then the potential difference activates the electrochemical circuit. It is necessary a small potential difference to do so. The cathode is the only component that corrodes, and the corrosion velocity depends on how many ions flows.

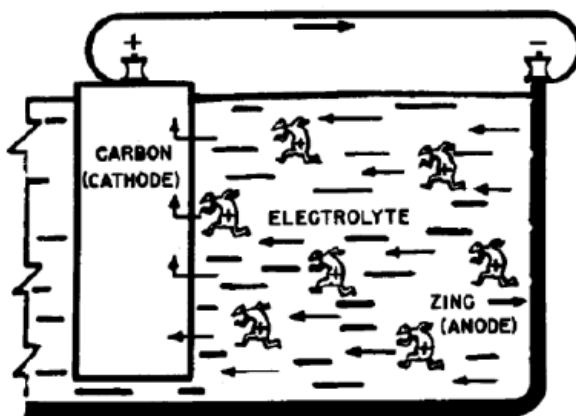
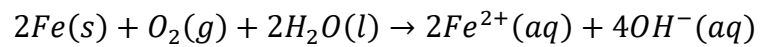


Figure 1 Galvanic cell

In general, the reaction in a humid environment is:



Where s stands for solid, g for gas, l for liquid and aq for aqueous.

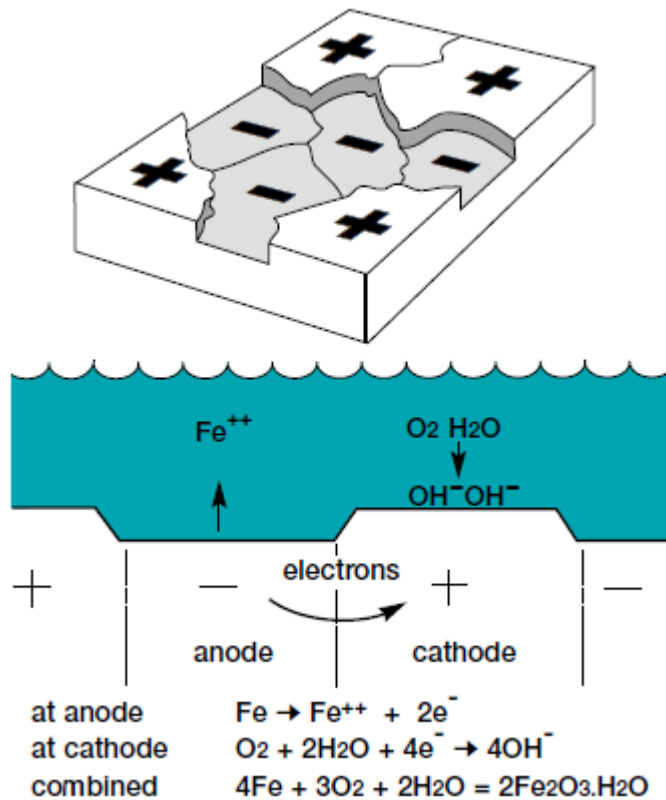
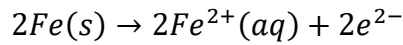
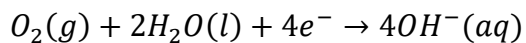


Figure 2 Schematic representation of corrosion mechanism

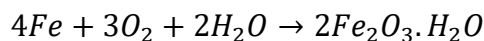
Specifically, water and oxygen start the superficial attack on the anodic region and steel makes an oxidation reaction:



Electrons are released from the anode and they move throughout the metallic structure toward the cathodic region, where they make a reduction reaction with oxygen and water to make movable OH⁻ ions.



The OH⁻ ions reacts with the Fe²⁺ ions to make (Fe(OH)₂), ferrous hydroxide, which is a barely soluble in water product. It is commonly called rust.



Through the first Faraday law it is possible to define the mass loss as:

$$|\Delta m| = \left| \frac{M}{zF} \right| q$$

Where q is the charge proportional to the number of lost ions, M is the metal molar mass (g/mole), z is the ion's valence, F is the Faraday constant which is equal to 96487 C.

So, the mass loss velocity v_m can be expressed in g/(m²year) and the thinning velocity v_p just dividing v_m over the material specific weight ρ; v_p is formulate in μm/year

$$v_m = \frac{1}{At} |\Delta m|$$

The ions' number released from the anodic reaction in a unit of time has to be equal to the one consumed in the cathodic reaction, so even the current which flows either in the environment than in the metal must be the same. The current value I_{corr} measures the corrosion velocity. To establish if a metal can corrode in a certain

environment, it is possible to compare the equilibrium potentials of the anodic and cathodic process; if $E_{eq,anodic} < E_{eq,cathodic}$ then corrosion happens.

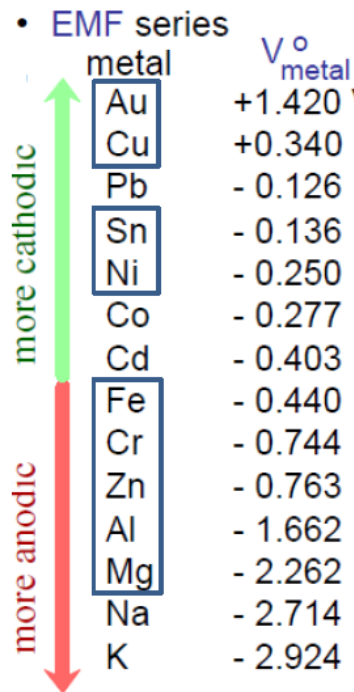


Figure 3 Major metals' potential

DEGRADATION EVOLUTION

It is important to evaluate the degradation evolution to predict when a certain damage occurs, for example the cover cracking, but more importantly to study how the different corrosion effects influence the behavior of a structure and its resisting capacity to external loads.

Mainly, people become aware of corrosion degradation when it is already activated. In these situations, in addition to plan the right maintenance operations, it is necessary to determine if the structure can still resist to the design stresses or corrosion has compromise security.

The corrosion process is mainly initiated by the following causes:

- Neutralization of the environment surrounding the metal, e. g. carbonation.

- Activation of strongly corrosive anions, e. g. chlorides.

According to the traditional (Tuutti, 1982) setting, the service life of a concrete structure, focusing on the reinforcement corrosion, is split into two fractions:

- Initiation stage, in which the conditions to create a damage on the metal surface, and so of the passivate film, are established; The length of the initiation period is determined by how rapidly the concrete cover is changed as a result of the fact that neutralizing or activating substances penetrate to the steel, and by the concentrations of those substances which are required for the start of the corrosion process.
- Attack propagation stage, which, in the long term, will provoke a progressive resisting bar's cross section reduction, concrete cover cracking and at last structural collapse.

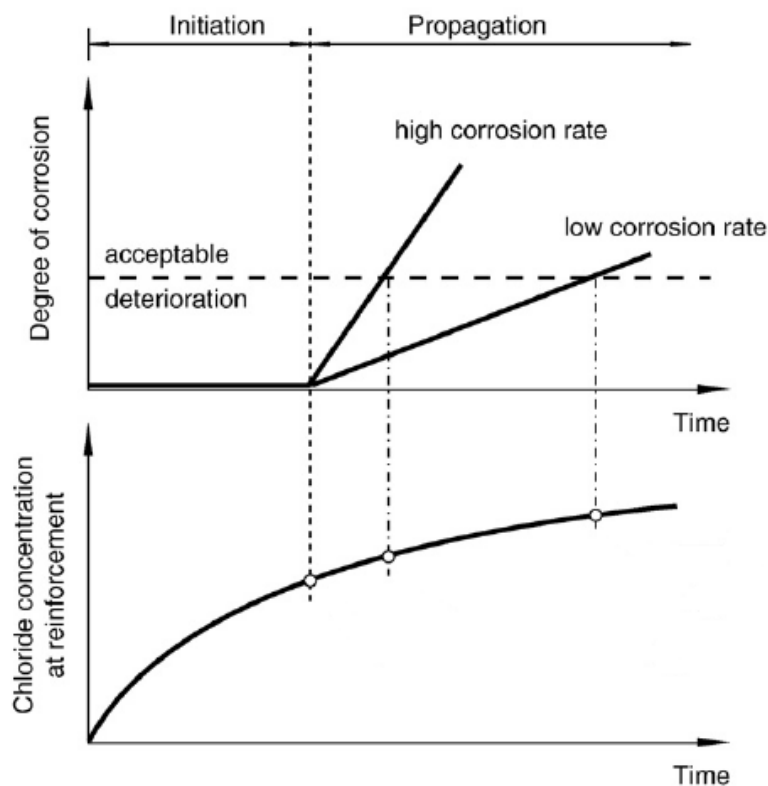


Figure 4 Evolution of steel corrosion in concrete (Tuutti, 1982)

This subdivision is suitable since the primary parameters differ in the two subprocesses. In fact, environment types were divided by the main parameters

which are concentrations of initiating substances, moisture and temperature conditions.

This model shows that it is incorrect to consider that the serviceable structural life ends when corrosion starts to degrade the metal surface because chlorides or carbonation have passed through the concrete cover.

At the same time, this model does not allow to examine the effective time depending evolution of the structure and its resisting capacity. For example, a cross section reduction could produce a resisting bending moment reduction as much as collapse can occur even before the concrete cover detachment, particularly in case of pitting corrosion.

CORROSION TYPES

There are different types of corrosion depending on the mechanisms with which it appears. The classification can be done in function of the morphologic aspect of the corroded material. In general, corrosion types are:

- General corrosion
- Galvanic corrosion
- Pitting
- Crevice corrosion
- Interstitial corrosion
- Intergranular corrosion
- Stress corrosion cracking

There are two causes of major importance, that provokes corrosion, in the civil field, which are carbonation corrosion and corrosion due to chlorides.

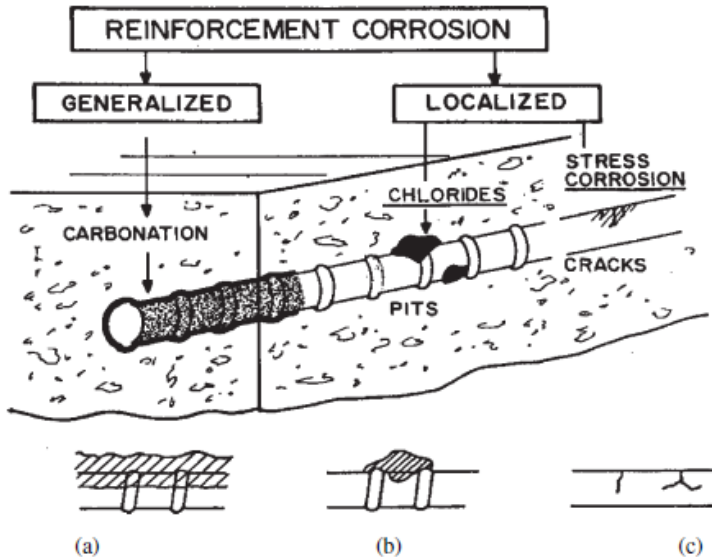
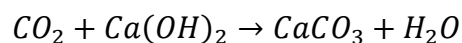


Figure 5 Types of corrosion of reinforcement: (a) carbonation, (b) chloride attack and (c) stress corrosion cracking.

CARBONATION

The carbonation process is an initiation mechanism in the corrosion process.

Concrete carbonation is due to the reaction between carbon dioxide in the atmosphere and the alkaline composite in the concrete pores (NaOH , KOH) and $\text{Ca}(\text{OH})_2$.



Because of the reaction, solution PH goes from high values to values close to neutral. This situation does not allow the formation of the passivation film around the bars.

The impermeability of concrete, the reserve of hydroxide and the low concentrations CO_2 are the primary reasons why the carbonation process proceeds slowly in the concrete.

Carbonation expands from the surface to the inner parts. The penetration in time can be expressed with the following formulation which shows how it decreases along time:

$$s = Kt^{1/n}$$

Where n is a coefficient function of the concrete' porosity; K is the carbonation coefficient and it is measured in mm/year^{1/n} and it depends form the RH, temperature and CO₂ concentration.

The carbon dioxide transportation is easier in pores filled with air, so the diffusion velocity decreases if it increases the relative humidity, up to be null if the concrete is saturated. At the same time, in contrast, the carbonation reaction needs water to be activated, so for RH<40% the velocity is negligible. The highest carbonation velocity values are measured for a RH range between 60% and 80% so, it can be said that it is higher in protected zones than in external.

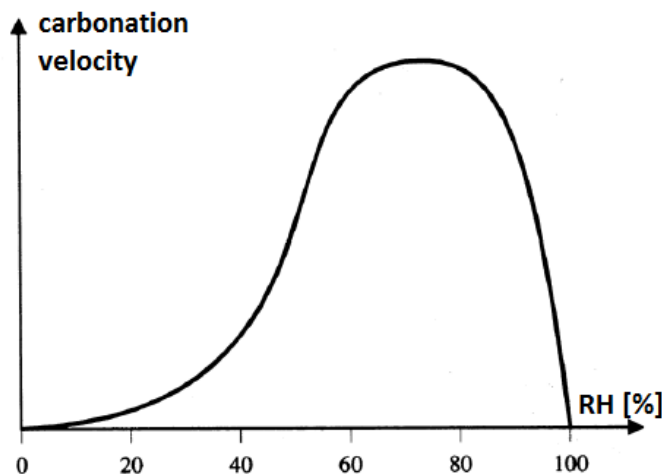


Figure 6 Evolution of carbonation velocity in function of RH with no wetting (Bertolini, 2006)

In existing structures, the carbonation depth can be measured to find the K value. Common values measured on real structures vary between 2 and 15 mm/year^{1/2}. For example, if K=7 the penetration depth can exceed 50 mm after 50 years.

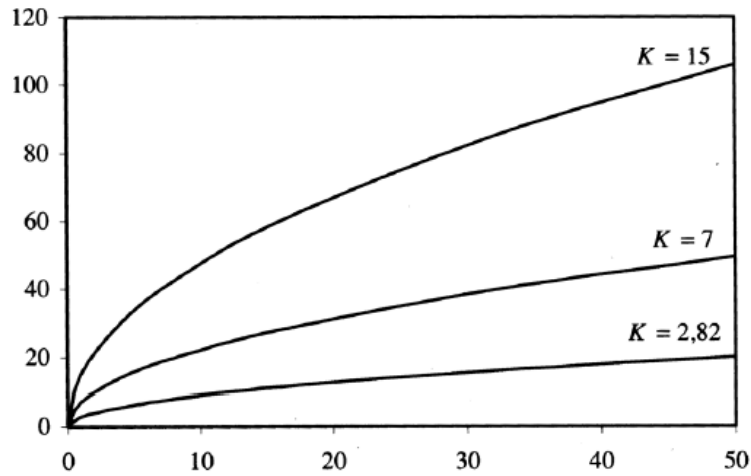


Figure 7 K evolution in function of time (abscissa in years) and penetration depth (ordinate in mm)

It has been observed that, for good quality concrete, corrosion velocity remains negligible if the relative humidity is less than 80%, in fact, it is assumed that corrosion spreads only during the wet time, that is the period in which the relative humidity is over 80%. The maximum values measured of the corrosion velocity are about 100-200 $\mu\text{m}/\text{yr}$ if the relative humidity is close to 100%; in opposition, it is about 5-50 $\mu\text{m}/\text{yr}$ in frequent conditions. Just if the carbonated concrete is exposed to a growth of RH that vary the water concentration at the bars level then corrosion velocity is not negligible. So, the worst situation is if the concrete is exposed to a succession of wet and dry conditions.

In addition, if chlorides exist in concrete, even for low concentrations, corrosion velocity turns to high values for low humidity.

In other words, most of all corrosion damage is caused by the neutralization of the concrete through carbonation or by the fact that the pore solution surrounding the reinforcement has too high a concentration of chlorides.

CHLORIDE ATTACK

Corrosion due to the presence of chlorides causes a localized break of the reinforcements' passivation film due to a chloride penetration in concrete to when a critic content is reached. This penetration can happen in structures exposed to a marine environment or in infrastructures in which antifreeze salts are used.



(c) 2000 RHAdler
www.RESnapshot.com

Figure 8 Example of pit corrosion

When the PH is high, the break is localized, just like the corrosion model and the mechanism is called pitting. Inside the pits there is a very aggressive environment in which the PH is less than 5.

The chlorides critic content, needed to initiate the corrosion process, depends from the concrete characteristics and environment exposure. For example, in a non-carbonate concrete made with Portland cement, corrosion risk is low, for chlorides content less than 0.4%, while, it is high, for chlorides content over 1%.

Furthermore, the chlorides critic content is even function of the attitude of concrete to alloy with chlorides.

In other words, it is possible to have some chloride concentration even in the concrete mix elements; or they can come from the outside, because of an exposure

to a marine environment or due to the use of de-icing salts. In the first situation, there can be immediate corrosion reactions, if more chlorides are added, such as the critic content is exceeded. In opposition, in the second case, the chloride ions concentration increases with time up to the critic threshold.

When the chlorides critic content is reached at the steel level, then the attack is launched. Corrosion velocity can change from few $\mu\text{m}/\text{yr}$ to 1 mm/yr when the relative humidity, from 70% to 90%, and the chloride content, from 1% to 3%, increases.

The chlorides transportation take place just in water, therefore without humidity inside the concrete element, there is no ions diffusion.

The time necessary to reach the critic content is defined as the activation time and it depends by the chloride's concentration on the external surface and the concrete characteristics which define the chloride transportation though the reinforcement concrete cover.

To describe the chlorides penetration over time it can be used a concentration profile obtained through the Fick's law for non-stationary diffusion:

$$\frac{\partial C}{\partial t} = -D \frac{\partial^2 C}{\partial x^2}$$

Assuming that the concentration of the element that diffuses is constant in time on the surface ($C=C_s$), and D is a constant material property in time; it can be hypothesized that the material initially does not contain the component that diffuses ($C=0$; $t=0$).

$$\frac{C}{C_s} = 1 - \operatorname{erf}\left(\frac{x}{2\sqrt{Dt}}\right)$$

This solution is used to estimate the chlorides diffusion coefficient adapting the theoretical profile to experimental test results. Actually, chlorides penetrate for

pure diffusion only for saturated concrete, otherwise there are different transportation mechanisms, but the Fick's solution interpret in an acceptable way the real behavior. In general, profiles are characterized by a high concentration on the surface which decreases with the increase of depth.

The main problem is to evaluate with a certain reliability the effective chlorides diffusion coefficient and the superficial chlorides content that vary over time. For structures exposed to a marine environment the highest C_s values are in the spray zone and they range between 0.6 to 1% of concrete weight, increasing the cement content from 300 to 600 Kg/m³. In addition, the D_{ce} value vary from 10^{-13} to 10^{-10} m²/s depending on the concrete characteristics, above all on the permeability and composition; in fact, in pozzolanic cements or slag cement the D_{ce} value decreases significantly.

CRITICAL CHLORIDE CONTENT

The critical chloride content is the amount necessary for steel passivation. Therefore, a structure visible deterioration is dependent to it.

Generally, the critical chloride content is expressed as the total chlorides' quantity in function of the concrete weight. Moreover, it can be expressed even as the ratio between Cl/OH⁻, that depends by the PH.

It is necessary a small concentration to break the steel passivation film, but the prospect to develop corrosion depends by other influencing factors which govern the corrosion velocity.

In (U. Angst, 2009) are collected a large number of literature's chloride threshold values and the respective experimental detail. In general, for structures exposed to the atmosphere, the critical content over the concrete weight $Cl_{crit}/W_{concrete}$ goes from 0.1% to 1.96%. Although according to the multiple studies there is no a unique

method to define and to determine the critical content. For this reason, it highlights the need for a practice-related test method.

In fib "Model Code for Service Life Design" is recommended to use statistical model defined by a beta distribution with mean value of 0.6 by % weight of cement to evaluate the critical chloride content, as reported in figure [].

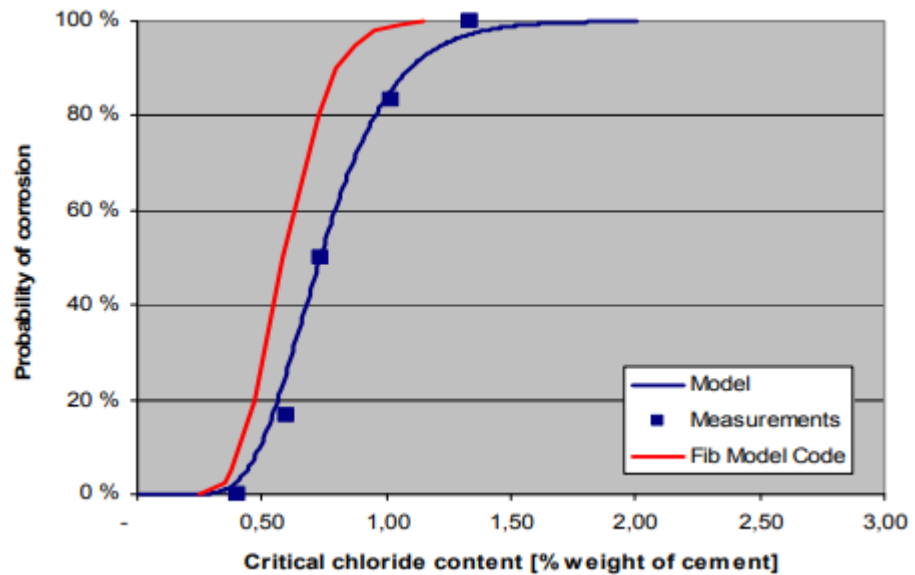


Figure 9 Critical chloride content according to fib "Model Code for Service Life Design"

STRESS CORROSION CRACKING

Stress corrosion cracking, or SCC, is a particular case of localized corrosion and is due to the parallel action of stress, corrosion and material properties. The wire failure take place in a relatively short time and in a brittle manner.



Figure 10 Example of SCC of a ZTA in an inox steel which is inclined to it because of nitrogen

It occurs only in elements stressed (tensed) to a certain level and in contact with a specific aggressive agent, for this reason is common in prestressing wires. Because one important parameter of SCC is the mechanical loading, the damage diffuses preferentially at notches or cracks where stress becomes concentrated. Because corrosion pits could also be considered as surface defects or notches, the evolution of stress corrosion cracks from pits is also a possibility in prestressing wire damage (Ngoc Anh Vu, 2009).

CORROSION SPEED

Corrosion speed is the penetration speed of corrosion in the bars, and it depends by multiple parameters, like the environment conditions. It is important to define the corrosion speed to study the evolution of the process through time ones the initiation time is passed.

Generally, the unit of measurement used to define the corrosion velocity is $\mu\text{m/year}$, but in experimental tests the electrochemical unit $\mu\text{A/m}^2$ is used.

In literature there are several empiric formulations, but the more common method is to use the Faraday's law, with which the velocity is evaluated in function of the corrosion current intensity i_{corr} [mA/m^2].

$$V_{corr} = 1.16i_{corr}$$

On account of this, the i_{corr} can be considered as an indirect measure of the corrosion level and it is function of the chlorides content, time and temperature.

Over time corrosion velocity is not constant, as revealed in different experimental studies. For example, in (Y. Liu, 1998) the corrosion level is dependent on the various parameters previously listed, in fact as suggested in figure 11, it increase when both temperature and chlorides content increase, in opposition, at the corrosion initiation, it rapidly decreases to an almost constant value after about 1 year.

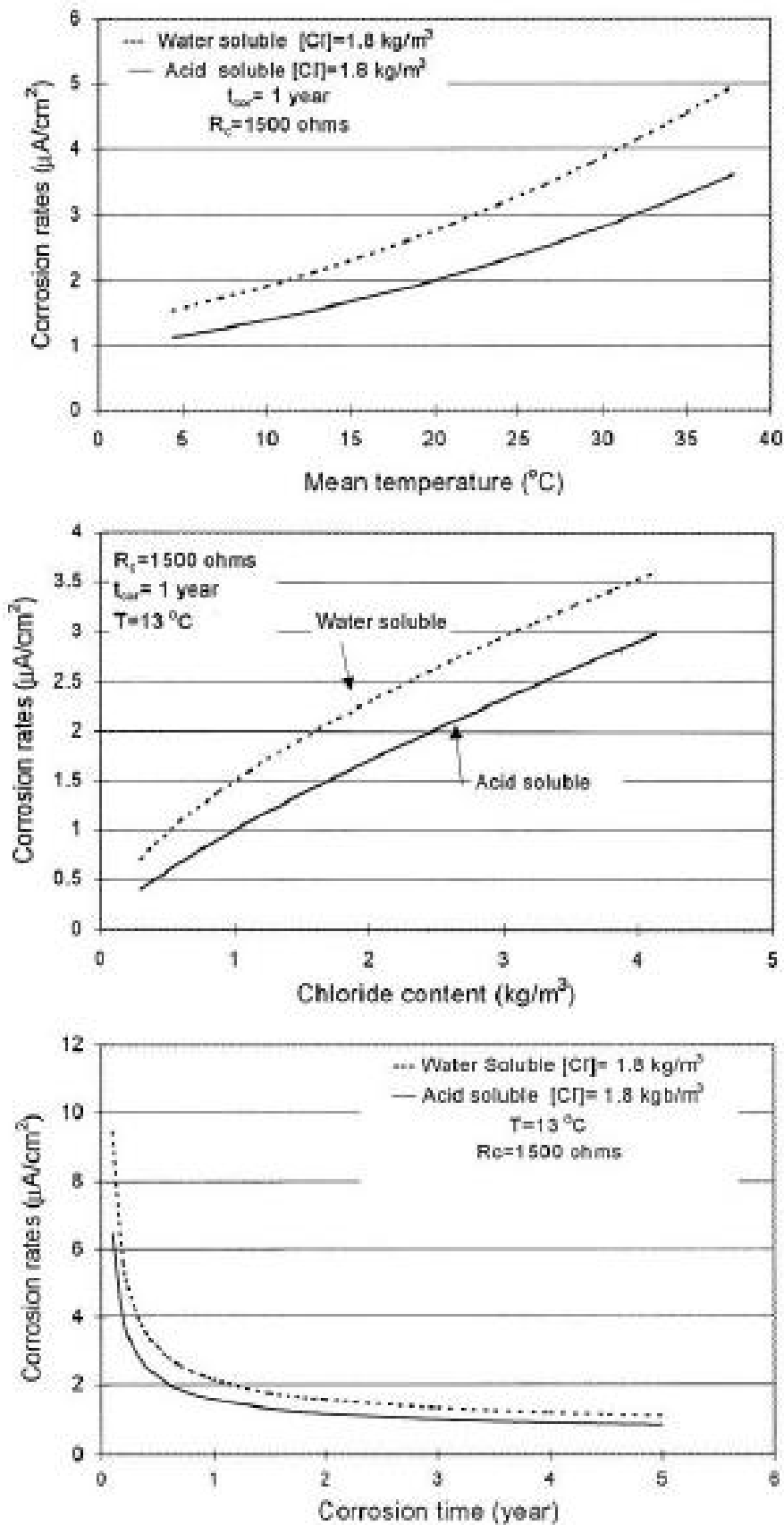


Figure 11 Corrosion level trend in function of the chlorides content, time and temperature.

Even more, corrosion speed is meaningful just for high humidity, in situations with stagnated water, and above all for elements exposed to rain.

The depth of corrosive attack penetration over time can be defined as:

$$x(t) = Vw_t(t - t_I)$$

Where w_t is a coefficient that depends on the environment conditions and t_I is the initiation time.

CORROSION CONSEQUENCES

The two main causes that affects durability are environmental conditions (4.2-EC2) and the concrete cover (4.4.1-EC2). Evidently, those characteristics are function of corrosion attacks which, for example, is advantaged in an aggressive environment and with a small concrete cover.

The exposure conditions can be distinguished into 6 classes according to the EC2 (prospect 4.1):

1. No risk of corrosion [X0]
2. Corrosion induced by carbonation [XC(#)]
3. Corrosion induced by chlorides [XD(#)]
4. Corrosion induced by chlorides from sea water [XS(#)]
5. Freeze/Thaw attack [XF(#)]
6. Chemical attack [XA(#)]

Similarly, the exposure classes are divided into just 4 classes according to NTC08.

Moreover, the Eurocode defines a minimum concrete class depending either on the environment than on the cover. Concrete type and quality influences both reinforcement conservation inside the concrete member and the concrete defense against corrosion attacks.

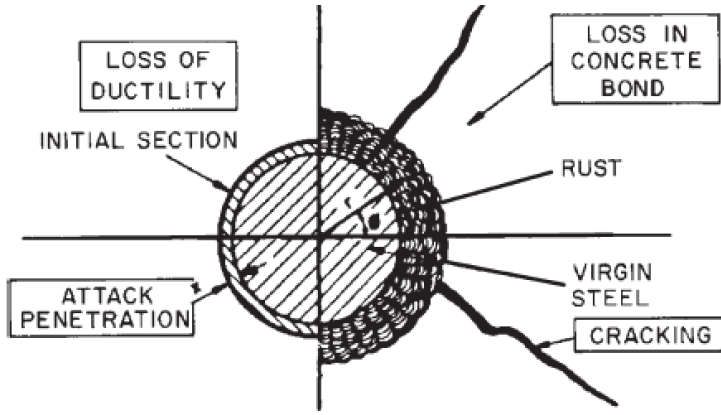


Figure 12 Consequences of reinforcement corrosion

EFFECTS ON STEEL

UNIFORM CORROSION

Once the steel passivation occurs in carbonated cement, with no relevant chloride concentration, corrosion develops uniformly around the bar circumference.

According to (J. Rodriguez, 1996), attack penetration can be calculated from the measured loss of steel mass, which presents the relationship between corrosion (pitting attack or homogeneous corrosion) and reinforcement diameter decrease.

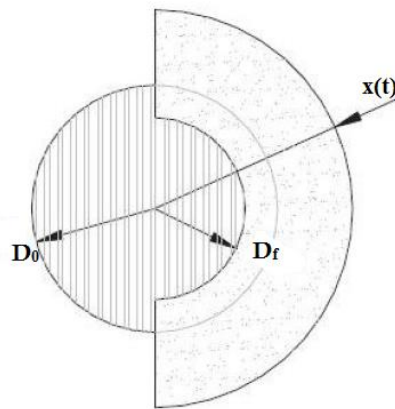


Figure 13 Evolution of the bar cross section because of corrosion

The reduction in the diameter of a corroded bars after time t [years] can be estimated as:

$$\varphi(t) = \varphi_0 - 2x(t)$$

The remaining resisting area is defined as depending on the penetration depth:

$$A_s(t) = \pi \left(\frac{D_0}{2} - x(t) \right)^2$$

To take into account that the corrosive attack can occur just from one or two sides of the bar, (Saetta, 1999) proposes:

$$A_s(t) = \frac{\pi(D_0 - nx(t))^2}{4}$$

Where n has a parabolic evolution from 1 if the attack comes from one side, so carbonation reaches the bar level, to 2 if it comes from both sides, do passivation involved the entire bar.

LOCALIZED CORROSION

When the chloride content is relevant, corrosion appear to be localized in pits. The cross-section reduction has to be evaluated otherwise in relation to the uniform case.

Localized corrosion due to chloride ingress is the predominant corrosion pattern at the cracking initiation stage and the first stage of cracking propagation, so pitting corrosion is the main factor that influences the cracking process. (Ruijin Zhang, 2010)

Corrosion

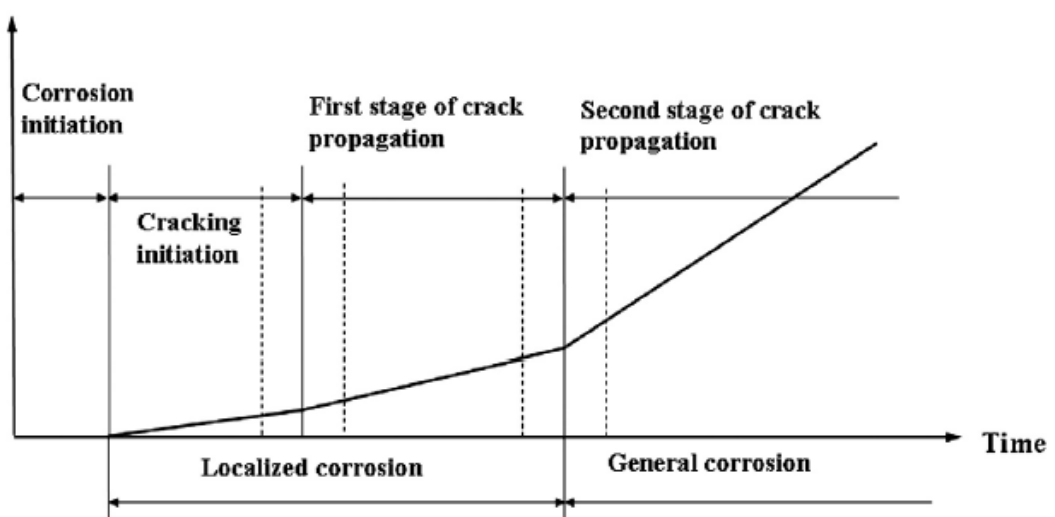


Figure 14 Corrosion pattern evolution according to (Ruijin Zhang, 2010)

The main concern is to define the maximum depth of the pitting attack because the corrosion current intensity has an average value highly lower than the maximum one.

In some cases, as accelerated corrosion tests, it can occur to have both uniform than localized section loss, so Rodriguez proposed a model that allows to define it in either case.

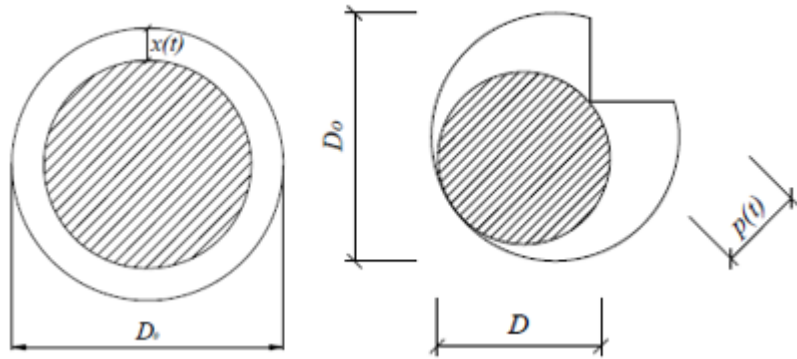


Figure 15 Cross section loss because of both homogeneous corrosion and pitting

The pitting factor R is equal to the ratio between the penetration depth maximum value over the average value.

$$R = \frac{x(t)_{max}}{x(t)_{middle}}$$

The amount of resisting area loss from the formulation for homogeneous corrosion using a pitting factor of 2:

$$\Delta A_s = \frac{\pi}{4} (2\alpha x(t) D_0 - \alpha^2 x(t)^2)$$

It depends on the initial diameter because it takes into account the case when two different diameters are subjected to the same attack.

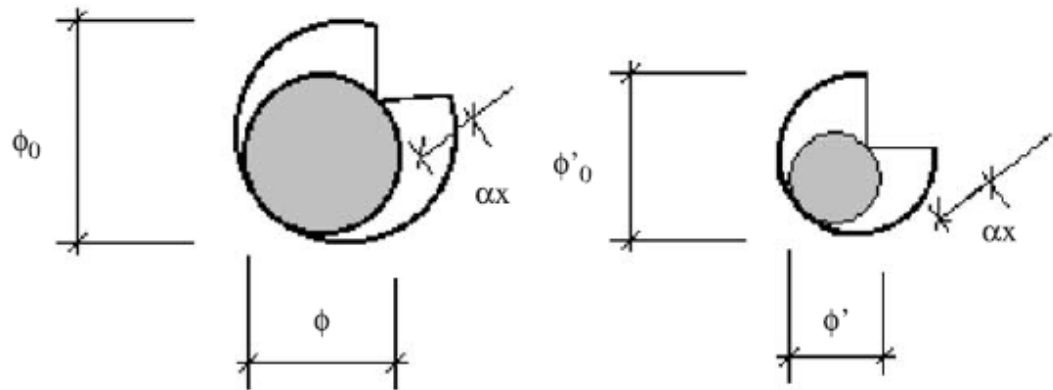


Figure 16 Same attack penetration on two different diameter reinforcements

Moreover, according to (Stewart, 2009), the pit area can be considered as shown in figure 17.

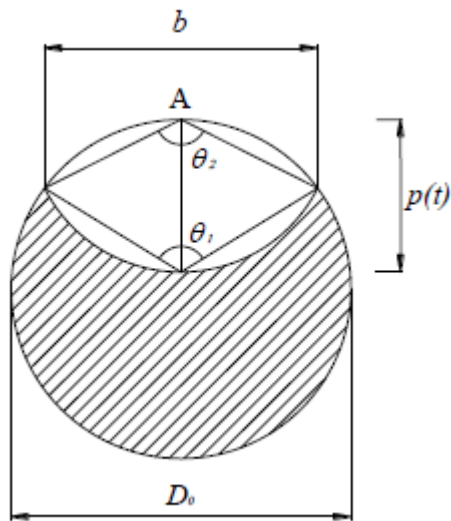


Figure 17 Section loss because of pitting according to (Stewart, 2009)

It hypothesizes that a pit starts from point A and develops over time following a circle with a $x(t)$ radius, where $x(t)$ is essentially the corrosion penetration depth.

$$x(t) = x(t)_{middle} R$$

At this point, the reduction percentage because of pitting can be defined:

$$\alpha_{pit} = \frac{A_{pit}}{A_0}$$

DUCTILITY

Corrosion may also affect the mechanical properties of the steel. Various experimental tests available in the literature show that steel ultimate elongation, and so its ductility, may be reduced, even for small area reductions. Consequently, a transition from a ductile behavior to a brittle one can occur.

Some experimental tests (Andrade, 2001) show a significant reduction of steel elongation at maximum load, that is a loss of steel ductility. Such reductions reach values of 30% and 50% for losses of steel section of 15% and 28%, respectively.

In (D. Coronelli, 2004) is suggested a linear reduction to describe the evolution of the ultimate strain of the steel from $\varepsilon'_{su} = \varepsilon_{su}$ in the virgin material ($\alpha_{pit}=0$) to $\varepsilon'_{su} = \varepsilon_{sy}$ ($\alpha_{pit} = \alpha_{pit}^{max}$ complete loss of ductility) for a severe percental reduction of the pitted section (α_{pit}^{max}):

$$\varepsilon'_{su} = \varepsilon_{sy} + (\varepsilon_{su} - \varepsilon_{sy}) \left(1 - \frac{\alpha_{pit}}{\alpha_{pit}^{max}} \right) \quad \text{for } \alpha_{pit} \leq \alpha_{pit}^{max}$$

The application is therefore linked to the parameter α_{pit}^{max} , whose evaluation is critical for the description of bar ductility.

STEEL MECHANICAL PROPERTIES

Strand corrosion deteriorates the material property and it can be considered by the corrosion loss and the deteriorated constitutive law.

In literature, several approaches are suggested. In (LeiWang, 2017) all the corroded strands are assumed having the same constitutive law before it yields. After that, the σ - ε diagram changes with increasing the corrosion loss. Strands with corrosion loss less than a critical value (η_c) will experience the hardening stage, but their

ultimate strains decrease linearly with increasing the corrosion loss. The further corroded strand, however, will fail immediately just after strand yielding.

The critical corrosion loss (η_c) was taken as 11% based on the experimental results. The constitutive law for strands with different corrosion losses can be expressed as:

$$f_p = \begin{cases} f_{py} + E_{pp}(\varepsilon - \varepsilon_{py}) & \varepsilon_{py} \leq \varepsilon \leq \varepsilon_{pu} - \frac{\eta}{\eta_c}(\varepsilon_{pu} - \varepsilon_{py}) \\ E\varepsilon & \varepsilon \leq \varepsilon_{py} \end{cases} \begin{cases} \varepsilon \leq \varepsilon_{py} \\ \eta \leq \eta_c \end{cases}$$

where f_p and ε are the stress and strain of strand, respectively; E_p , E_{pp} , ε_{py} , ε_{pu} and f_{py} are the elastic modulus, hardening modulus, yield strain, ultimate strain and yield strength of virgin strand, respectively.

This deterioration of the σ - ε diagram causes both a reduction of the material resistance and of the section ductility.

The stress-strain relationship of the steel reinforcement is idealized to be linear elastic-plastic with a post-yield strain hardening of 1%.

The compression stress-strain relationship of concrete is described by a parabolic relationship:

$$f_c(\varepsilon_c) = f'_c \left[\frac{2\varepsilon_c}{\varepsilon_{c0}} - \left(\frac{\varepsilon_c}{\varepsilon_{c0}} \right)^2 \right]$$

where f'_c is the specified compressive strength of concrete and ε_{c0} is the corresponding strain.

EFFECTS ON CONCRETE

An important aspect regarding a corroded element is how steel corrosion affects the concrete in which it is embedded. The corroded bar cracks the concrete cover up to the cover spalling because of corrosion products that have a higher volume than the basic metal. In other words, when steel corrosion develops, the corrosion

products spread throughout the material and mix with the hydrated products of cement. They slowly stress the concrete cover until the resulting tensile stress in the enclose concrete cover reaches the tensile strength limit of concrete.

As corrosion cracking develops and becomes wider, the aggressive agents can reach the steel surface more easily, so the protective task of the concrete cover is reduced as though corrosion velocity increases. Moreover, corrosion cracks propagation modifies the corrosion pattern which change from localized dominant to generalized (Ruijin Zhang, 2010).

The design of the longitudinal reinforcement defines the pattern of cracks propagation. Longitudinal cracks constitute an important characteristic because they offer a visual sign of corrosion. As a matter of fact, the time elapsed between steel passivation and the appearance of the first crack in the surface is comparatively very short, as suggested by (C. Alonso, 1998).

Above all, the factors conditioning the cover cracking are the c/d ratio (cover/diameter) and the cement quality. In agreement with (C. Alonso, 1998), assuming a generalized corrosion, for c/d ratios > 2 , radius losses of around $50 \mu\text{m}$ induce crack widths of about 0.05 mm, while for c/d ratios ≤ 2 , only attack penetrations of $15-30 \mu\text{m}$ are necessary. In other words, for a small c/d ratio, the corrosion products provoke immediate cracking, on the other hand, a high c/d ratio brings a cracking delay.

Many studies, in literature, are aimed to link the reinforcement corrosion state to cracking evolution, in particular, to crack width.

For example, referring to (C. Alonso, 1998), after the generation of the crack, the growth of its width seems to follow a lineal trend with the attack penetration until levels of around $200-300 \mu\text{m}$.

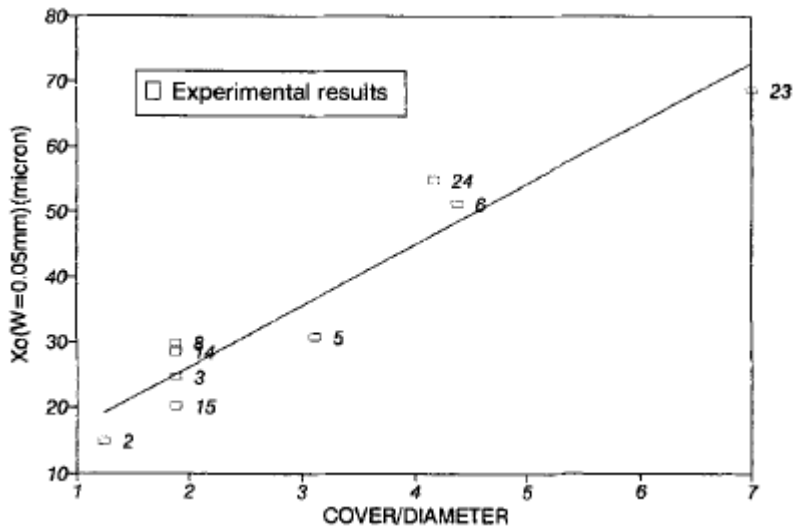


Figure 18 Linear relationship between crack width growth and radius loss according to (C. Alonso, 1998)

The attack penetration required for corrosion cracking initiation (μm) is:

$$x_0 = 7.53 + 9.32 \frac{c}{d}$$

During the cracking propagation phase, a general form of the linear relation between crack width and attack penetration proposed by (J. Rodriguez, 1996) is:

$$w = 0.05 + \beta(x - x_0)$$

where, x is the attack penetration (μm) and β is the coefficient depending on the position of rebar: $\beta=0.01$ for top cast bar; $\beta=0.0125$ for bottom cast bar.

However, in this model, the steel bar's position only affects the value of attack penetration that initiates cracking, and it has no influence on cracking development.

In (Ruijin Zhang, 2010), it is related the average steel cross-section loss to the cracking propagation, in the second stage of cracking propagation, though an empirical linear expression predicting crack propagation under the general corrosion pattern is:

$$w = 0.1916\Delta A_{sm} + 0.164$$

Because of cracks, before the cover spalling, the cement surrounding the bar present a reduced compressive strength. Nowadays, some studies have been performed to define the flexural strength of corroded beams.

In general, it can be defined a damage coefficient δ_{fc} :

$$f_c = f_{c0}(1 - \delta_{fc})$$

An example is the formulation developed in (D. Coronelli, 2004):

$$f_{c,rid} = \frac{f_c}{1 + k \varepsilon_t / \varepsilon_{c0}}$$

Where k is coefficient depending on the bar diameter and roughness. The deformation is:

$$\varepsilon_{c0} = 0.0017 + 0.001 \left(\frac{f_{cm}}{70} \right)$$

Considering f_{cm} in MPa

The compressive strength reduction is considered up to the cover spalling, after that the damage coefficient is applied to the cover area reduction:

$$A_c = A_{c0}(1 - \delta_{Ac}) = 0 \text{ because } \delta_{Ac} = 1$$

The transverse deformation can be expressed as:

$$\varepsilon_t = \frac{n_{bars} w}{b_i}$$

Where b_i is the section width in correspondence with the reinforcements.

STEEL-CONCRETE BOND

Corrosion can affect the anchorage of pre-tension strand and lead to a lack of the structures load-carrying performance and serviceability performance, such as anchoring-bond failure of pre-tensioned structures.

Bond strength improves before the cover concrete cracks then decreases when the crack is wide enough. This critical width depends on factors such as reinforcement design and diameter, concrete strength and cover depth.

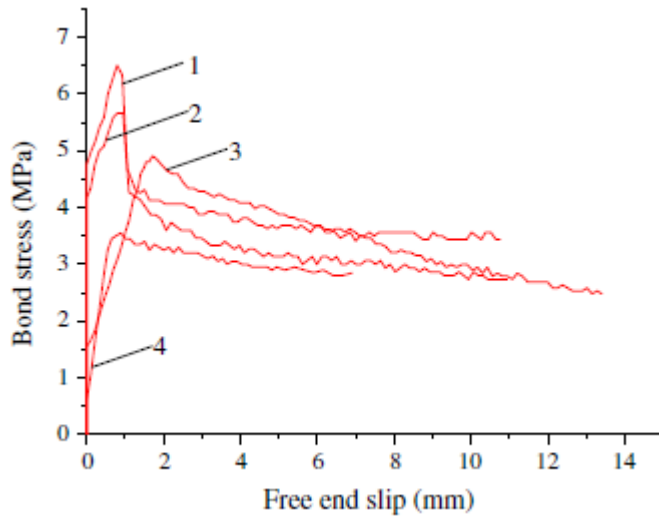


Figure 19 Bond-slip diagrams by (Fumin Li, 2013): (1) no corrosion, (2) corrosion crack of 0.2mm (3) corrosion crack of 0.5mm (4) corrosion crack of 0.8mm

In pre-tensioned structures, the anchoring bond length is very long and the influence of tendons corrosion on the redistribution of anchoring bond stress should be considered, as suggested by (Fumin Li, 2011).

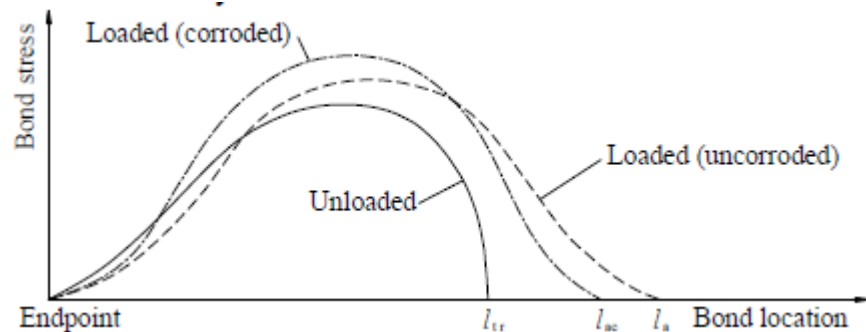


Figure 20 Bond redistribution by (Fumin Li, 2011)

How shows figure 21, when the applied strand force (F_p) is greater than the sum of effective bond force and prestressed force ($F_{eb}+F_{pe}$), the effective bond region begins to shift. The slip region extends, and the residual bond force increases. The shifting will not stop until the total of the effective bond force, the residual bond force and the prestressed force ($F_{eb}+F_{pe}+F_{rb}$) is equal to the applied force (F_p).

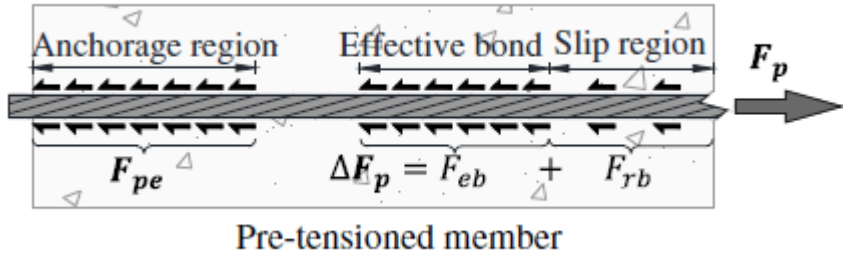


Figure 21 Bond force shift

Some studies have been performed to identify the effect of bond degradation for corroded RC beams. However, most of the existed studies just provide some empirical bond deterioration factors based on experimental tests. These empirical factors could not be suitable for prestressed concrete beams.

In (LeiWang, 2017) the excessive slip is treated as constant, obtained based on the equivalence of energy dissipation:

$$\tau_{ave} = \frac{\int_0^{s_2} \left[\tau_{max} \left(\frac{s}{s_2} \right)^\alpha \right] ds + \int_{s_2}^{s_3} \left[\tau_{max} - (\tau_{max} - \tau_f) \left(\frac{s - s_2}{s_3 - s_2} \right) \right] ds}{s_3}$$

That can be approximately simplified as:

$$\tau_{ave} = \frac{s_2}{(\alpha + 1)s_3} \tau_{max} + \frac{s_3 - s_2}{2s_3} (\tau_{max} + \tau_f) \approx 0.7\tau_{max}$$

The effective bond length of the strand tension force increment:

$$l_{eb} = \frac{f_{py} - f_{pe}}{7} d_p$$

where l_{eb} is the effective bond length; f_{py} is the yield strength of the strand; f_{pe} is the effective stress of strand; d_p is the diameter of strand.

The effective bond force of the strand with different corrosion loss can be calculated as:

$$F_{eb} = 0.7R(\eta)\tau_{max}L_p l_{eb}$$

where F_{eb} is the effective bond force of strand; L_p is the circumference of strand and $R(\eta)$ is the normalized maximum bond stress, which is the ratio between the maximum bond stress for corroded members and the value of virgin members; η is the corrosion loss of strand.

In addition, based on pull out tests, (Jianren Zhang, 2016) determined an empirical formulation to obtain the influence of corrosion-induced crack on τ_p and τ_m , which represents the bond stress of initial slip occurred at free end and bond stress at maximum pull-out force:

$$\begin{aligned}\tau_m &= -4.03W_{ave} + 4.96 \\ \tau_p &= 3.23\exp(4W_{ave})\end{aligned}$$

It can be seen that the τ_p and τ_m presents a linear decrease and an exponential descent with the increasing of corrosion induced crack width.

PRESTRESS FORCE

Accurate determination of residual prestress forces is a key parameter when assessing existing prestressed concrete bridges because it strongly influences their responses and capacities at both serviceability and ultimate limit states.

Prestress loss is deeply dependent on corrosion, especially for pretensioned structures, because of the multiple parameters already discussed; such as bond degradation, which increases the transfer length, and cross section loss, that limits the amount of force that can be transferred.

Thus, there are clearly difficulties in determining residual prestress forces using code models related to uncertainties associated to the prestressing system and time-dependent phenomena, such as steel relaxation, both shrinkage and creep of concrete and also degradation processes.

Several researchers have performed studies to determine the effective prestress force.

In (Niklas Bagge, 2017) a combination of both non-destructive and destructive tests in conjunction with FE analyses is proposed; moreover, due to the pursuit of practical applications for existing bridges, the main focus was on non-destructive methodology.

CHAPTER 2: CASE STUDY

The Corso Grosseto's flyover, in Turin, Italy, has been an important hub for the city for 45 years because it links two urban arterial road which are Corso Potenza, which connects the uptown (north side) to the downtown (south side), and Corso Grosseto, which covers the uptown from West to East.



Figure 22 Satellite view of the situ from Google Earth Pro

The project dates back to 1970, in a period of economic boom in the Italian history. Over the course of these years, Turin becomes the icon of this thriving society thanks to the presence of the biggest industries in the country. For this reason, the city becomes an immigration destination. Therefore, the local authorities highlight the need of multiple overpasses and underpasses in the strategic hubs to remedy the urban drivability problems.

The overpass bridge presents different spans: 24m, 20m, 19.60 m, 17.30m, 16m, 15.60m and 10m.

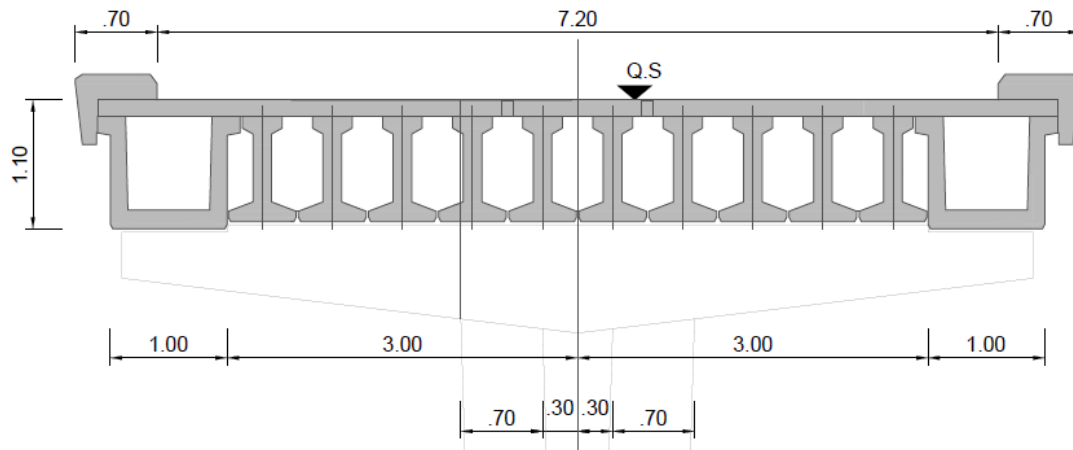


Figure 23 Corso Grosseto's flyover: deck's section "A type" relatively to the 24 m, 20 m, 19.60 m, 18 m, 16 m, and 15.60 m spans

The demolition process started around a year ago to permit the construction of a tunnel and it is not over yet.

The bridge has been subjected to different kinds of corrosion which even includes the chloride attack due to the use of antifreeze salts during the winter season and pollution agents.

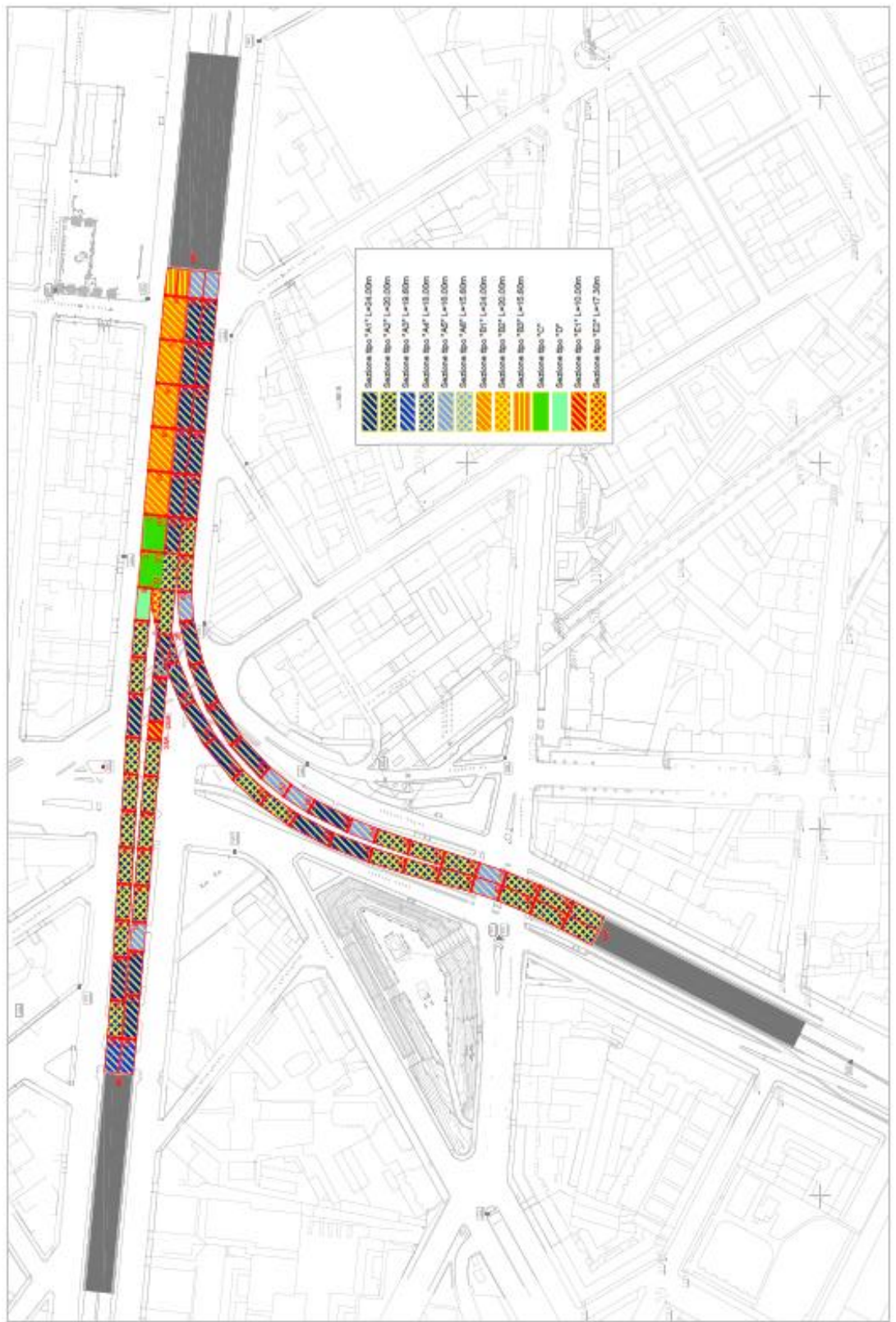


Figure 24 Corso Grosseto's flyover planimetry

CHAPTER 3: ANALYTICAL ANALYSIS

In this section an analytical analysis is provided to gain further parameters for the numerical modelling and, in general, to have a magnitude of what is or would act on the Corso Grosseto's overpass bridge beams under different scenarios.

The scheme used is an isostatic, simply supported beam with 4 different span lengths, which are equal to 24, 16, 8 and 6 meters. The firsts two lengths are the two biggest spans in situ. On the other hand, the 6- and 8-meters ones have been analyzed to take into account further experimental tests, so to fit into a laboratory.

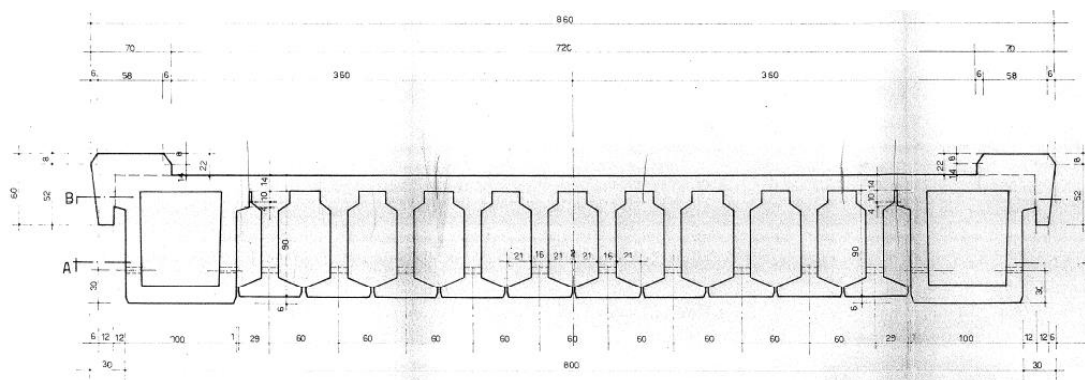


Figure 25 Transversal deck's section as reported in the executive report

The deck is composed by two different sections and reinforcement designs for the border beams and for the intermediate ones, as reported in figure 26. In particular, the border beams are U shaped sections with a height of 960 mm and the intermediate beams are 900 mm, double T sections.

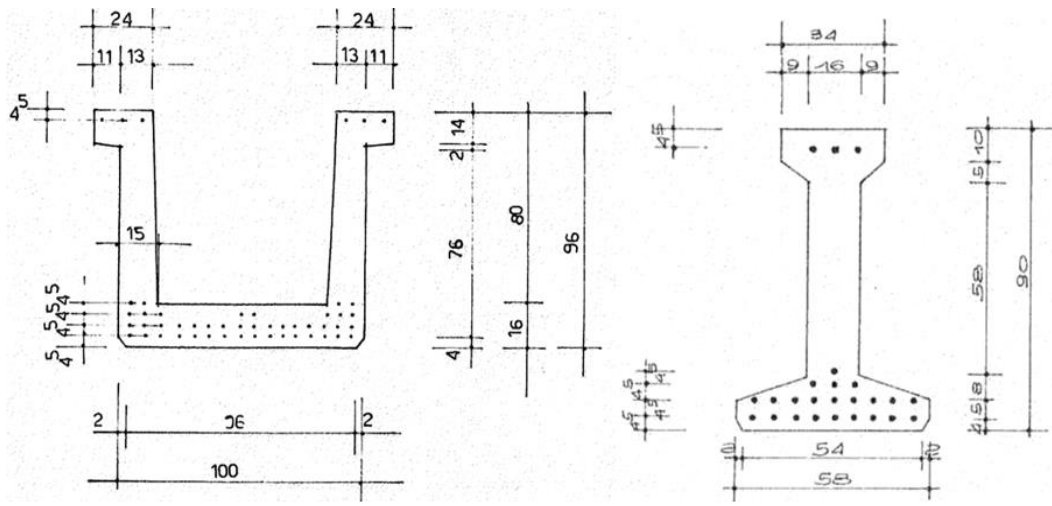


Figure 26 Cross sections geometry

The intermediate beams are spaced out of 600 mm from the central axis respectively, instead, the border beam is distant from the first intermediate beam of 800 mm.

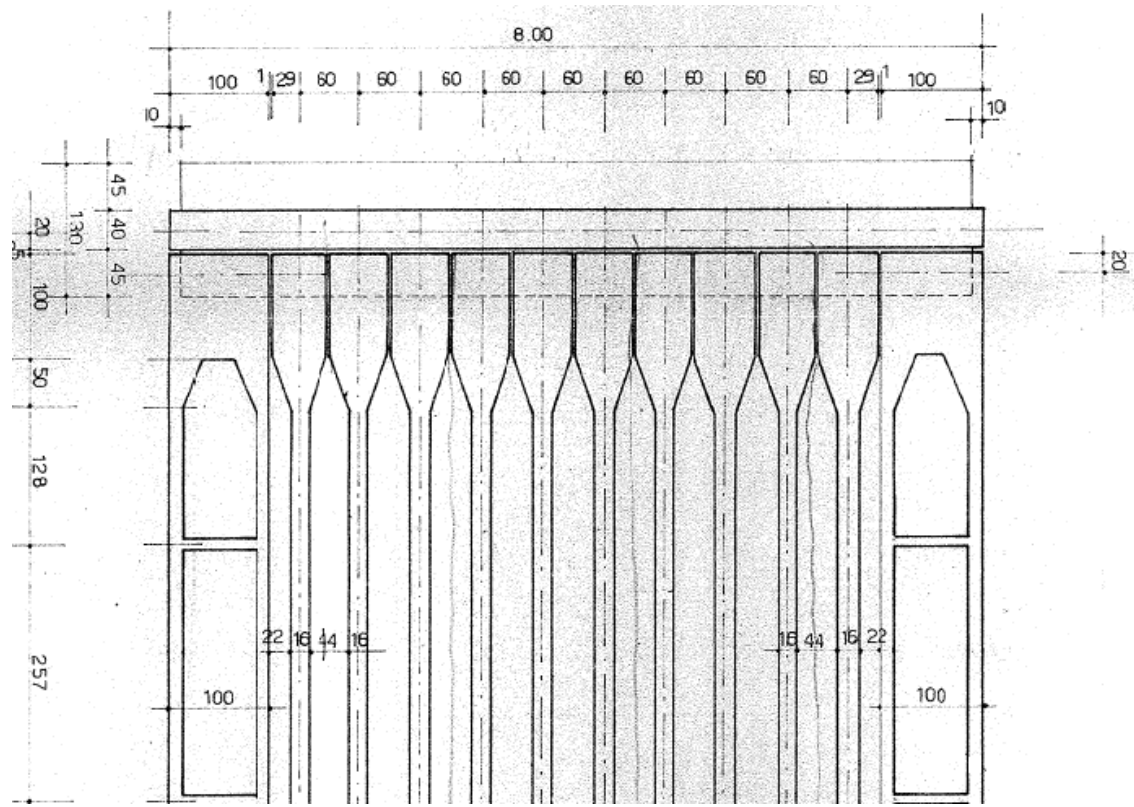


Figure 27 Deck's horizontal section closeness to the support

On the beams we can find a slab 140 mm thick, for this reason, in the analytical analysis, two situations are considered, the first one with no working slab on the beams, which is took into account just as a dead weight, and the other one with a working slab.

The analysis can be split in 3 macro steps: definition of the transferring length for the different beams and reinforcements designs; tensional analysis and the resisting characteristics just like the resisting bending moment and shear. Moreover, thinking about future experimental tests in situ, it is been analyzed a configuration with the intermediate beams overturned, to understand if those beams could be used as a test base in rupture tests.

MATERIALS

To define the materials used for the construction of the Corso Grosseto's bridge, the historic executive report has been essential because there are no experimental tests to help. The design values have been defined, but for the analysis the characteristic values have been used. This choice because the design values are defined with the safety coefficients in the prospectus 2.1N-EC, and they are related to new materials, realized with modern techniques, so to apply them to these materials has not sense because they are materials produced over 70 years ago. In other words, for the analysis the characteristic values have been used above all because of the aleatory nature of the data.

The characteristic value is the one to which is assigned a probability to be not reached in a hypothetical test after an unlimited sequence. According to the EN1990 the characteristic value of a generic material's property as 5% fractile of a probability distribution in which a low value is unfavorable or 95% fractile a probability distribution in which a high value is unfavorable.

In reference to the rigidity parameters, like the elastic modulus, the characteristic values are equal to the average value because these coefficients can either be favorable or not in relation to the different cases.

So, from the report, the following characteristics can be expressed:

Concrete:

After 28 days:

E_{cm}	35376.28 MPa	
α_e	5.79	
γ_{cls}	25 kN/m ³	
R_{ck}	500 Kg/cm ²	49.05 MPa
$R_{ck, min}$	468.16 Kg/cm ²	45.93 MPa
	433.16 Kg/cm ²	42.49 MPa
f_{ck}	40.71 MPa	
f_{cm}	48.71 MPa	
f_{cd}	23.07 MPa	
f_{ctd}	1.66 MPa	
f_{ctm}	3.55 MPa	

After the tendons' distention:

R_{ck}	396.67 Kg/cm ²	38.91 MPa
f_{ck}	32.30 MPa	
f_{cm}	40.30 MPa	

f_{cd}	18.30 MPa
f_{ctd}	1.42 MPa
f_{ctm}	3.04 MPa
E_{cm}	33420.05 MPa
α_e	6.13

Therefore, the concrete used can be classified as an ordinary concrete C40/50 kind.

Steel:

E_p	205000 Mpa			
f_{ptk}	167.48 Kg/mm ²	1642.979 MPa		
f_{p01k}	150.73 Kg/mm ²	1478.681 MPa	ε_{pyk}	7.21 %o
γ	1.15			
f_{ptd}	1428.68 MPa			
f_{p01d}	1285.81 MPa			

GEOMETRY

To define the geometry and dimensions of the deck, as well as for the materials, the data comes from the executive report. Two sections are considered, each one in two different conformations: with and without the working slab. Furthermore, it has even been considered the configuration of a simple concrete section and the configuration of the same section but with steel homogenized to concrete. In addition, it has been calculated the prestress center for the two sections and for the different reinforcement designs, which for the intermediate beams are three different ones.

FOR THE BORDER BEAMS

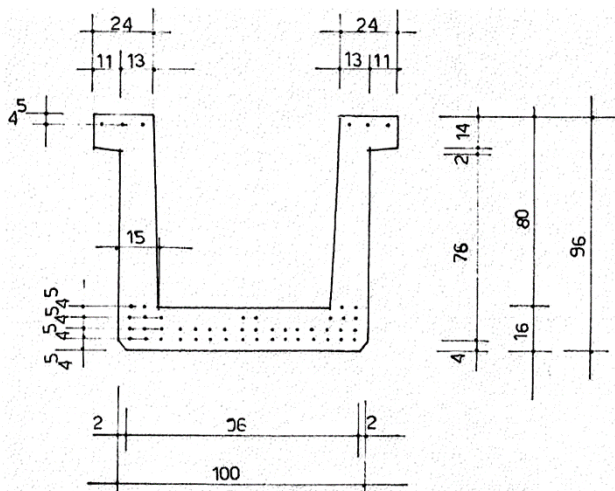


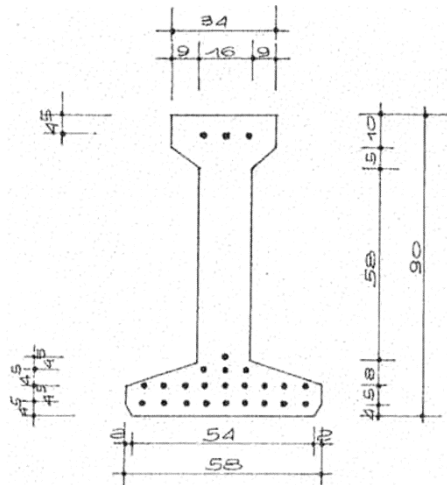
Figure 28 Border beam cross section

GEOMETRY	
b_{sup1}	240 mm
Δb_{sup}	110 mm
s_{sup}	140 mm
$h_{sup,link}$	20 mm
h_{web}	760 mm
$b_{web, sup}$	130 mm
$b_{web, inf}$	150 mm
b_{inf}	1000 mm
s_{inf}	160 mm
$h_{inf,link,2}$	40 mm
$b_{inf,link,2}$	20 mm

n	50 # of tendons		
φ	1/2"	\rightarrow	10.82 mm
$A_{p,i}$	92.00	mm^2	
A_p	4600.00	mm^2	
$h_{inf wire}$	100.00	mm	
$h_{G,precompression}$	197.20	mm	
A_c	403200.00	mm^2	
S_c	159490026.7	mm^3	
y_G	395.56	mm	

\underline{I}_c	33488642250 mm ⁴	
HOMOGENIZED SECTION		
$A_{c,om}$	431416.60 mm ²	
$S_{c,om}$	165088199.6 mm ³	
y_{om}	382.67 mm	
$\underline{I}_{c,om}$	36355213419 mm ⁴	
SECTION WITH COLLABORATIVE SLAB		
A_c	558600.00 mm ²	
S_c	319552026.7 mm ³	
y_G	572.06 mm	
\underline{I}_c	81040124627 mm ⁴	
HOMOGENIZED SECTION WITH COLLABORATIVE SLAB		
$A_{c,om}$	586816.60 mm ²	
$S_{c,om}$	325150199.6 mm ³	
y_{om}	554.09 mm	
$\underline{I}_{c,om}$	87436979121 mm ⁴	

FOR THE INTERMEDIATE BEAMS



GEOMETRY	
b_{sup}	340 mm
Δb_{sup}	90 mm
s_{sup}	100 mm
$h_{\text{sup,raccordo}}$	50 mm
h_{web}	710 mm
b_{web}	160 mm
$h_{\text{inf,raccordo},1}$	80 mm
Δb_{inf}	210 mm
b_{inf}	580 mm
s_{inf}	90 mm
$h_{\text{inf,raccordo},2}$	40 mm
$b_{\text{inf,raccordo},2}$	20 mm

Figure 29 Intermediate beam
cross section

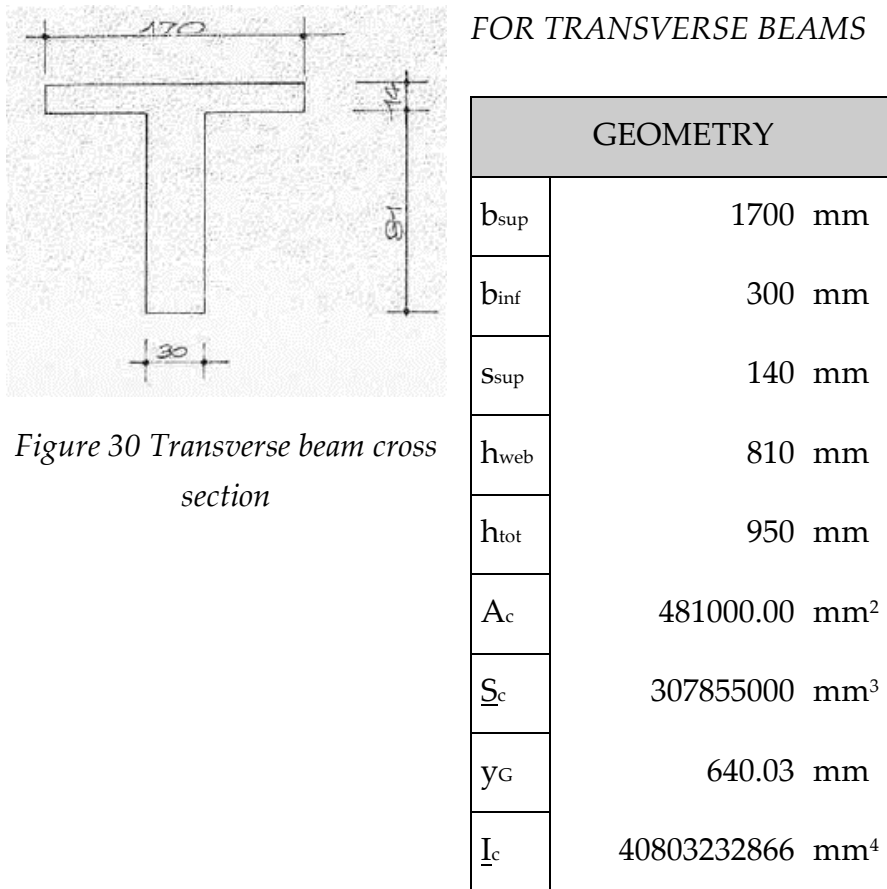
n	25 # trefoli in mezzeria		
	22 # trefoli tra 1,5 e 3		
	m		
	19 # trefoli tra 3 e 6 m		
φ	1/2"	\rightarrow	10.82 mm
$A_{p,i}$	92.00 mm ²		
A_p	2300.00 mm ²		

	25	22	19	φ
$h_{\text{cavo inf}}$	90.91	97.37	96.88	mm
$h_{G,\text{prestress}}$	182.00	200.00	215.79	mm
A_c	162800.00	169700	176600	mm^2
S_c	87275333.33 mm^3			
y_G	536.09 mm			
I_c	22933452337 mm^4			

HOMOGENIZED SECTION	
$A_{c,om}$	231764.19 mm^2
$S_{c,om}$	89780416.62 mm^3
y_{om}	387.38 mm
$I_{c,om}$	18053227347 mm^4
SECTION WITH COLLABORATIVE SLAB	
A_c	304300.00 mm^2
S_c	168755333.3 mm^3
y_G	554.57 mm
I_c	44886693313 mm^4

HOMOGENIZED SECTION WITH COLLABORATIVE SLAB	
$A_{c,om}$	315764.19 mm ²
$S_{c,om}$	171260416.6 mm ³
y_{om}	542.37 mm
$I_{c,om}$	47128570060 mm ⁴
HOMOGENIZED SECTION WITH COLLABORATIVE SLAB 22φ	
$A_{c,om}$	314388.49 mm ²
$S_{c,om}$	171012661.1 mm ³
y_{om}	543.95 mm
$I_{c,om}$	46796858639 mm ⁴
HOMOGENIZED SECTION WITH COLLABORATIVE SLAB 19φ	
$A_{c,om}$	313012.79 mm ²
$S_{c,om}$	171012661.1 mm ³
y_{om}	546.34 mm
$I_{c,om}$	46524199929 mm ⁴

Moreover, the deck has some transverse beams with the following dimensions:



DATA ON PRESTRESSING

In the midway section 50 tendons can be find in the border beams and 25 tendons in each intermediate beam. Each tendon has a diameter of $\frac{1}{2}''$ which is equal to 12.5 mm. As the 70s legislative proposed, the following tensions have been used:

Tolerable tension on the prestressing enactment:

$$\sigma_{api} = 0.95 f_{p0.1k} = 143.20 \frac{kg}{mm^2} = 1404.75 MPa$$

Tolerable tension to an infinite time:

$$\sigma_{ap} = 0.60 f_{ptk} = 709.77 \frac{kg}{mm^2} = 985.79 MPa$$

These values can be compared with the EC2 suggested values:

$\sigma_{p,max} = \min(0.8 f_{ptk}; 0.9 f_{p0.1k}) = 1314.38 MPa$ which is the maximum intensity of the force in the jack. This limit because the application of the prestress force has not to damage the concrete element.

$\sigma_{p,max} = \min(0.75 f_{ptk}; 0.85 f_{p0.1k}) = 1232.23 MPa$ is the force intensity once the release happens, so the prestress is transferred to concrete.

$\sigma_{p,max} = 0.80 f_{p0.1k} = 1182.94 MPa$ Tension to an infinite time

It is clear that the tension used to make the prestressed state in the beams has a value that exceed the modern limits according to the Eurocode, so the materials were “pushed further”; in fact, the EC2 limits are imposed to avoid a brittle failure of the tendons. As well as, to an infinite time it is accepted a smaller tension, so bigger rheological effects, that reduce the prestressing force, are allowed.

TRANSFER OF PRESTRESS

The transmission of prestress force from wires to the concrete section is not immediate but happens along a transfer length. This length is the required distance in order to have a constant distribution of the prestressing force in the entire section. This space is necessary because the force is applied punctually. Along this distance there is an instable zone called D-Region. In other words, at the end of the member, the strain, just like the force, is null and then it gradually increases through the transfer length up to the strain due to the effective prestress force. This strain remains almost constant once the D-region has overtaken. To estimate the D-Region, a huge number of formulations have been proposed in literature.

For this analysis, the EC2 proposed formula has been used. This formulation is inspired by fib Model Code 1990. According to it, the length required to have a constant force distribution, with no disturbs, is the sum (squared under square

root) of a part related to the transmission length (prestressing reinforcement anchorage zone) and the diffusion length required to have a gradual diffusion of tensions up to have a linear distribution in the section, which is the actual transfer. This last amount is equal to the section effective height which is the section height minus the reinforcement's concrete cover. This formula guarantees more safety than the approximate ones, in fact, it almost doubled those values, because the estimated expression do not consider the tension's diffusion but just the transferring part.

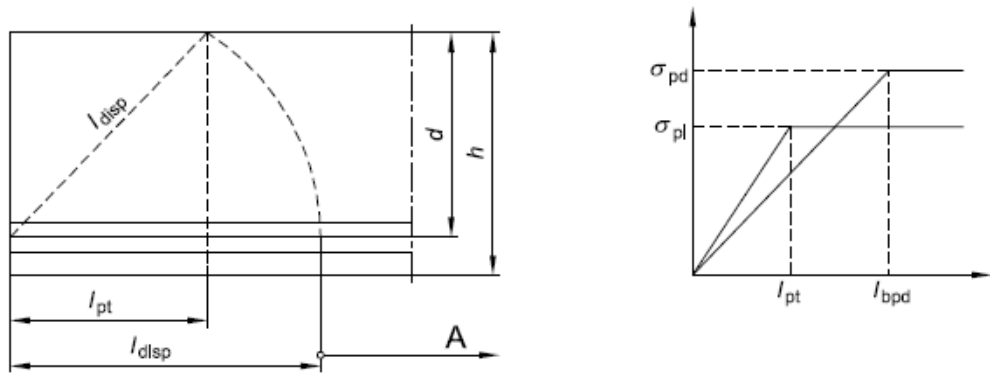


Figure 31 Prestress force transfer in pre-tensioned elements

$$l_{disp} = \sqrt{l_{pt}^2 + d^2}$$

$$l_{pt} = \alpha_1 \alpha_2 \phi \frac{\sigma_{pmo}}{f_{bpt}}$$

Where α_1 considers the type of release and α_2 the tendon area factor;

α_1	1 for gradual release 1.25 for sudden release
α_2	0.25 Tendons with circular cross-sections 0.19 for 3 and 7 wires strands

ϕ is the strand diameter, σ_{pm0} is the steel stress just after stress release and f_{bpt} is the constant bond stress that transfer the stress, at tendons release, to concrete, it is equal to:

$$f_{bpt} = \eta_{p1}\eta_1 f_{ctd}(1)$$

Where, $f_{ctd}(1)$ is the design tensile strength at time of release and η_{p1} and η_1 are two coefficients in function of the tendon's type and the bond situation, i.e. push-in at release and the position of the tendon during casting:

η_{p1}	2.7 for indented wires
	3.2 for 3 and 7 wires wire strands
η_1	good bonding conditions
	0.7 otherwise

FOR THE INTERMEDIATE BEAMS

l_{pt}	1030.386 mm
----------	-------------

19φ SECTION

h_{Gs}	215.79 mm
----------	-----------

With no slab

d	684.21 mm
l_{disp}	1236.87 mm

With slab

d	824.21 mm
l _{disp}	1319.48 mm

19φ+3φ SECTION

h _{Gs}	100.00 mm
-----------------	-----------

With no slab

d	800.00 mm
l _{disp}	1304.49 mm

With slab

d	940.00 mm
l _{disp}	1394.74 mm

22φ+3φ SECTION

h _{Gs}	50.00 mm
-----------------	----------

With no slab

d	850.00 mm
l _{disp}	1335.74 mm

With slab

d	990.00 mm
l _{disp}	1428.91 mm

ANCHORAGE LENGTH

According to Eurocode 2, the total anchorage length for anchoring a tendon with stress σ_{pd} is:

$$l_{bpd} = l_{pt2} + \alpha_2 \phi \frac{(\sigma_{pd} - \sigma_{pm\infty})}{f_{bpd}}$$

Where l_{pt2} is the upper design value of transmission length, (8.10.2.2 (3)), α_2 as defined in the previous paragraph, σ_{pd} is the tendon stress and $\sigma_{pm\infty}$ is the prestress after all losses; f_{bpd} is the strength for anchorage in the ultimate limit state

$$f_{bpd} = \eta_{p2} \eta_1 f_{ctd}$$

Where η_{p2} is a coefficient that considers the type of tendon and the bond situation at anchorage ($\eta_{p2} = 1,4$ for indented wires or $\eta_{p2} = 1,2$ for 7 -wire strands).

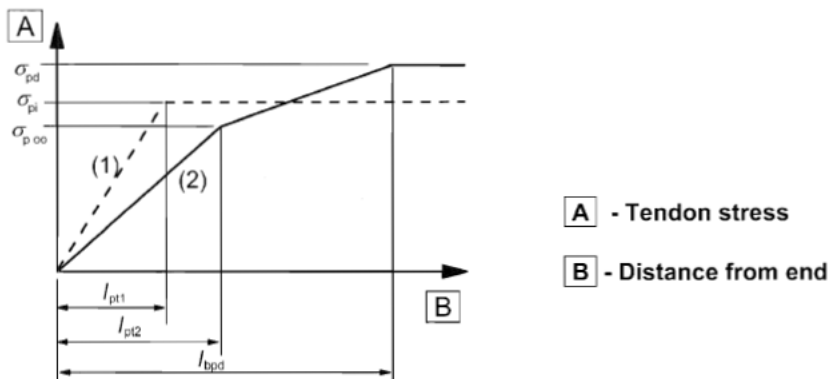


Figure 32 Stresses in the anchorage zone of pretensioned members: (1) at release tendons
(2) at ULS

	25φ	22φ	19φ	
σ_{pd}	18.01	15.21	12.62	MPa
$\Delta\sigma_{p,c+s+r}$	164.07	198.54	226.60	MPa
$\sigma_{pm\infty}$	-146.06	-180.52	-208.59	MPa
f_{bpt}	3.18	MPa		
l_{bpd}	1342.55	1402.98	1424.66	mm

TRAFFIC LOAD

The load can be concentrated or distributed, in any case they are multiplied by the adjustment factors α which depends on the relevance of the bridge and by the expected traffic.

$\alpha_Q Q_k$ for concentrated loads

$\alpha_q q_k$ for distributed loads

- 1st category bridges: $\alpha_Q = \alpha_q = 1.0$
- 2nd category bridges: $\alpha_Q = \alpha_q = 0.8$

In absence of specifications, these factors should be taken equal to unity.

Furthermore, there is a dispersal of concentrated loads through pavement and the concrete slab that increases the application area. This phenomenon is less accentuated in concrete bridges than in steel bridges because the stress variation is slower.



Figure 33 Concentrated load dispersion

There are 6 load models used to describe all the vertical actions:

- Load model 1 (LM1): tandem and distributed loads for general and local verification
- Load model 2 (LM2): tandem and single tie load for general and local verification
- Load model 3 (LM3): concentrated load for local verification (0.4x0.4m)
- Load model 4 (LM4): concentrated load for local verification (0.1x0.1m)

- Load model 5 (LM5): distributed crowd loads for general and local verification
- Load model 4 (LM4): distributed load for long span bridges

Some of these models are meant for global verifications, others for local verification.

For the study the load model 1 has been used:

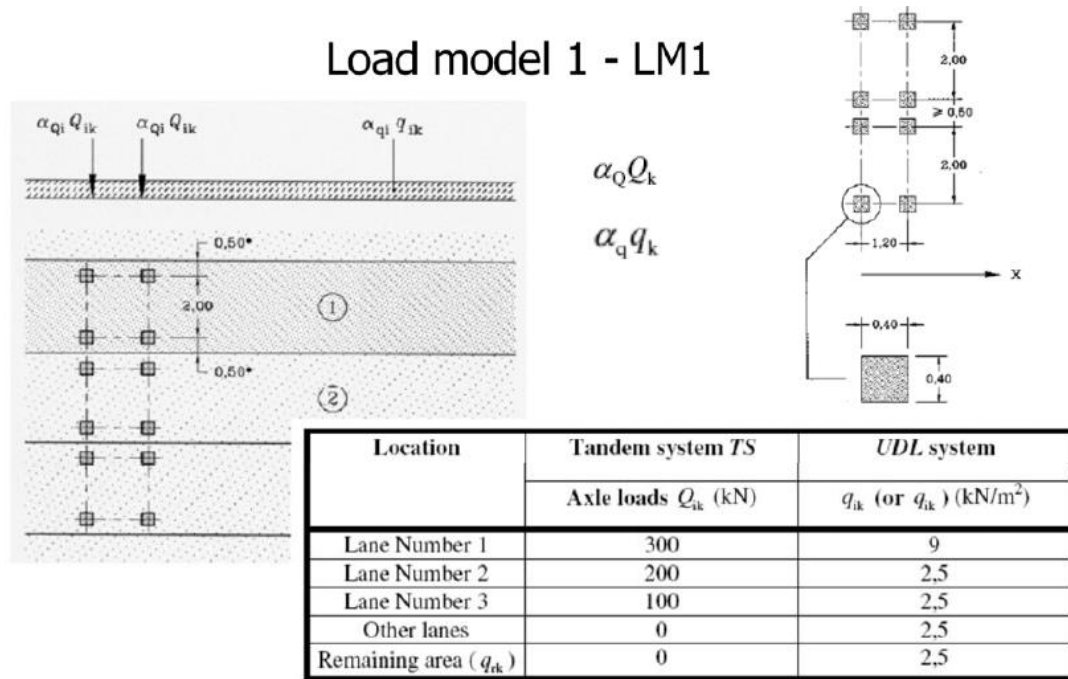


Figure 34 Load model 1

The number of notional lanes n_l depends by w the transverse length that in the case study, it is equal to 8, so n_l results:

$$n_l = \text{int} \left(\frac{w}{3} \right) = 2$$

To define the influence of the tandem system on the deck, the Courbon method has been used. It is based on the hypothesis that there is an infinite (or high number) number of transverse which have an infinite flexural rigidity ($Q_E=\infty$) while longitudinal beams have null torsional rigidity ($\gamma_p=0$).

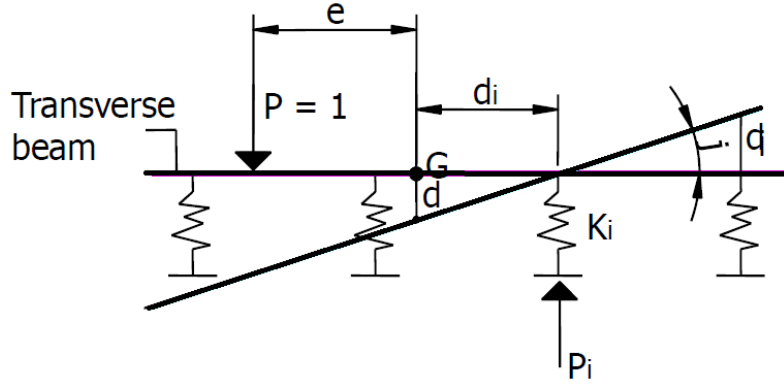


Figure 35 Courbon method: static scheme of transverse beam

The static scheme analyzed considers the slab as a continuous beam supported by springs, then an eccentric load P ; G is the spring rigidity gravity center, δ the displacement of the beam in correspondence to the rotation center and φ the rotation angle of transverse beam. The global displacement of transverse beam is:

$$\delta_i = \delta + \varphi d_i$$

The force in the generic beam is:

$$P_i = K_i \delta_i = K_i (\delta + \varphi d_i)$$

The equilibrium in the vertical direction:

$$\sum_{i=1}^n P_i = 1 \Rightarrow \sum_{i=1}^n (K_i \delta + K_i \varphi d_i) = \sum_{i=1}^n K_i \delta + \varphi \sum_{i=1}^n K_i d_i = 1$$

The second summary is equal to zero because G is the centroid of rigidities, so by definition of static moment; the previous becomes:

$$\delta = \frac{1}{\sum_{i=1}^n K_i}$$

Imposing the rotation equilibrium:

$$\sum_{i=1}^n P_i d_i = 1e \Rightarrow \sum_{i=1}^n (K_i \delta + K_i \varphi d_i) d_i = \delta \sum_{i=1}^n K_i d_i + \varphi \sum_{i=1}^n K_i d_i^2 = 1e$$

$$\varphi = \frac{e}{\sum_{i=1}^n K_i d_i^2}$$

If the beams are identical with the same restraints $K_i=K=\text{cost}$.

It is now possible to calculate the percentage of load $P=1$ with eccentricity e acting on the i -th beam=

$$\rho_{i,e} = \frac{K_i}{\sum_{i=1}^n K_i} + \frac{K_i d_i e}{\sum_{i=1}^n K_i d_i^2} = \frac{K}{nK} + \frac{K d_i e}{K \sum_{i=1}^n d_i^2} = \frac{1}{n} + \frac{d_i e}{\sum_{i=1}^n d_i^2}$$

This percentage represent a repartition parameter which explains how the load is distributed along the deck.

Instead of considering the deck composed by 2 U sections and 10 I sections, it has been simplified in 14 beams with the I section rigidity because the rigidity of the U sections is doubled compared to the one of the I section. This assumption has been made even in the executive design.

From the analysis results that:

$R_{1,F}$	63.28	kN
$R_{1,q}$	4.88	kN/m

In the executive design, another method has been used to define the traffic load, which is the Massonet method. This method considers 2 eccentric loads from which the repartition coefficients can be calculated.

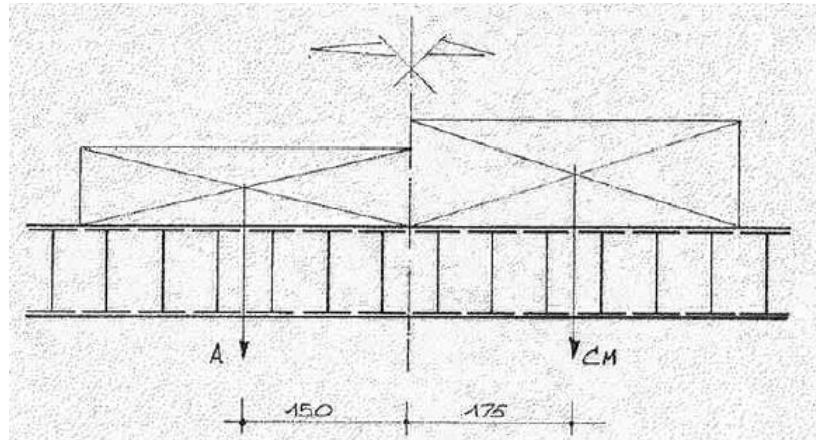


Figure 36 Load distribution from the executive report

So, from the executive report results:

P	0.64	t/m	6.31	kN/m		
k_{cm}	1.67	t/m	16.42	kN/m	121.28	kN
k_a	0.41	t/m	4.00	kN/m	29.55	kN

TENSIONAL ANALYSIS

Tensional analysis is useful to quantify the beam's prestress losses and to better check the software's results, or rather, to validate the modelling process. Moreover, it is interesting to compare the executive project results with the nowadays ones, evaluated with the Eurocode formulations.

For this reason, the two beam sections have been analyzed, both considering the collaborative slab and not, in the 4 span configurations. In other words, the tensional analysis has been done considering a constant step of 0.5 m, according to the future model which will present beams elements of the same length. It has been considered a variable prestress force, which enters in the element gradually throughout the transmission length, function of the reinforcement design, along the maximum span beam. A total of 24 sections are took into account from the

midspan to an end because of the problem's symmetry. Same assessment has been done for the 16 m beams.

The two smaller beams considered for potential experimental tests are not going to be modeled so to evaluate the tensional state, starting from the midspan, 5 sections every 250 mm are analyzed for the 6 m beams and others 5 sections every 550 mm for the 8 m ones. So, in both the smaller beams, the D-Regions have been cut off.

First of all, let's have a look to the executive results. From the executive report, in fact, it is possible to extract the following information:

FOR THE BORDER BEAMS

TENSION LOSSES			
IMMEDIATE			
$\Delta\sigma_{el}$	9.11 Kg/mm ²	89.37 MPa	Elastic reduction
RHEOLOGICAL			
$\Delta\sigma_{sh}$	6.00 Kg/mm ²	58.86 MPa	Shrinkage
$\Delta\sigma_{creep}$	20.95 Kg/mm ²	205.56 MPa	Creep
$\Delta\sigma_{pr}$	22.44 Kg/mm ²	220.18 MPa	Steel's relaxation
TOTALE	58.51 Kg/mm ²	573.97 MPa	TOTAL
STEEL STRESSES			
$\sigma_{p\infty}$	84.69 Kg/mm ²	830.77 MPa	at $t\infty$
σ_{p0+}	129.78 Kg/mm ²	1273.19 MPa	At tendons' distention

FOR THE INTERMEDIATE BEAMS

TENSION LOSSES			
IMMEDIATE			
$\Delta\sigma_{pe}$	8.93 Kg/mm ²	87.60 MPa	Elastic reduction
RHEOLOGIC			
$\Delta\sigma_{sh}$	6 Kg/mm ²	58.86 MPa	Shrinkage
$\Delta\sigma_{creep}$	20.55 Kg/mm ²	201.60 MPa	Creep
$\Delta\sigma_{pr}$	22.87 Kg/mm ²	224.35 MPa	Steel's relaxation
TOTALE	58.35 Kg/mm ²	572.41 MPa	TOTAL
STEEL STRESSES			
$\sigma_{p\infty}$	84.85 Kg/mm ²	832.33 MPa	at t_∞
σ_{p0+}	129.97 Kg/mm ²	1274.96 MPa	At tendons' distention

The executive report offers some additional data like that the elastic reduction is been evaluated considering the lowest tendons' row and hypothesizing the relaxation loss, ones the tendons distention occurred, is equal to 3% of the tension acting initially in each cable. In addition, the relaxation loss has been defined considering a parabolic variation as recommended at point 2.7.1 of "Le nuove norme per le strutture in c.a.p." in effect at the time.

To define the initial losses, in the analysis it has been considered the beams' self-weight quota in which it is possible to distinguish different parts. Concrete and slab weight are structural weight portions, instead, finishing and transverse beams weight are carried, not structural, weights. Each beam has been schematized as a simple supported isostatic beam, so the bending moment diagram has a parabolic path, with a maximum in the midspan. The self-weight quota has been

added to the beam initial tensional state, considering a variable prestress force and the different reinforcement configuration. This assessment has been done for the 4 spans and the 2 cross sections.

For the border beams there are no information about the reinforcement configuration, so the analysis considers those beams with a unique design with 50 tendons.

Shown belong the case of both sections with collaborative slab.

FOR THE BORDER BEAMS

SECTION WITH COLLABORATIVE SLAB	
P _{inf}	7585.09 kN
P _{sup}	1034.33 kN
P	8619.42 kN
M _{p,inf}	-3553.18 kNm
M _{p,sup}	384.31 kNm
M _p	-3168.87 kNm
q _{pp,cls}	10.04 kN/m
q _{pp, soletta}	3.89 kN/m
q _{pp, finiture}	3.47 kN/m
q _{pp, traverso}	1.67 kN/m
q _{pp, tot}	19.07 kN/m
q _{pp}	13.93 kN/m

FOR THE INTERMEDIATE BEAMS

SECTION WITH COLLABORATIVE SLAB				
	25φ	22φ	19φ	
P _{inf}		2580.41	2228.54	1876.66 kN
P _{sup}		351.87 kN		
P		2932.29	2580.41	2228.54 kN
M _{p,inf}		-1164.95	-1152.37	-1159.82 kNm
M _{p,sup}		111.77 kNm		
M _p		-1053.18	-1040.61	-1048.05 kNm
q _{pp,cls}		7.89	7.86	7.83 kN/m
q _{pp, soletta}		2.10 kN/m		
q _{pp}		9.99	9.96	9.93 kN/m
q _{pp, finiture}		1.87 kN/m		
q _{pp, traverso}		2.33 kN/m		
q _{pp, tot}	14.20	14.17	14.13 kN/m	

Defined the self-weight load, the bending moment, related to the initial state in which the elastic losses are extinguished, is evaluated for every span and cross section.

In particular, for the biggest span configuration the tensional state is the following:

Δ	$\sigma_{c,\text{inf}}$	$\sigma_{c,\text{sup}}$	$\sigma_{p,1}$	$\sigma_{p,2}$	$\sigma_{p,3}$	$\sigma_{p,4}$	$\sigma_{p,5}$
12	-16.62	-10.96	1184.64	1193.81	1202.97	1212.14	1119.08
	-16.62	-10.96	1184.64	1193.81	1202.97	1212.14	1119.08
11	-16.62	-10.96	1184.64	1193.81	1202.97	1212.14	1119.08
	-16.62	-10.96	1184.64	1193.81	1202.97	1212.14	1119.08
10.5	-16.62	-10.96	1184.64	1193.81	1202.97	1212.14	1119.08
	-16.62	-10.96	1184.64	1193.81	1202.97	1212.14	1119.08
10	-16.62	-10.96	1184.64	1193.81	1202.97	1212.14	1119.08
	-16.62	-10.96	1184.64	1193.81	1202.97	1212.14	1119.08
9	-16.62	-10.96	1184.64	1193.81	1202.97	1212.14	1119.08
	-16.62	-10.96	1184.64	1193.81	1202.97	1212.14	1119.08
8.5	-16.62	-10.96	1184.64	1193.81	1202.97	1212.14	1119.08
	-16.62	-10.96	1184.64	1193.81	1202.97	1212.14	1119.08
8	-16.62	-10.96	1184.64	1193.81	1202.97	1212.14	1119.08
	-16.62	-10.96	1184.64	1193.81	1202.97	1212.14	1119.08
7.5	-14.91	-9.83	1173.64	1181.87	1190.10	1198.33	1114.79
	-14.23	-9.38	1124.55	1132.40	1140.24	1148.09	1068.42
7	-13.53	-8.92	1075.05	1082.51	1089.98	1097.44	1021.65
	-13.18	-8.69	1202.54	1209.87	1217.19	1224.52	1150.38
6.5	-13.32	-8.72	1202.54	1209.87	1217.19	1224.52	1150.38
	-13.32	-8.72	1202.54	1209.87	1217.19	1224.52	1150.38
6	-10.16	-6.65	1199.10	1204.69	1210.28	1215.87	1159.28
	-9.53	-6.24	1141.85	1147.10	1152.34	1157.58	1104.53
4.5	-8.88	-5.82	1083.63	1088.52	1093.41	1098.30	1048.83
	-8.56	-5.60	1227.88	1232.61	1237.35	1242.09	1194.36
3							

2.5	-8.65	-5.60	1227.88	1232.61	1237.35	1242.09	1194.36
2	-8.65	-5.60	1227.88	1232.61	1237.35	1242.09	1194.36
1.5	-7.95	-5.14	1128.01	1132.37	1136.72	1141.07	1097.23
1	-4.88	-3.16	693.07	695.75	698.42	701.09	674.16
0.5	-1.63	-1.05	231.02	231.92	232.81	233.70	224.72

RHEOLOGICAL LOSSES

The rheological losses took into account are:

- concrete shrinkage,
- concrete creep phenomena due to the prestress force and to the loads
- steel' relaxation.

Each quota has been defined through the Eurocode formulations, shown in detail belong.

SHRINKAGE

The negative shrinkage deformation ε_{cs} is function of the situ humidity and of the average radius $h_0=2A_c/u$; for this reason, it is defined as sum of two parts:

- drying shrinkage deformation ε_{cd} which is function of the water migration from harden concrete; it develops slowly;

$$\varepsilon_{cd,\infty} = k_h \varepsilon_{c0}$$

$$\beta_{ds}(t - t_s) = \frac{t - t_s}{(t - t_s) + 0.04h_0^{3/2}}$$

$$\varepsilon_{cd}(t) = \varepsilon_{cd,\infty} \beta_{ds}(t - t_s)$$

- autogenous quota ε_{ca} , which develops in the first days after poured.

$$\varepsilon_{ca,\infty} = 2.5(f_{ck} - 10)10^{-6} \text{ where } f_{ck} \text{ in MPa}$$

The relative humidity RH from which the ε_{c0} term depends has been considered equal to 70%.

1 Shrinkage	
k_h	0.95
$\varepsilon_{cd,0}$	-0.31 %o
$\varepsilon_{cd,\infty}$	-0.295 %o
$\varepsilon_{ca,\infty}$	-0.056 %o
$\varepsilon_{c,sh,\infty}$	-0.351 %o
t	14600 days
t_s	28 days
h_0	119.7 mm
$\beta_{ds}(t-t_s)$	1.00
$\varepsilon_{c,sh,0}$	-0.349 %o
$\Delta\sigma_{p,sh}$	-71.60 MPa

CREEP

Concrete creep deformation to an infinite time, $\varepsilon_{cc}(\infty; t_0)$, is due to a constant compression stress in time σ_c which has been applied at time t_0 :

$$\varepsilon_{cc}(\infty, t_0) = \varphi(\infty, t_0) \left(\frac{\sigma_c}{E_c} \right)$$

$\varphi(\infty, t_0)$ is the creep coefficient referred to the tangent elastic modulus E_c . if the compression stress σ_c at time t_0 is at least $0.45f_{ck}(t_0)$ the evaluation of the creep coefficient can take place graphically [3.1-EC2]. Those values are valid for relative humidity between 40% and 100% and temperature between -40°C and +40°C. Moreover, they are function of the concrete age when the load is applied, in days; of the conventional dimension, or average radius, h_o and of the concrete class.

RELAXATION

The relaxation loss can be defined either with experimental certificates supplied by the manufacturing or with empirical formulations. The EC2 suggests three different expression to define the ratio between the relaxation losses value and the initial stress in the tendons depending on the three relaxation classes. For this ratio it is necessary the Q_{1000} coefficient which is the relaxation losses in percentage after 1000 hours after the tendon is stretched in an environment with an average temperature of 20°C.

All the rheological prestress losses can be defined, in general, though the following expression:

$$\Delta P_{c+s+r} = A_p \Delta \sigma_{c+s+r} = A_p \frac{\varepsilon_{cs} E_p + 0.8 \Delta \sigma_{pr} + \frac{E_p}{E_{cm}} \varphi(t, t_0) \sigma_{c,QP}}{1 + \frac{E_p}{E_{cm}} \frac{A_p}{A_c} \left(1 + \frac{A_c}{I_c} z_{cp}^2\right) [1 + 0.8 \varphi(t, t_0)]}$$

CORROSION

First of all, for the definition of the real corrosion level of the beam, it is necessary to define the initiation time through the Fick's law as defined in chapter 1.

$$C_{crit} = C_s \left[1 - erf \left(\frac{x}{2\sqrt{Dt_I}} \right) \right]$$

Where t_i is the initiation time and C_{crit} is the chloride threshold that coincide with corrosion initiation. To evaluate t_i , the ratio C_{crit}/W (W =cement weight=776 kg/m²) has been taken equal to 0.6% as suggested in the Model Code. X is the distance between the bar and the closest section edge and C_s is the concentration on the surface depending on the environment, in this case it has been considered an aggressive environment, almost marine, for which the ratio $C_s/W=1.23\%$. At last, the diffusion coefficient D has been evaluated as equal to 1.13E-0.4 m²/year. Then, the initiation time results to be 15 years.

Thereafter, the Faraday's law to define the corrosion speed has been used. A current intensity of 70 mA/m² has been considered. This value is normally attributed to a marine environment, but it has been chosen because, from visual estimations, close to the supports, it seems to reach this value. Moreover, it permits to carry the big corrosion dispersion.

The corrosion velocity has been calculated using the Faraday's law.

$$V_{corr} = 1.16i_{corr} = 8.12 \frac{\mu m}{year}$$

The corrosion penetration can be evaluated in view of an initiation period of 15 years and a propagation of 35 years:

$$x(t) = V_{corr}t = 0.28 mm$$

So, the strand resisting area of the corroded element is:

$$A_s = \pi \left(\frac{\varphi_0}{2} - x(t) \right)^2 = 82.73 mm^2$$

The resisting area loss results to be equal to 10%.

CHAPTER 4: MODELLING

The definition of the model is a crucial part for the study. The purpose was to define a possible automatic method to express a prestress beam behavior through a mono dimensional model; which could be able to identify all the characteristics deriving from the prestress state and to take into account the transfer and anchorage lengths. To do so, the beam section is expressed through the M- χ diagram. Along the beam, geometry remains the same but, it changes the reinforcement design and the prestress force acting. For this reason, the M- χ diagrams have been calculated every 50 cm.

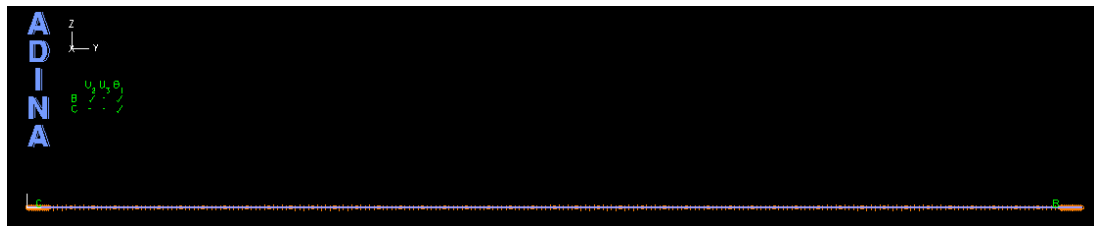


Figure 37 Adina model

The prestress force is considered in part as an acting force and in part as a resisting effect. The acting quota differs along the transfer length and due to changes in the reinforcement design. This force is meant to reduce the external actions deriving, for example, from the traffic load. The maximum value reached from this prestress portion is equal to the maximum prestress force that the element can archive.

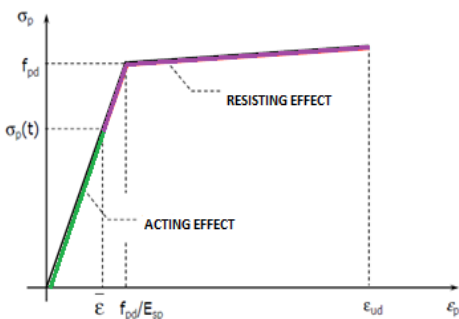


Figure 38 Prestress force acting and resisting quota

The model has been made considering only the resistant part of the σ - ε diagram, that actually means to take just the residual material properties and to consider the tendons to act like a common reinforcement. To evaluate the resistant σ - ε diagram is necessary to shift the axis origin of the tendons σ - ε diagram to the point $(\bar{\varepsilon}; \sigma_p(\bar{\varepsilon}))$; where $\bar{\varepsilon}$ is the pre-deformation and $\sigma_p(\bar{\varepsilon})$ is the tension related to it.

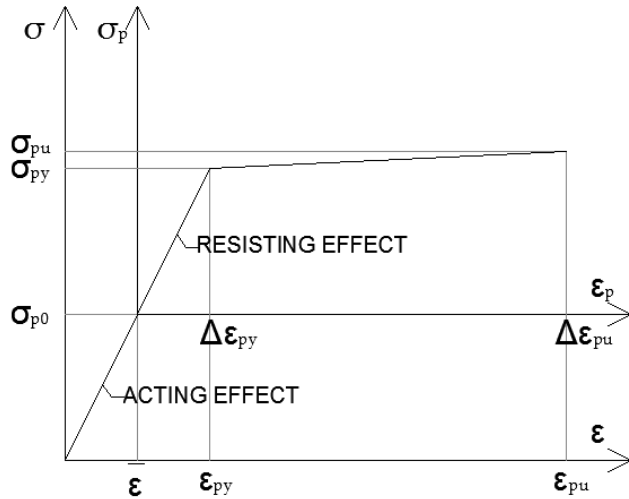


Figure 39 Resistant σ - ε diagram

Moreover, in the anchorage zone the σ - ε diagram is limited to the amount of force that the tendons can transfer indeed.

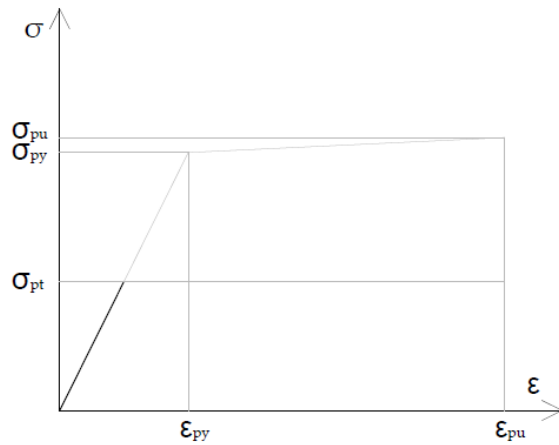


Figure 40 Tendons σ - ε diagram along the transfer length because of anchorage

EXCEL PROGRAM

Because the prestress force is considered to be divided into two parts (resisting and acting), then a section of a prestress element can be defined as a common reinforced concrete section subjected to either an axial force N and a bending moment M .

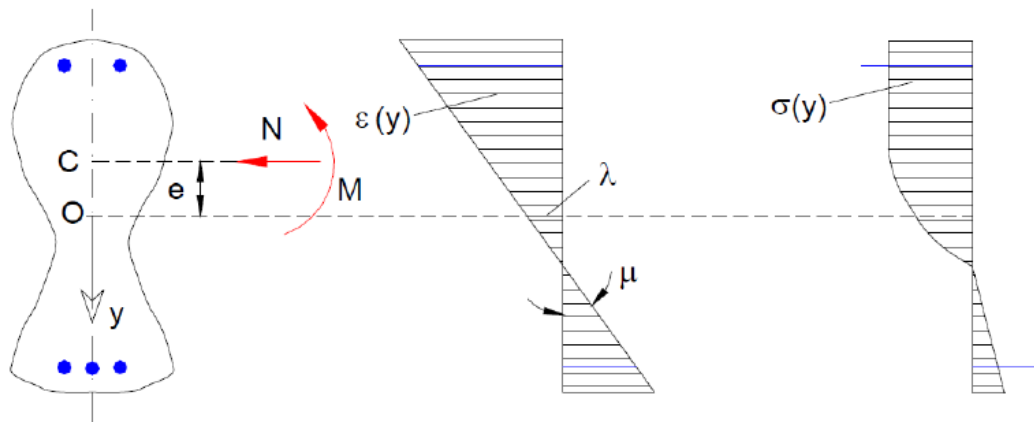


Figure 41 Generic section subjected to both axial force and bending moment

To evaluate a relation between N and M , for a given curvature χ a numerical process is used.

The relation between deformations and curvature exerts the congruence of the system:

$$\varepsilon(y) = \lambda + \chi y$$

Where λ is the barycentric deformation and χ a generic curvature.

So, stresses can be expressed as:

$$\sigma = E\varepsilon = E(\lambda + \chi y)$$

The λ value is defined iteratively imposing the equilibrium of:

$$N = \int \sigma(y)dA$$

Once λ is known, the curvature and bending moment are calculated:

$$M_R = \int \sigma(y) y dA$$

When the curvature varies even the M value changes till the calculation reaches the resisting bending moment referred to a specific acting N.

The section, symmetrical along the y axis, is divided in multiple fibers. In this way, it is possible to evaluate the forces by way of summations and not by integrals.

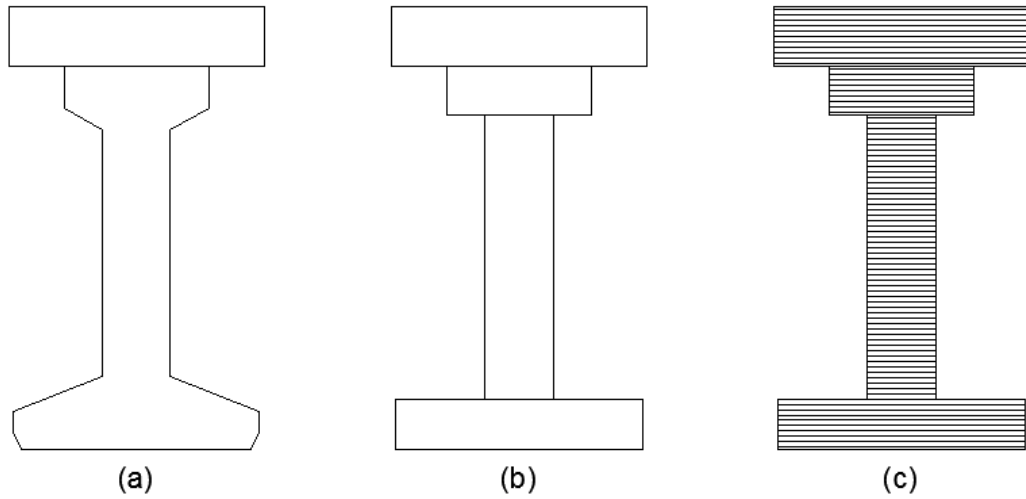


Figure 42 Intermediate beam cross section: (a) real, (b) approximated and (c) approximated and divided in fibers

So, it is possible to define the deformation of the generic fiber:

$$\varepsilon_i = \lambda + \chi y_i$$

The stress is $\sigma_i = \sigma(\varepsilon_i)$

The integral, that guarantees the equilibrium, becomes a summation:

$$N_R = \sum_{i=1}^n \sigma_i b_i h_i + \sum_{j=1}^m A_{s,j} \sigma_{s,j}$$

The second part is related to the m reinforcement fibers.

At this point, it is possible to evaluate M:

$$M_R = \sum_{i=1}^n \sigma_i b_i h_i y_i + \sum_{j=1}^m A_{s,j} \sigma_{s,j} y_i$$

In other words, starting from N and χ values, an early λ value is hypothesized so, the first iteration can be launched, from which some N_R and M_R values are obtained. Iterations stop when the difference between N (input) and N_R is less than a certain tolerance value.

The program's script is assembled by 5 sheets:

- Section 1: in this part the input data is defined, like geometry, reinforcement and their position, and so on.
- Section 2: in this part there is a definition of the fiber model though N_{stri} which is the number of subdivisions (the default value is 100). Furthermore, it is described the variability range of χ and λ .
- Section 3: in this sheet the concrete formulations are defined to evaluate the stresses in function of the deformations. It is possible to choose between two models of the σ - ϵ diagram: parabola rectangle or Sargin's law.
- Section 4: in this sheet the steel σ - ϵ diagram is defined as a bilinear diagram because $f_y=f_u$ and equal either in tension or compression.
- Section 5: in this part the calculation system is defined for N_R and M_R knowing the λ and χ values.

FIRST IMPROVEMENT: DIFFERENT CONSTITUTIVE LAW FOR THE SUPERIOR AND INFERIOR TENDONS

Each beam cross section is subjected to an axial force which provokes the origin of a bending moment. This M_p is caused from the eccentricity of the application point of N in relation to the section' center of gravity. Moreover, in this case, it is due to the fact that the majority of the section reinforcement is located in the bottom part.

So, it is possible to consider the bottom reinforcement though an equivalent bottom tendon $\varphi_{\text{equ},B}$ and the upper ones though another equivalent tendon $\varphi_{\text{equ},U}$.

It is clear that, because of the acting bending moment, the stress in $\varphi_{\text{equ},B}$ is different from the $\varphi_{\text{equ},U}$ ones. For this reason, the program has been modified to consider two different resisting σ - ε diagrams referred to the bottom and upper reinforcement.

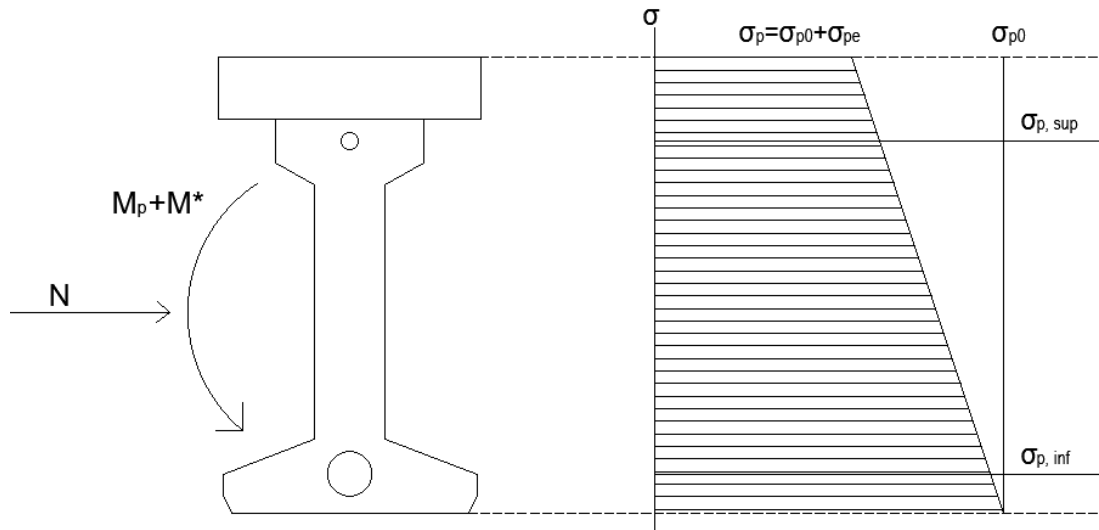


Figure 43 Stresses on a general section

Practically, in Section 4 two σ - ε diagrams are defined to characterize the bottom (sigacc) and upper (sigacccsup) reinforcement.

Referring to Narm which is the number of reinforcement levels from the bottom to the top, in Section 5 the evaluation of N and M uses sigacc from 1 to Narm-1 and sigacccsup for Narm; which is the last reinforcement level that is equal to the only upper reinforcement level of this section.

SECOND IMPROVEMENT: DIFFERENT TENSION STATE FOR TENDONS WHICH PROVOKES REINFORCEMENT DESIGN CHANGES

The beam, along its longitudinal development, present 3 different reinforcement designs:

- From the support to 3 m there are 19 tendons
- From 3 m to 6 m there are 22 tendons
- From 6 m to midspan there are 25 tendons

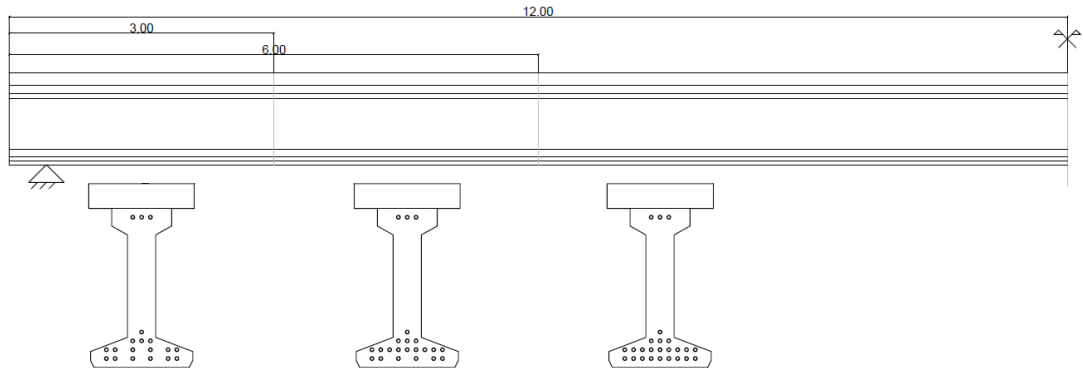


Figure 44 Beam's longitudinal development and cross sections

Initially, where new tendons are set they are not able to immediately transfer the final prestress force because of the anchorage, that is not totally performed, and there even is a linear increase of the prestress force along the transfer length.

For these reasons, the “new tendons” result to have a σ - ε diagram limited by the value of force that they can actually transfer. This happens to be true just in the first sections, where the transfer is small. In fact, excluding those sections, the “new tendons” show greater resisting characteristics than the “old” ones; because the acting force is smaller in them, so the resisting part is bigger. This situation can be translated through a more extended σ - ε diagram.

To consider this contribution, another improvement has been made to the Excel program. The old reinforcement is evaluated through Narm levels, on the other hand, the new reinforcements are defined by Narm1 which is a new fibers system, characterized by number of levels, steel area and σ - ε diagram independently to Narm.

So, as already defined, in Section 5 the evaluation of N and M uses sigacc from 1 to Narm-1 and sigaccsup for Narm, plus sigacc1 for Narm1.

ADINA MODEL

The mono dimensional model is composed by beam elements characterized through the moment-curvature diagram, in function, not just of the axial force, but even of a bending moment M^* .

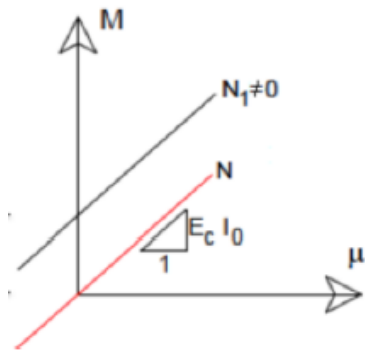


Figure 45 Translation of a generic linear $M-\chi$ diagram because of an axial force

This bending moment depends by the axial force because it is the moment related to a null curvature in presence of a high axial force, just like in a common prestressed structure.

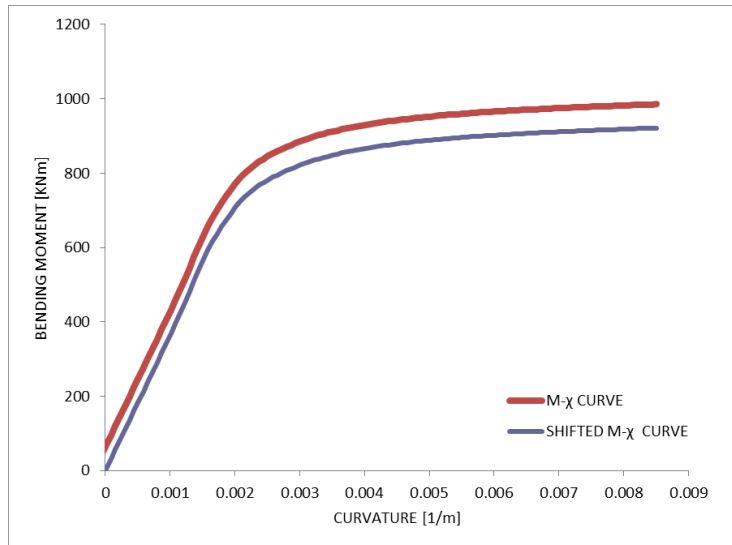


Figure 46 Example of the $M-\chi$ curves

Different $M-\chi$ diagrams are plotted into the FEM program, shifted of the M^* "factor" to make them pass throughout the axis origin. The shift is a rigid shift along the ordinate axis, so the shifted curve donates the same curvature of the unshifted one, but for an acting bending moment equal to the actual bending moment plus M^* .

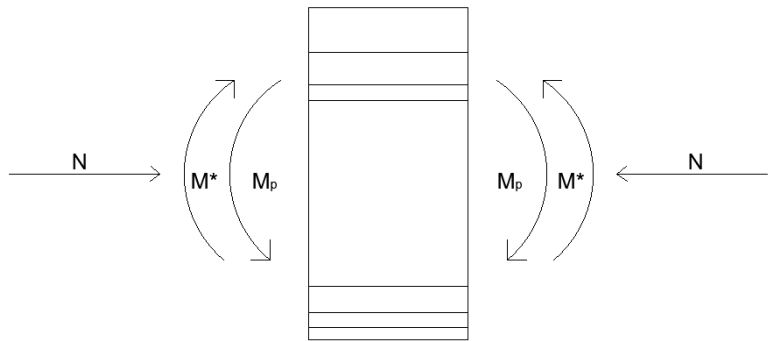


Figure 47 Generic loaded element

Moreover, a variable axial force has been modeled along the transfer and anchorage length and in function of the different reinforcement design along the beam's span. Corrosion scenarios have been modeled as a loss of the prestressing force which causes a reduction of the $M-\chi$ diagram. The loss of prestress is due to a loss of the tendons resisting cross section. Furthermore, a reduction of the bond

proportional to the tendons cross section loss has been taken in to account. The bond decrease provokes a variation of the transfer length.

The analysis is characterized by 3 different time steps which describe the following time function:

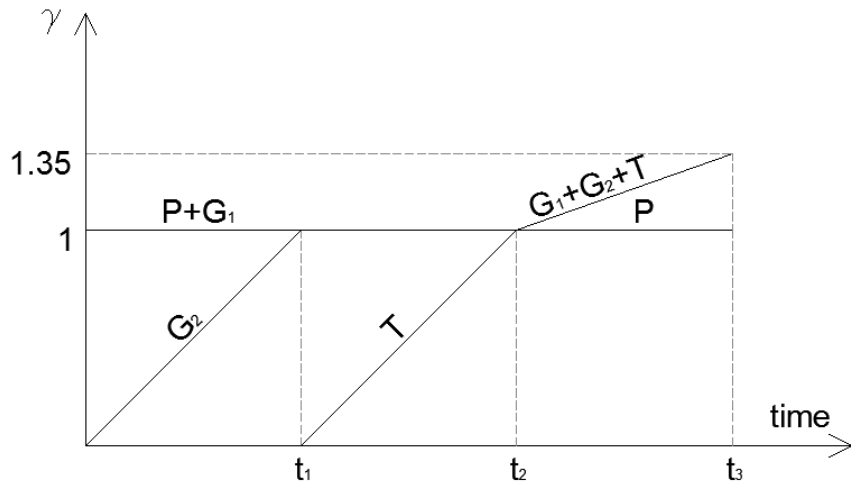


Figure 48 Time function

- from t_0 to t_1 , the forces acting on the model are the prestress force and dead loads.
- from t_1 to t_2 , the permanent loads are added to the model.
- from t_2 to t_3 , in addition to the previous ones, the traffic load is added, and they are all combined with the partial coefficient suggested by the Eurocode 2 which is equal to 1.35, excluding the prestress force.

CHAPTER 5: NUMERICAL ANALYSIS

Different scenarios have been considered to evaluate how the beams reacts under different load set ups and corrosion states. In particular, for each corrosion scenario, even the resisting characteristics are taken into account.

The comparison of the different configurations has been made in terms of a difference Δ between the actions and the resisting properties. In other words, the biggest is the gap between action and resistance, the greater the security level is.

TRAFFIC LOAD MOVEMENT

The traffic load is a moving load so to better evaluate every possible situation the tandem system is been placed in different positions which are:

- Midspan
- A quarter of the span
- An eighth of the span
- 1.5 meters from the left support
- In the middle of the 19φ part after the prestress is transferred
- In the middle of the 22φ part after the prestress is transferred

Moreover, the load has been considered both with no security coefficient and with security coefficient as expected in the Eurocode 2 (paragraph 6.8.3). The partial coefficient is equal to 1.35 and multiplies the permanent loads and the traffic actions, instead the prestress force has a coefficient equal to 1.

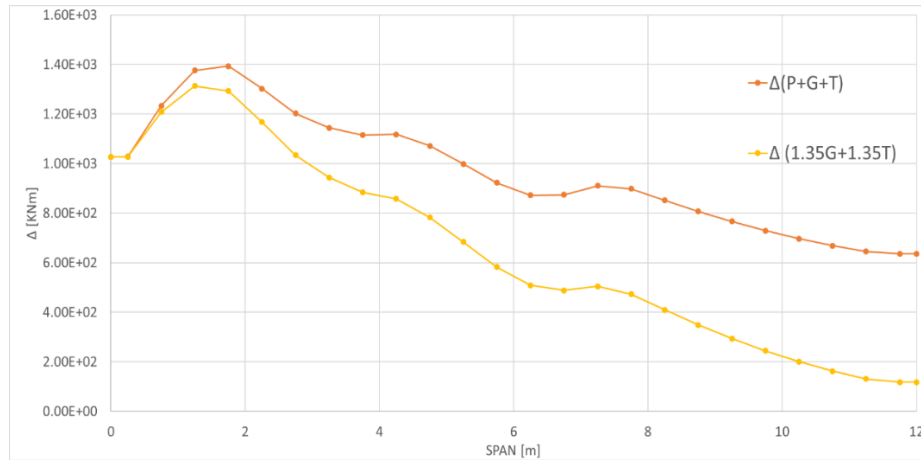
Shown below, the results deriving from SCENARIO0 model (no corrosion) and the traffic load in the midspan with and without partial coefficient. The analysis is divided in different time functions which simulate the various loads entrances. In the graph, there are 3 separate times:

1. prestress and dead loads,
2. prestress, dead loads and permanent loads

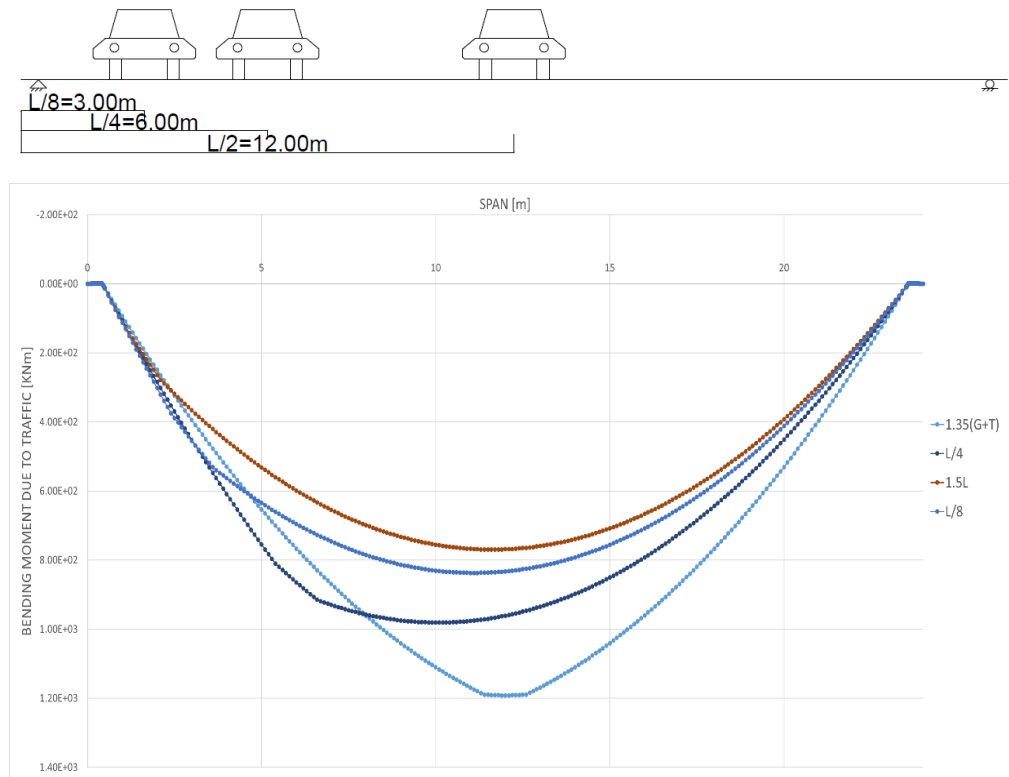
3. prestress, dead loads, permanent loads and traffic load, using the partial coefficients.

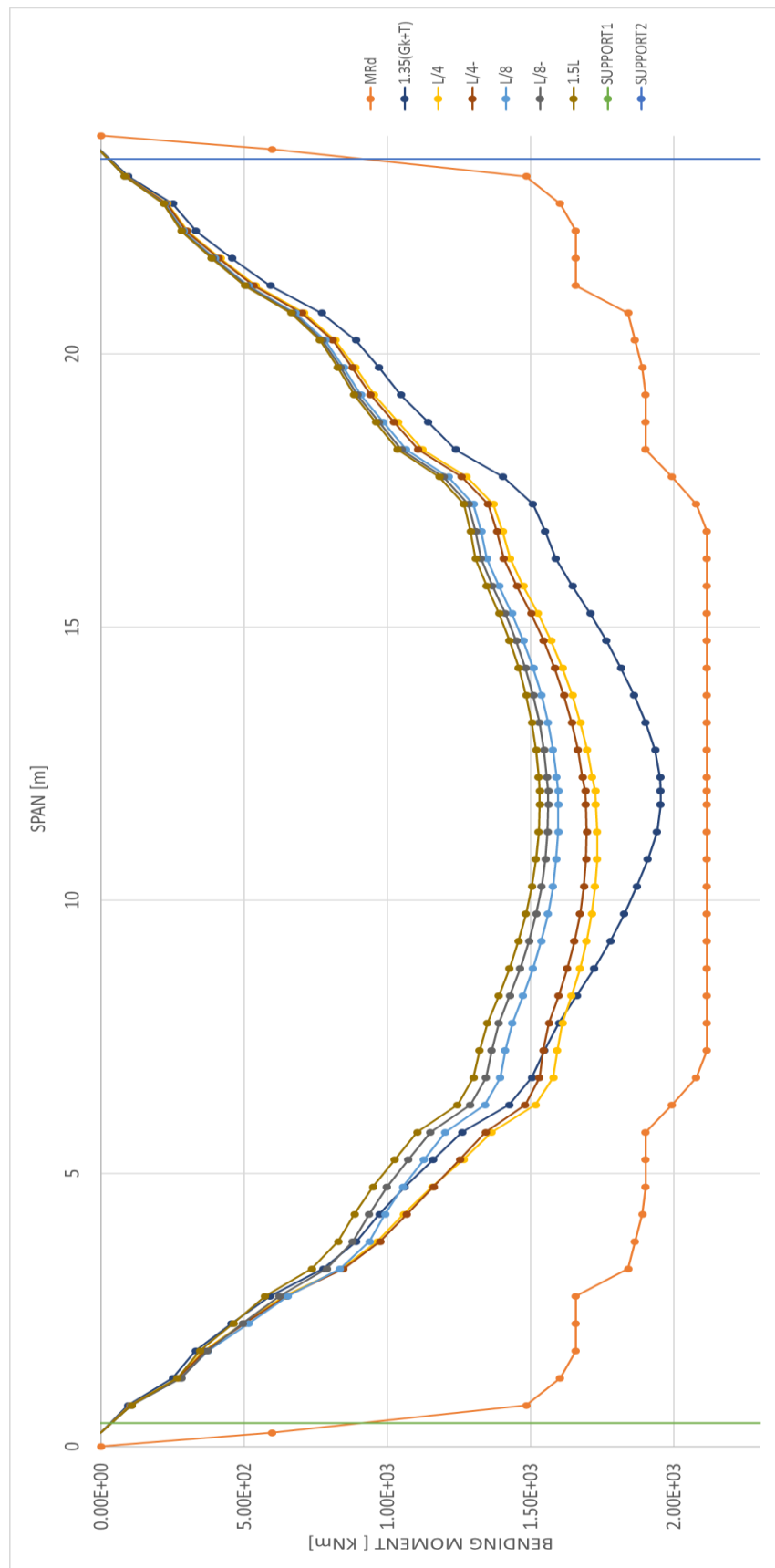
If the difference between the actions and resisting part is represented in a diagram, then it is easy to identify how the security coefficient, which is the delta itself, changes through the span:

$$\Delta(F) = M_R - M_E$$



If the traffic loads move from midspan to the left the bending moment diagram changes.





The Δ is big near the supports, so for this configuration it can be said that the worst situation is when the tandem system is in the midspan position.

CORROSION VARIATION

Corrosion is introduced through the change of two important parameters:

- loss of the tendons' cross section, which produce less prestress in the sections corroded and less resistance.
- loss of steel-concrete bond, which affects the prestress transmission length because it increases the transfer and the anchorage.

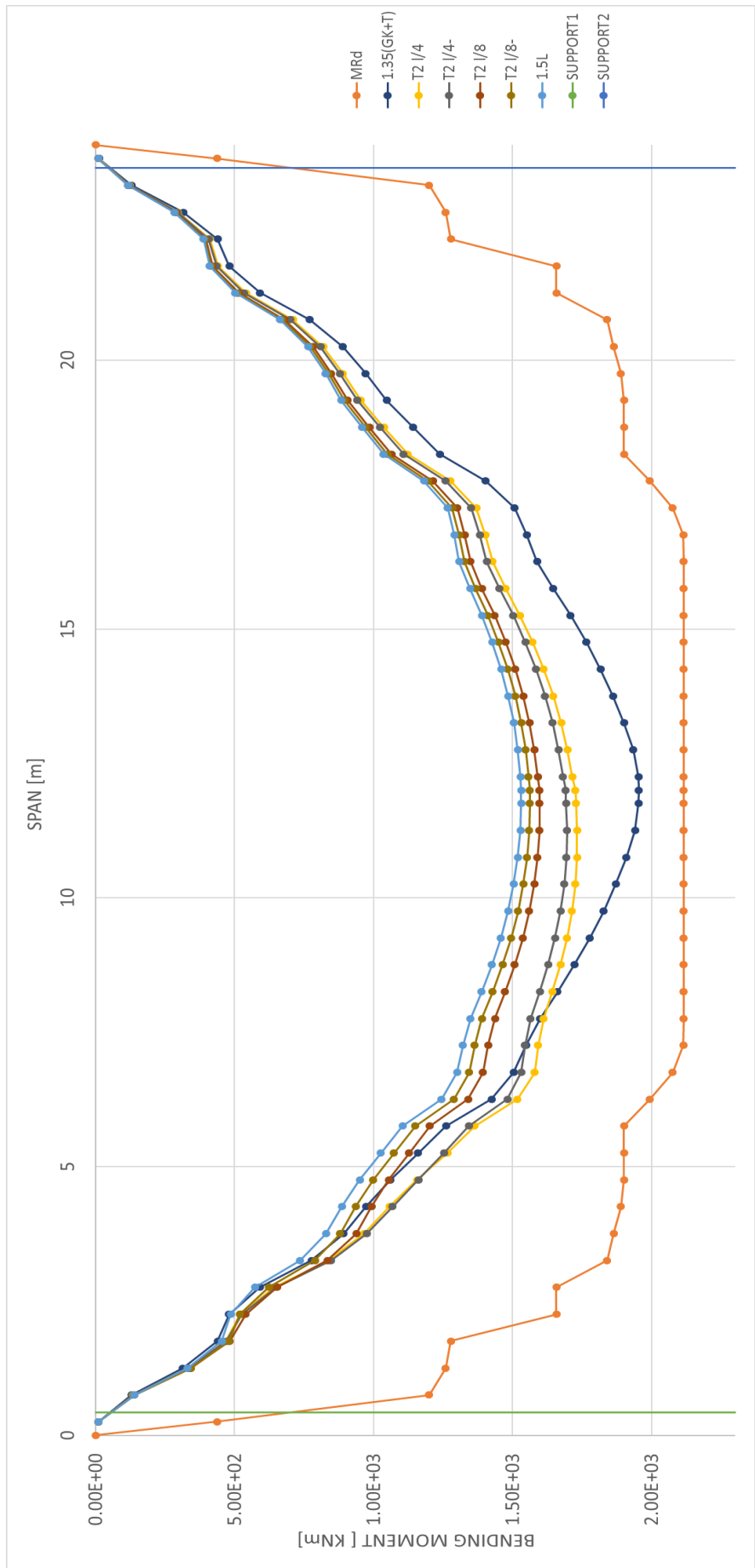
Moreover, in SCENARIO6 a variation of the material properties has been considered as a modification of the σ - ϵ diagram as defined previously.

In the last scenario, it has been considered a 20% loss of the prestress force not considering any loss of section and bond.

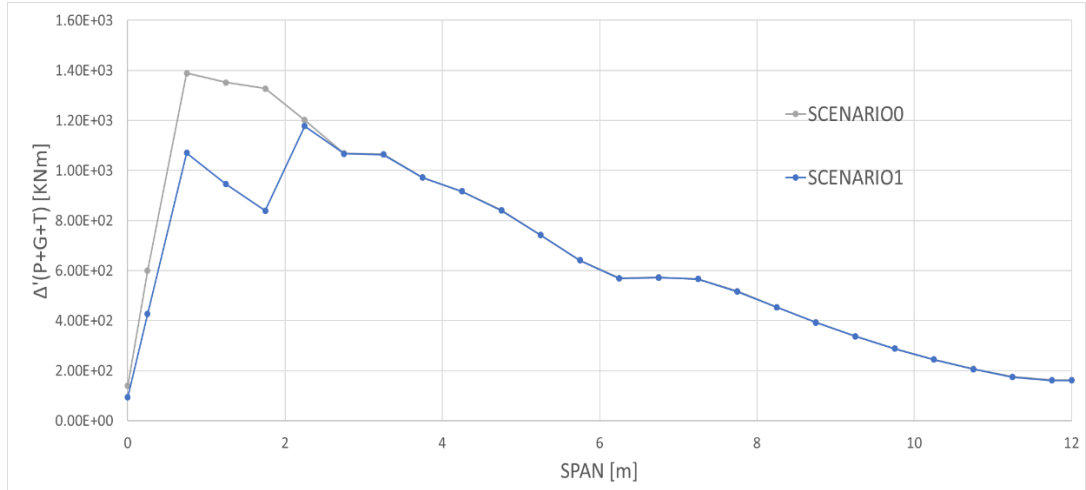
SCENARIO	
0	NO CORROSION
1	$Q_{CORR}=20\%$ UNIFORMLY FOR THE FIRST 2 m
2	$Q_{CORR}=20\%$ IN THE BOTTOM PART FOR THE FIRST 2 m
3	$Q_{CORR}=20\%$ UNIFORMLY FOR THE ENTIRE SPAN
4	$Q_{CORR}=10\%$ UNIFORMLY FOR THE ENTIRE SPAN
5	$Q_{CORR}=20\%$ UNIFORMLY FOR THE FIRST 2 m + $Q_{CORR}=10\%$ UNIFORMLY FOR THE REMAINING SPAN
6	$Q_{CORR}=10\%$ UNIFORMLY FOR THE ENTIRE SPAN CONSIDERING THE MATERIAL PROPERTIES
7	20% LOSS OF P

SCENARIO1

Corrosion in this scenario is concentrated in the first 2 meters from the supports, symmetrically, considering a reduction of all the tendons' cross section of 20%. This hypothesis derives from visual considerations about the real deck's state, that results to be particularly deteriorated in some parts, as shown in the next chapter.



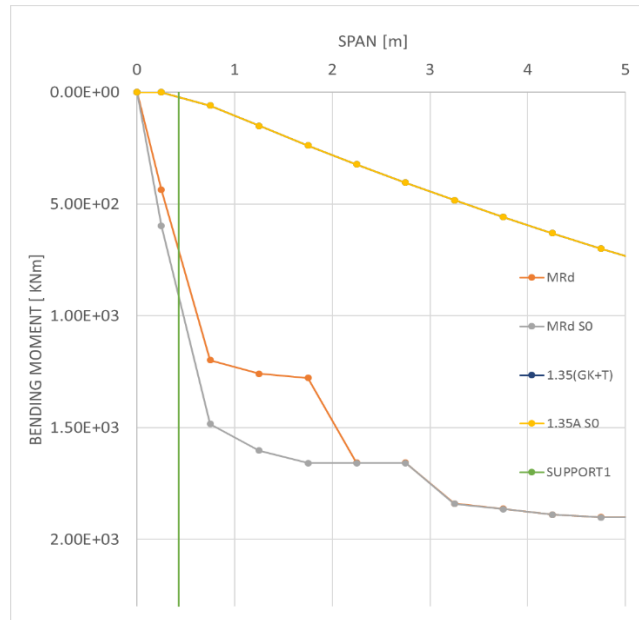
So, the delta can be compared with the ones from SCENARIO0.



It is clear a reduction of the delta due to corrosion which means a reduction of security of about 33%.

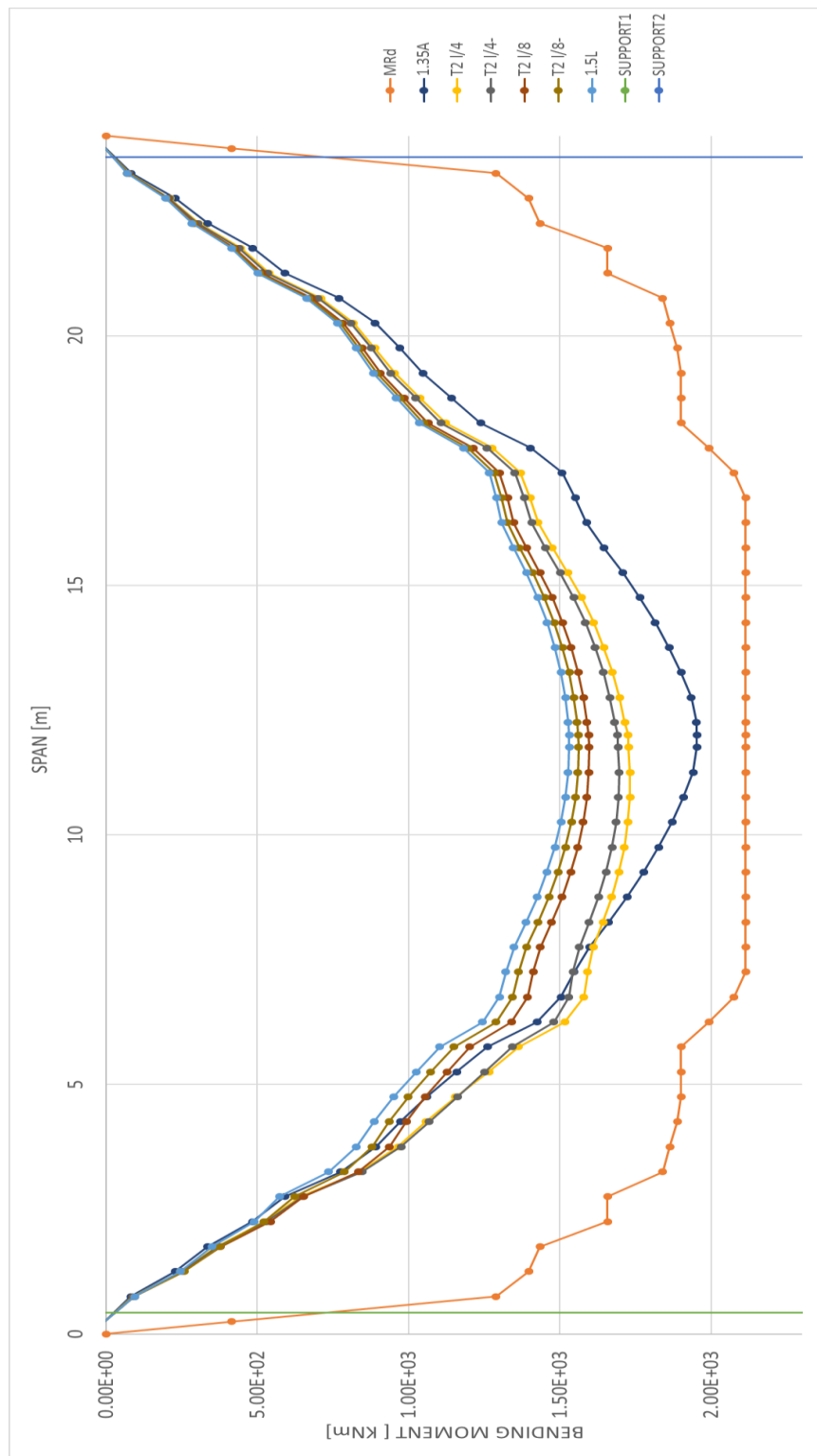
DISTANCE FROM THE SUPPORT [m]		0	0.25	0.75	1.25	1.75	2.25
Δ'	CORR	9.41E+01	4.27E+02	1.07E+03	9.46E+02	8.39E+02	1.18E+03
	NO CORR	1.40E+02	6.00E+02	1.59E+03	1.47E+03	1.33E+03	1.20E+03
		33%	29%	33%	35%	37%	2%

In conclusion, the appearance of corrosion provokes a reduction of resistance.

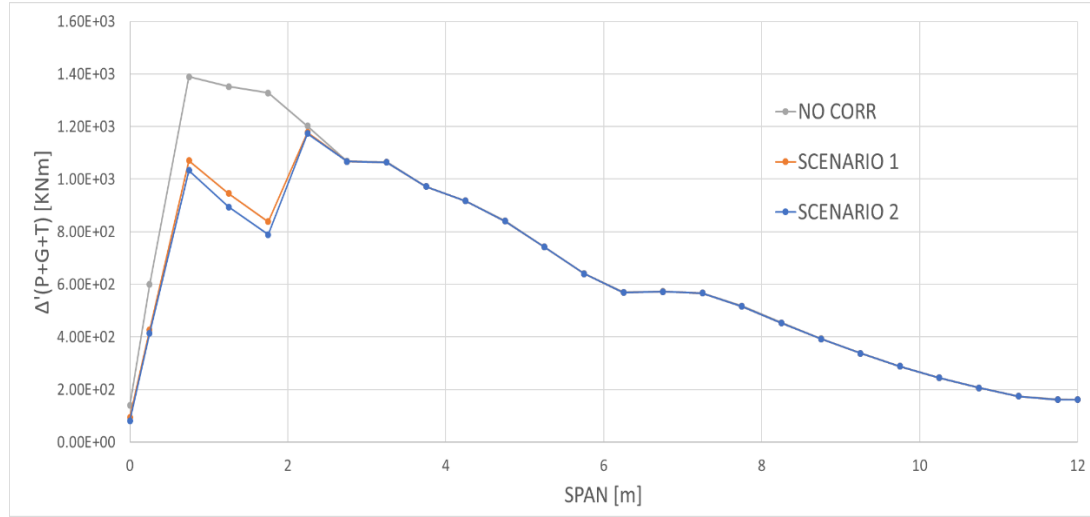


SCENARIO2

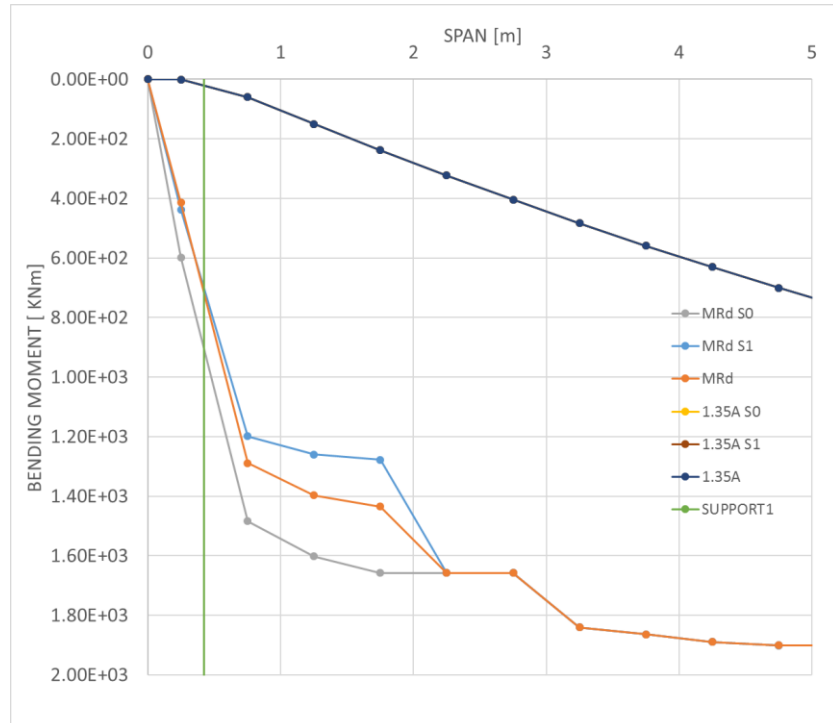
Corrosion in this scenario, just like the previous one, is concentrated in the first 2 meters from the supports, symmetrically. In this configuration the steel cross-section loss is concentrated in the bottom part of the entire section.



At this point, the delta can be compared with the ones from SCENARIO0 and SCENARIO1.



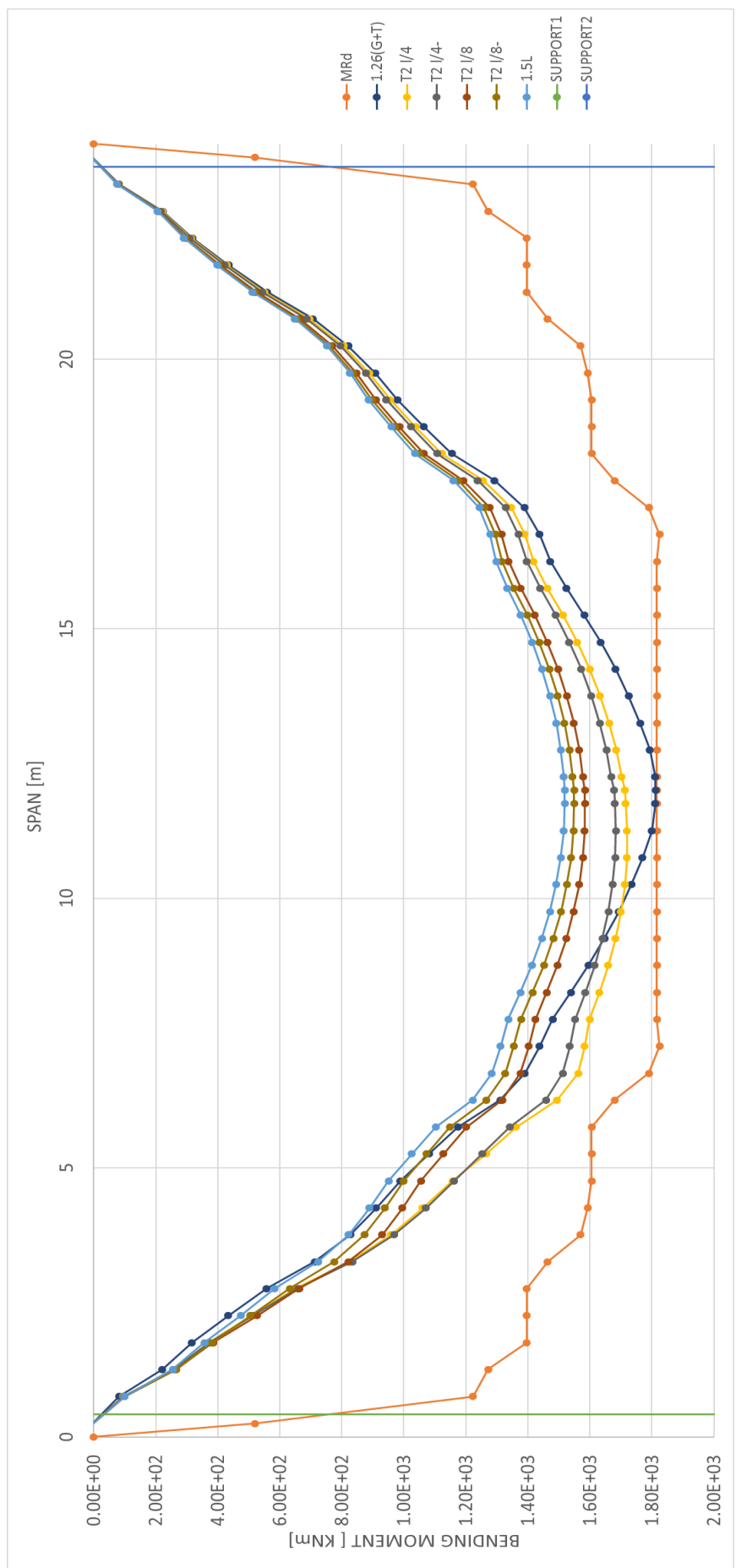
The difference between SCENARIO1 and SCENARIO2 results to be negligible, in fact the two curves almost coincides. The reason appears to be that the majority of the tendons are located in the bottom of the section, so it can be said that the lower tendons are the ones that influence the beam's behavior. Even on the resistance point there is a reduction that results to be close to the one already seen in SCENARIO1.



SCENARIO3

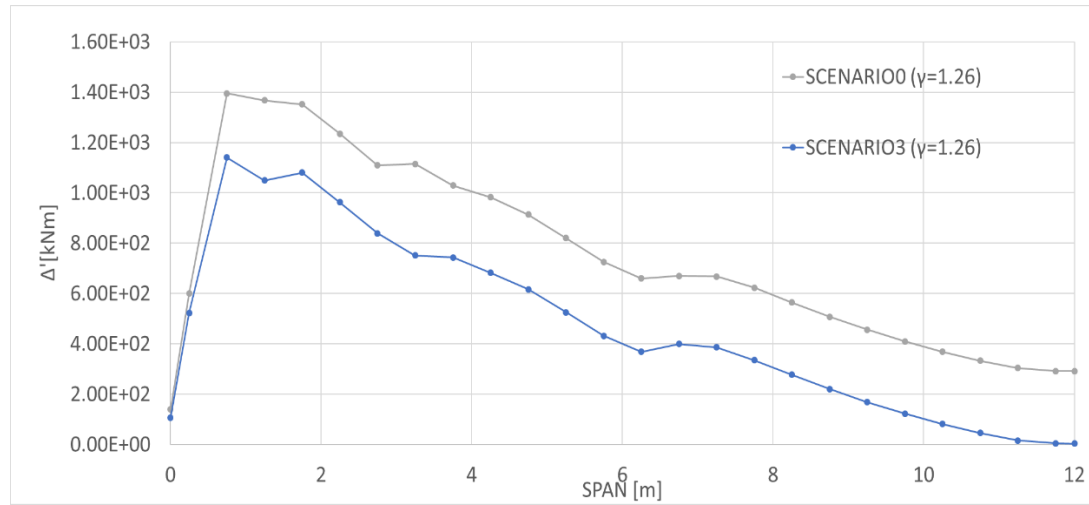
Corrosion is uniformly distributed along the entire beam span with a cross section reduction of 20%.

In this configuration the reduction of the resisting part is so intense that the actions do not arrive to perform the EC2 force combination using the partial coefficient equal to 1.35. The analysis is set to reach the 1.35 value at time 3, but, for example for the tandem system in midspan position, it stops at time 2.75 in which the coefficient reaches a value of 1.26. The analysis goes further moving the tandem system toward one of the supports and it does reach the 1.35 value.



The delta, even in this case, can be related with the ones from SCENARIO0, but it is not a real comparison because in this scenario the 1.35 coefficient has not been reached.

To have a cleaner view of the different behavior it is necessary to compare this situation with the not corroded one using a partial coefficient equal to the minimum reached in this scenario.



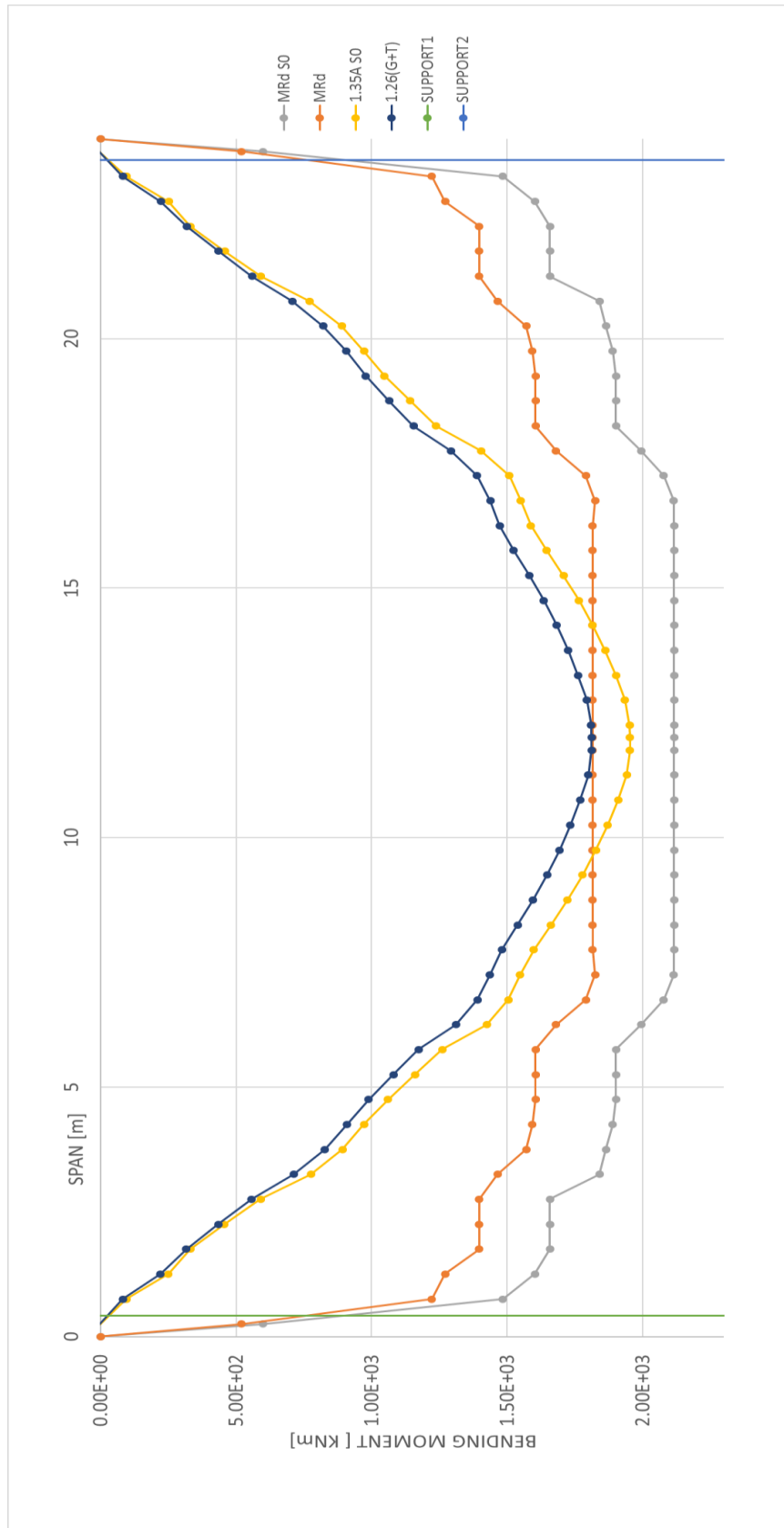
When corrosion is extended at the whole beam the reduction of the security level is clear, as shown in the following chart.

DISTANCE FROM THE SUPPORT [m]		0	2.25	4.75	7.25	9.75	12
Δ'	CORR	107.38	962.88	616.91	420.54	122.75	4.25
	NO CORR	139.56	1235.46	913.44	689.39	409.87	291.45
		23%	22%	32%	39%	70%	99%

The midspan delta of the corroded configuration does not go to zero because the analysis reaches the ultimate time step and cannot calculate further because it collapses in the next time step.

From the comparison between this setting and SCENARIO0, it is clear that the ultimate state of the corroded beam is reached because of two main reasons, that

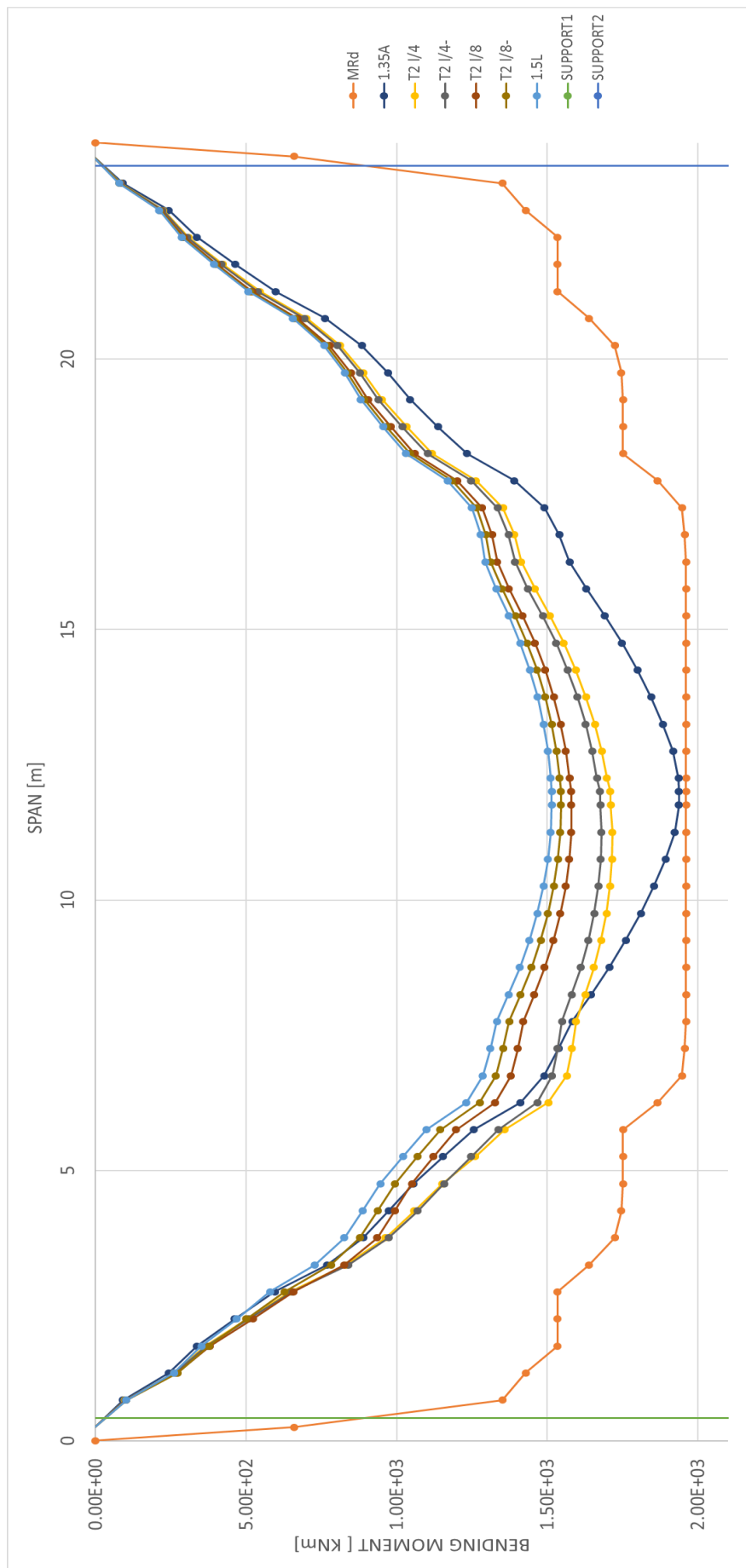
are a minor resisting property and a significant loss of the prestress force which makes the structure to be not able to resist larger forces.



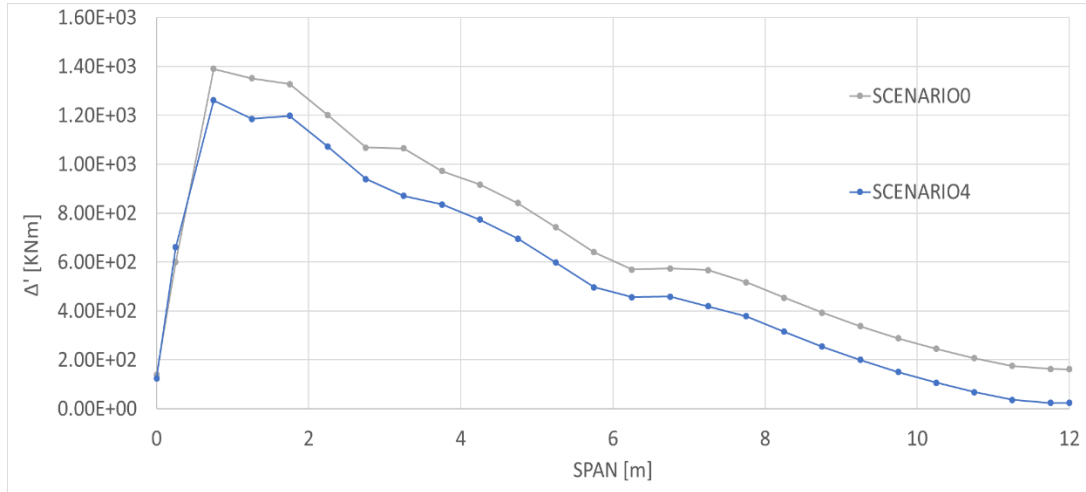
SCENARIO4

This scenario derives from considerations about the real corrosion state as defined in the previous chapter. For this reason, corrosion is uniformly distributed along the entire beam span with a cross section reduction of 10%.

Again, the reduction of the resisting part is so intense that the actions do not arrive to perform the EC2 force combination using the partial coefficient equal to 1.35. The analysis is set to reach the 1.35 value at time 3 and it is able to reach the coefficient for every load position, but when the load is in the midspan position, it is close to the maximum resistance. For this reason, this scenario can be considered as a limit case.



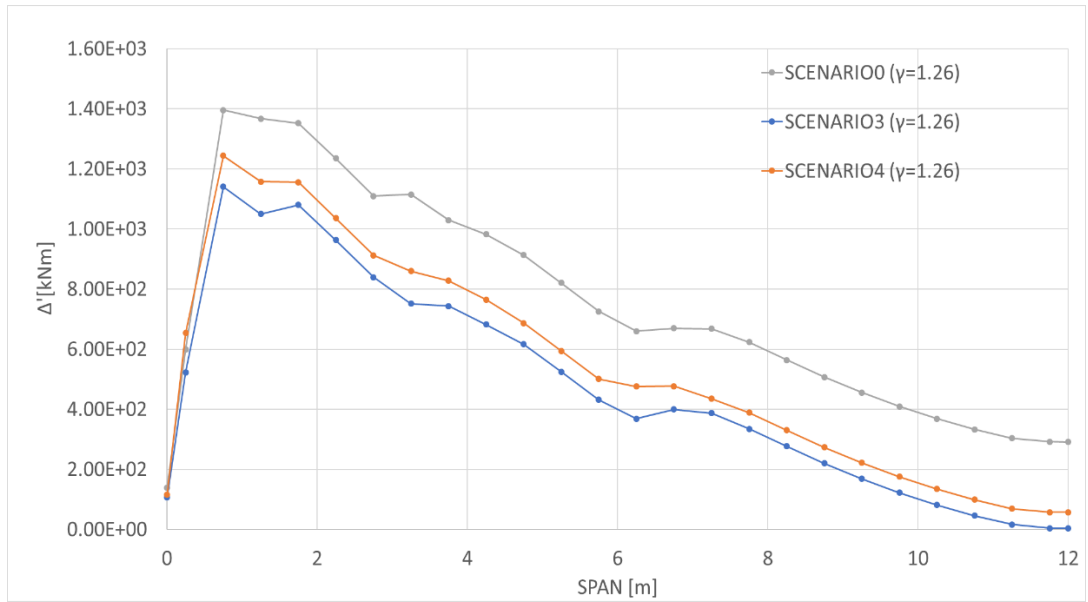
The delta, related to the load in the midspan position, can be compared with the ones from SCENARIO0.



Once again, there is a reduction of the Δ security. In particular, it highlights the big reduction in the midspan position.

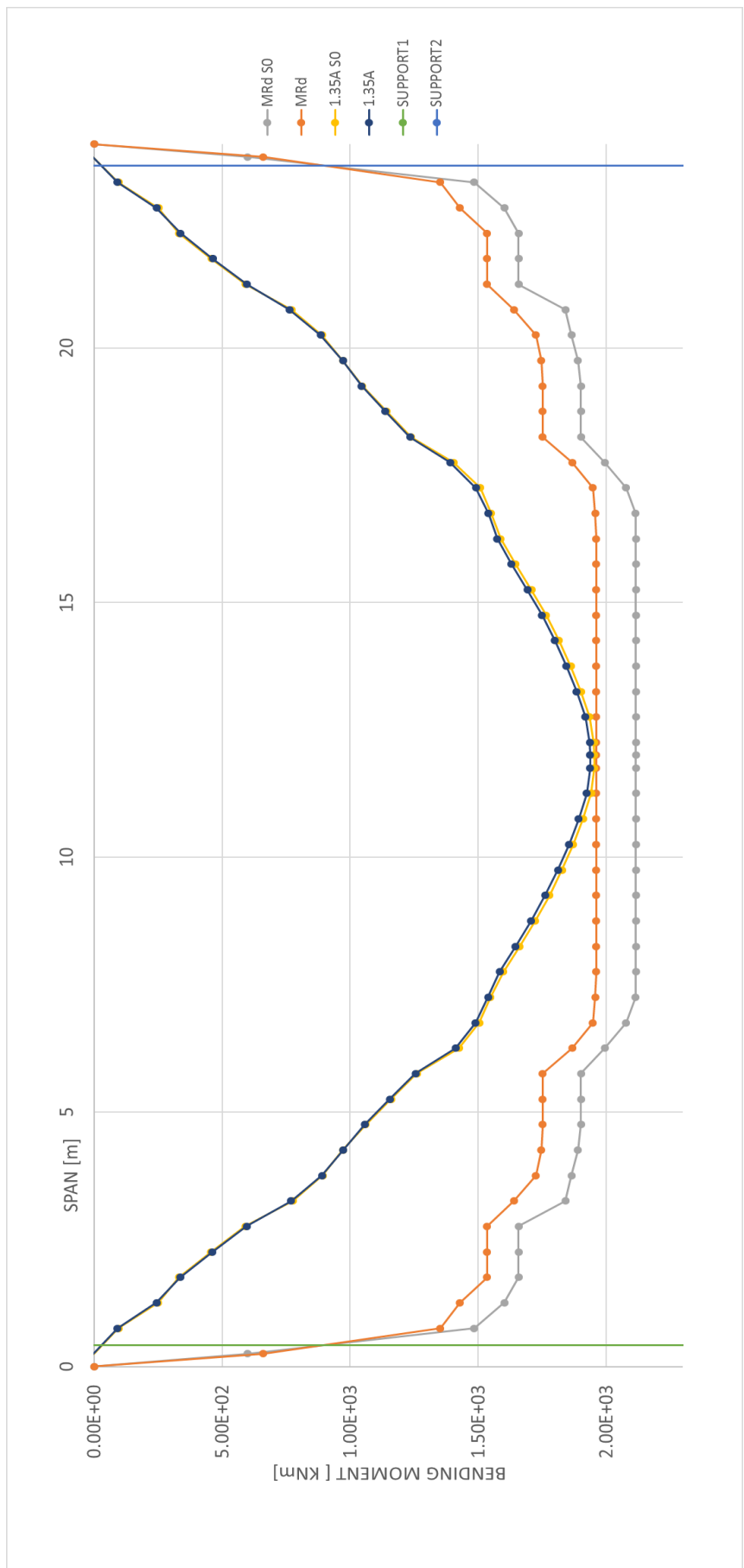
DISTANCE FROM THE SUPPORT [m]		0	2.25	4.75	7.25	9.75	12
Δ'	CORR	123.9	1072.1	696.2	463.7	150.3	23.7
	NO CORR	139.6	1201.8	841.3	587.9	288.6	162.0
		11%	11%	17%	21%	48%	85%

Moreover, to better compare this scenario with SCENARIO3 and SCENARIO0, the results have to be related to the same partial coefficient. This coefficient must be the minimum reached from the different configurations. For this reason, the following results are related to a partial coefficient equal to 1.26 as it results from SCENARIO3.



It is shown that the delta security level decreases with the increase of corrosion, as expected.

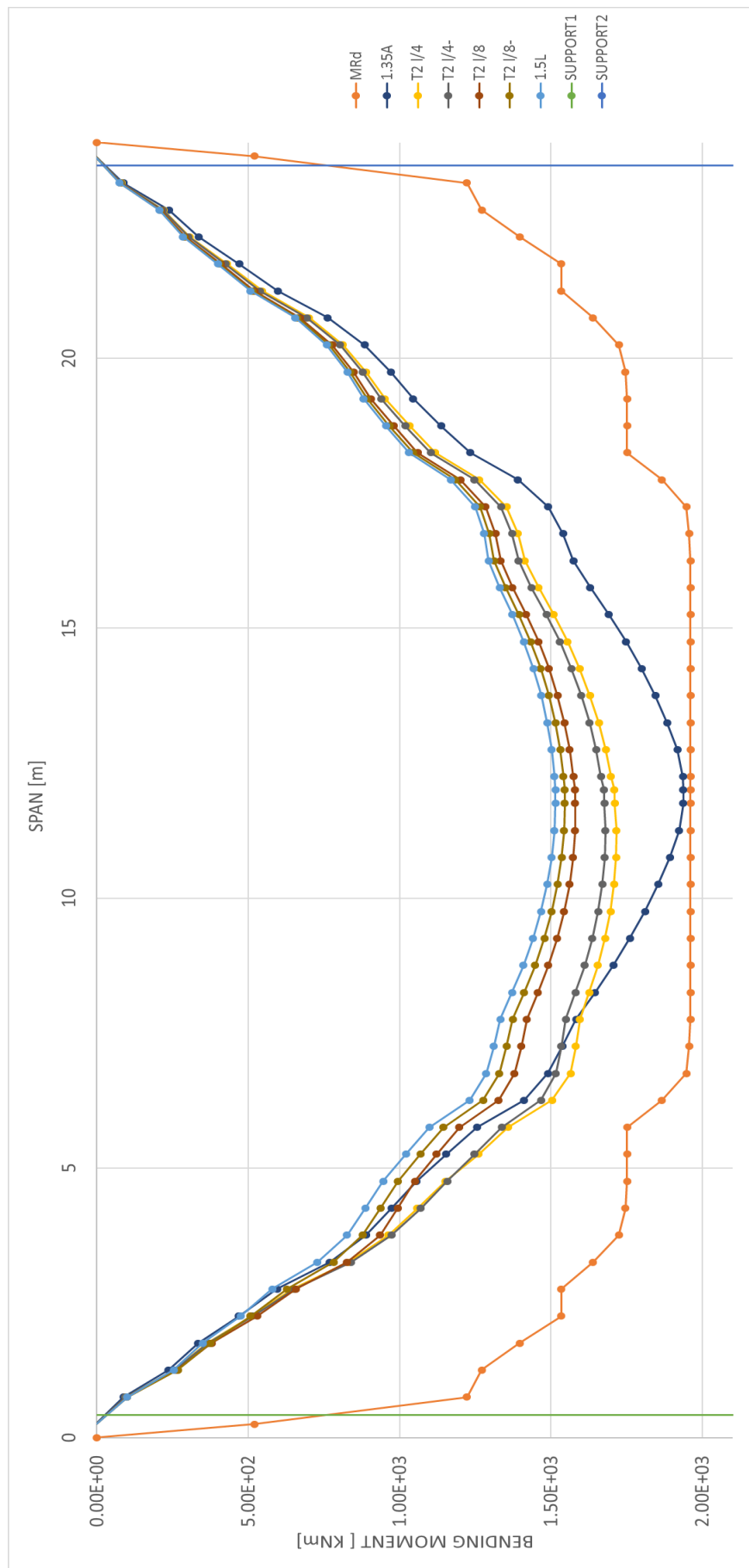
Analogizing this arrangement with SCENARIO0, the same situation of the previous scenario can be found, to wit there is a loss of both resistance and an increase of actions due to a loss of the prestress force.



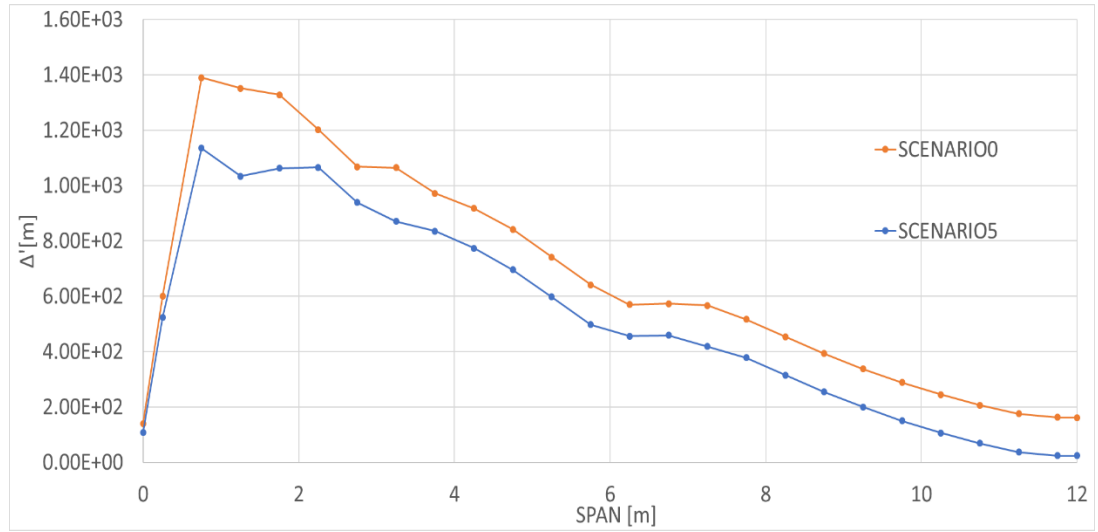
SCENARIO5

This scenario is a mix of SCENARIO3 and SCENARIO4, in fact, corrosion is uniformly distributed along the entire beam span with a cross section reduction of 10% except for the first 2 meters from the supports in which the reduction is equal to 20%. This situation is the one that could be closer to the real beam's state. Even though the real corrosion state result to be analytically equal to 10%, many beams, from visual inspection, appear to be more corroded because characterized by wide cracks.

As it results in SCENARIO4, even in this case the acting bending moment for the traffic load in midspan position is close to reach the resisting value.

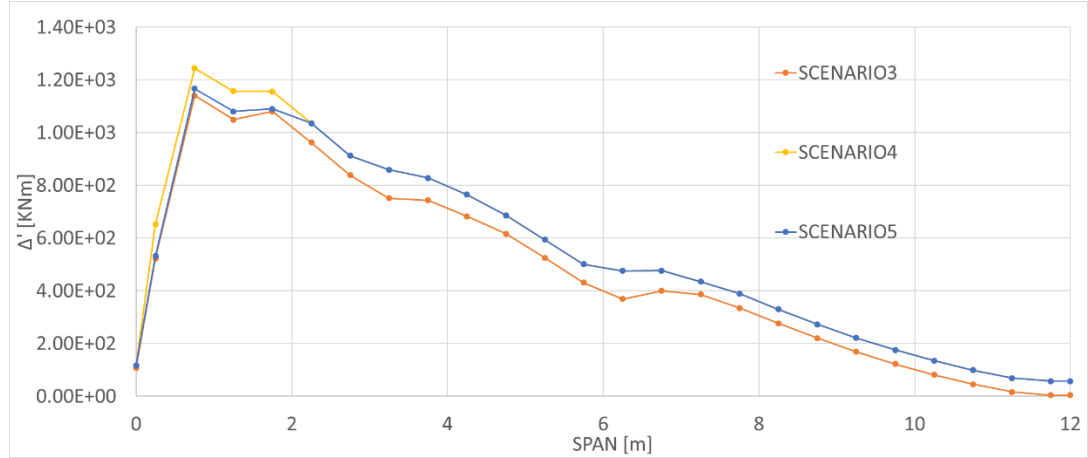


As expected, comparing the Δ with the one from SCENARIO0 is evident that the reduction is wider in the first 2 meters from support.

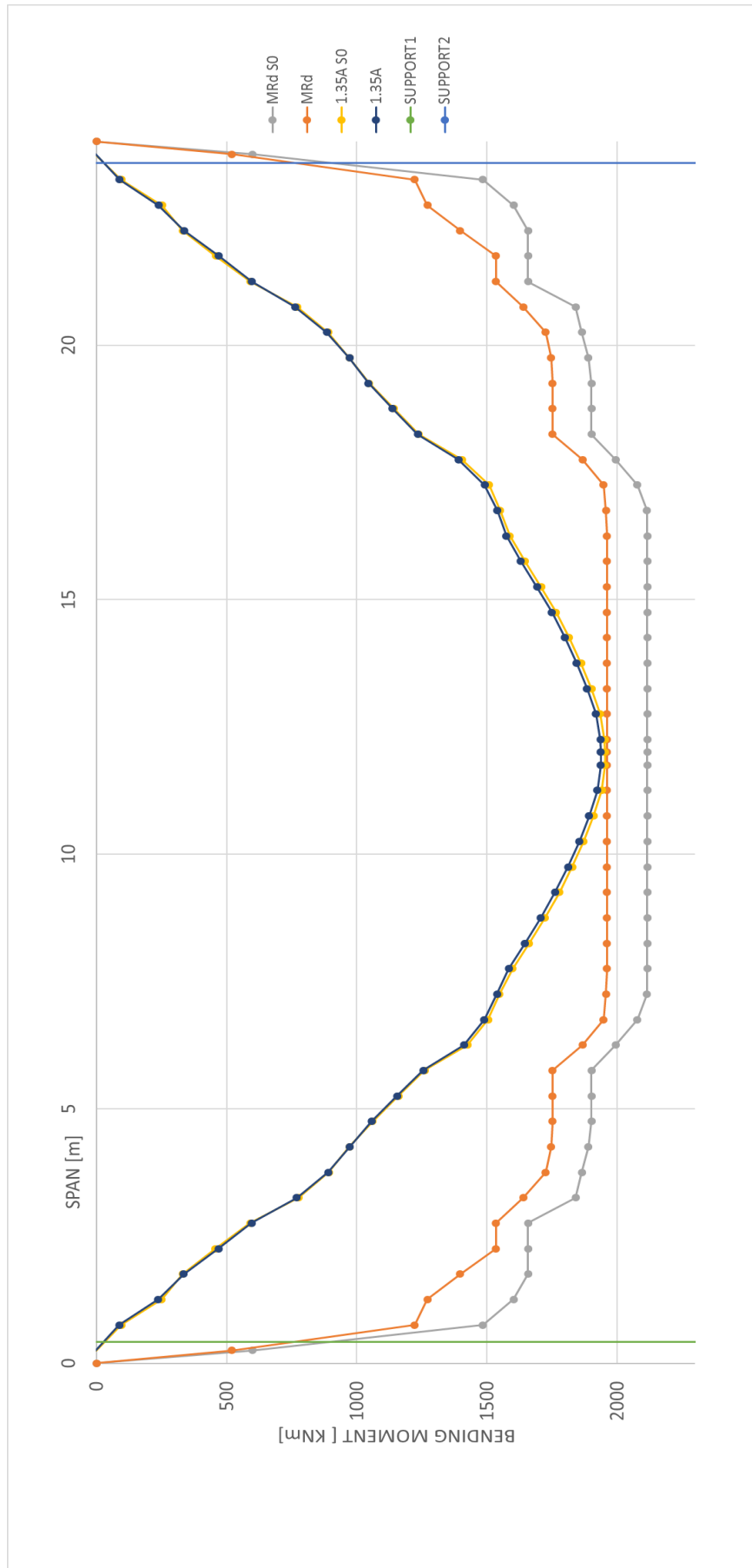


Accurately, if this setting is correlated to SCENARIO3 and SCENARIO4 it is visible that the behavior is closer to the one from SCENARIO4.

Once again it is more appropriate to compare the results deriving from two configurations in which the same partial coefficient is used.



Because the midspan behavior is driven by the element with a tendon cross section loss of 10%, the ultimate state is reached for a value of the partial coefficient close to the one of SCENARIO4.

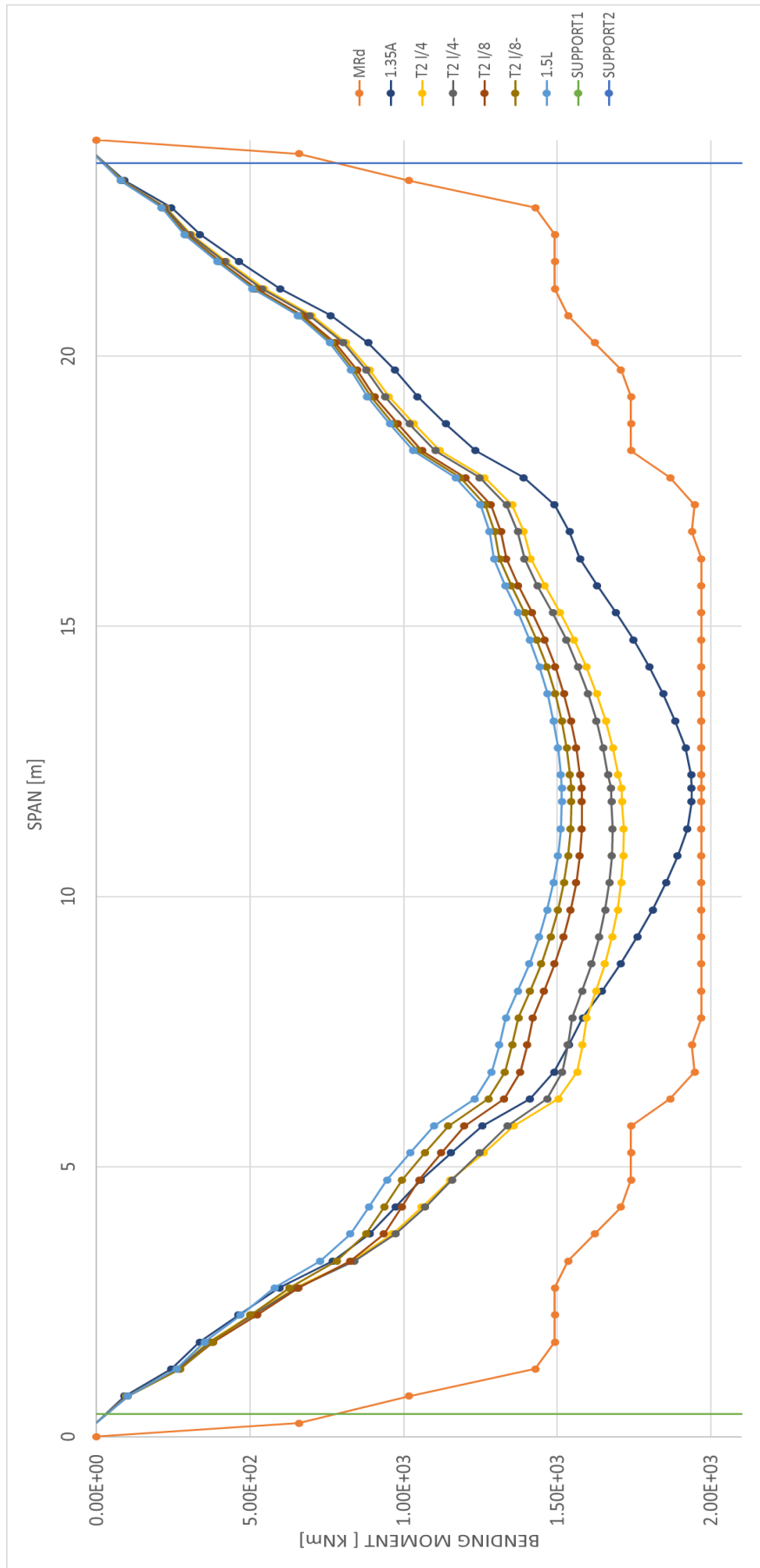


SCENARIO6

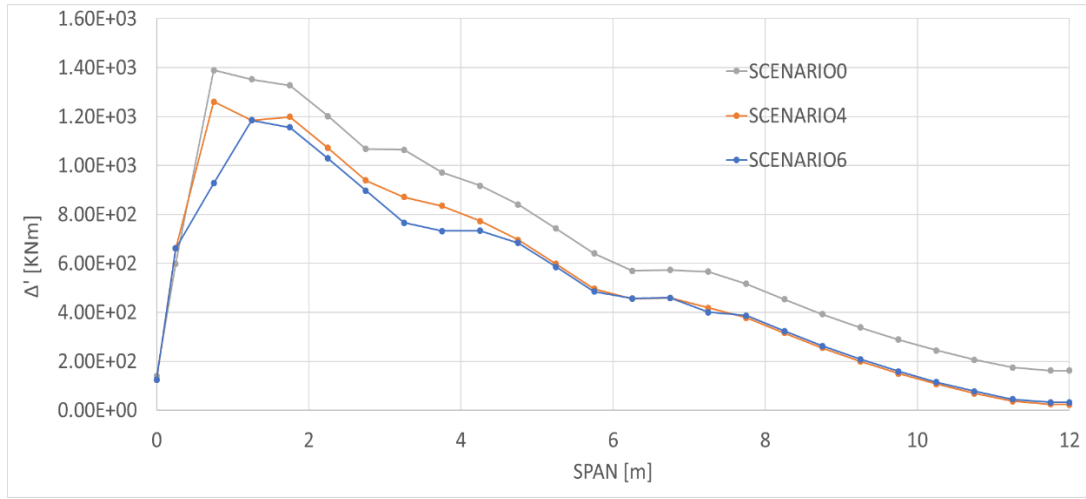
Regarding the real corrosion state analyzed in SCENARIO4, in this case a further improvement has been considered which is the variation of the steel material properties. To do so a degradation of the σ - ϵ diagram has been performed. The diagram considered is dependent on the corrosion loss, in fact, it changes with increasing the corrosion loss, as suggested in (LeiWang, 2017) and discussed in chapter 2.

So, the new constitutive law is:

f_{pu}	1308.601	MPa	ϵ_{pu}	8.71	%o
f_{py}	1285.81	MPa	ϵ_{py}	6.43	%o



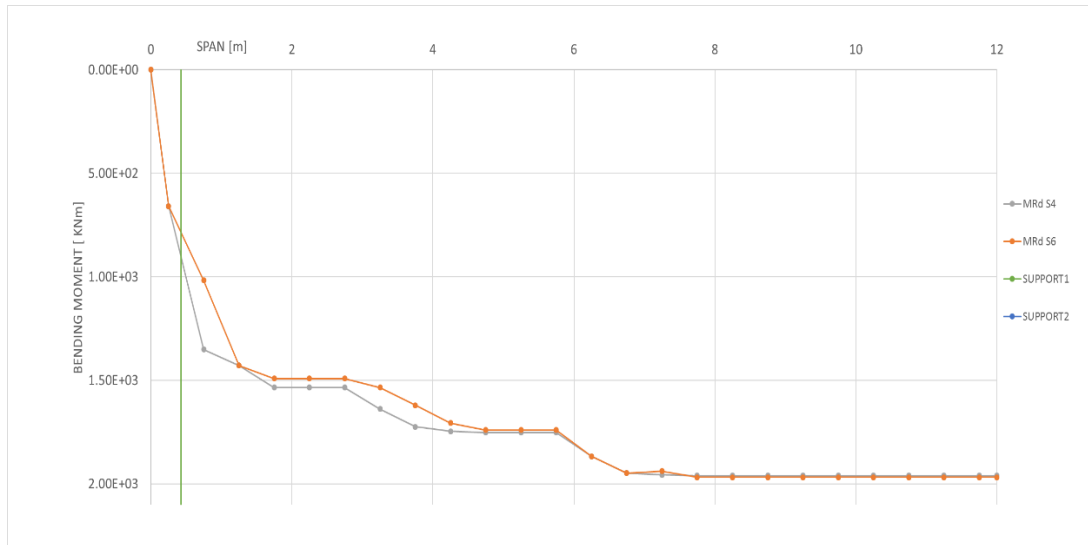
The Δ , related to the load in the midspan position, can be compared to both SCENARIO0 and SCENARIO4.



From the comparison, the variation in the Δ value between SCENARIO4 and SCENARIO6 is more evident close to the supports; where there is a reduction of the Δ , in opposition, moving toward the midspan the coefficient result to increase compared to SCENARIO4.

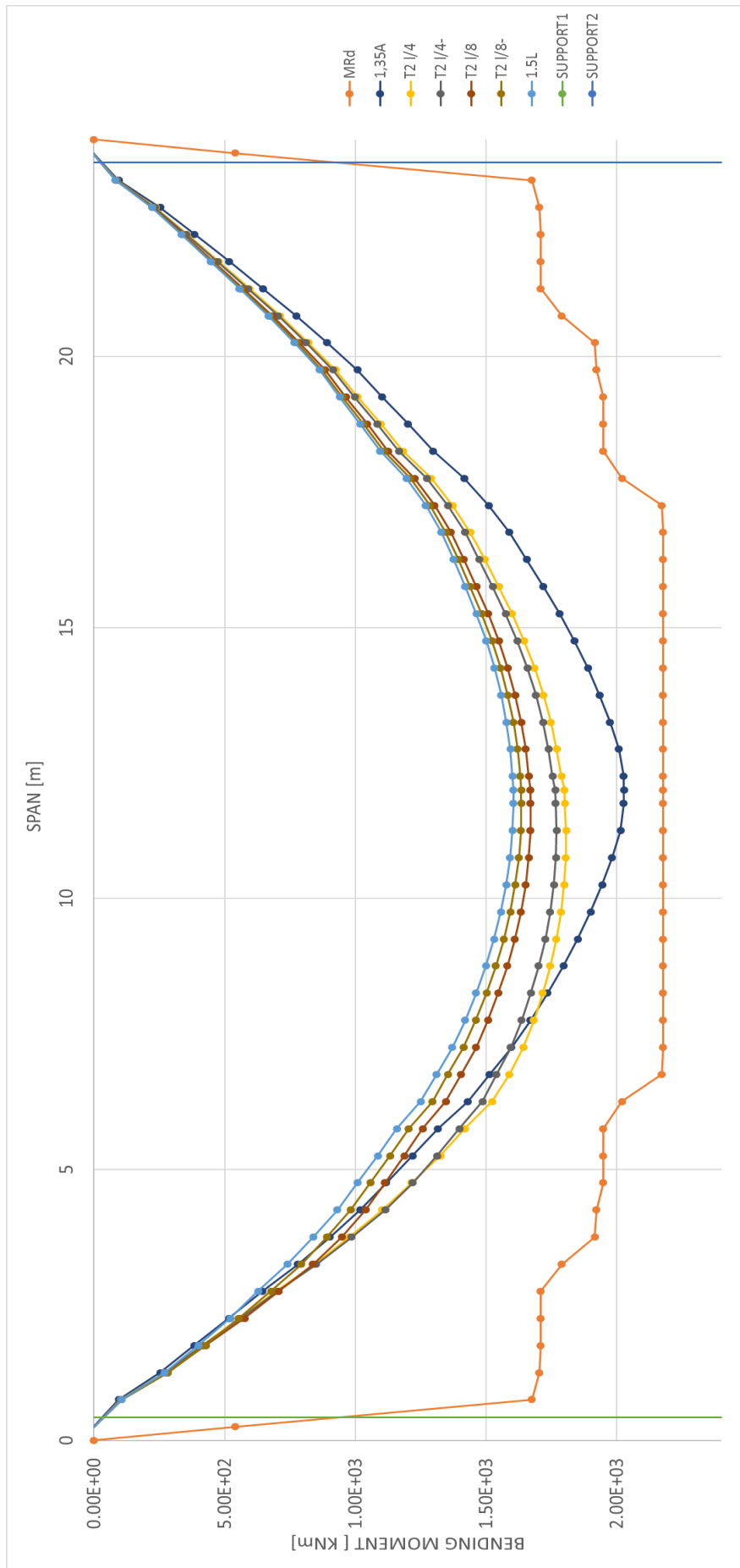
DISTANCE FROM THE SUPPORT [m]		0.75	2.25	4.75	7.25	9.75	12
Δ'	S5	927.3	1029.6	684.2	400.3	158.9	32.2
	S4	1260.7	1072.1	696.2	418.9	150.3	23.7
		-36%	-4%	-2%	-5%	5%	26%

This situation is due essentially to the resistance and not to the acting force. In fact, if the resisting bending moments, related to the two scenarios, are compared the same Δ trend is found. This behavior depicts a more ductile attitude of the section with 19 tendons than the one with 25 tendons.

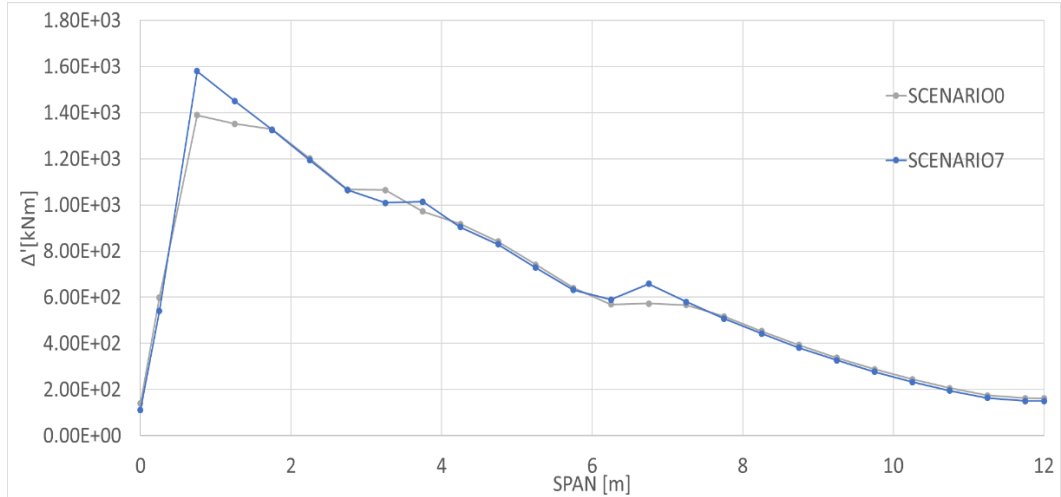


SCENARIO7

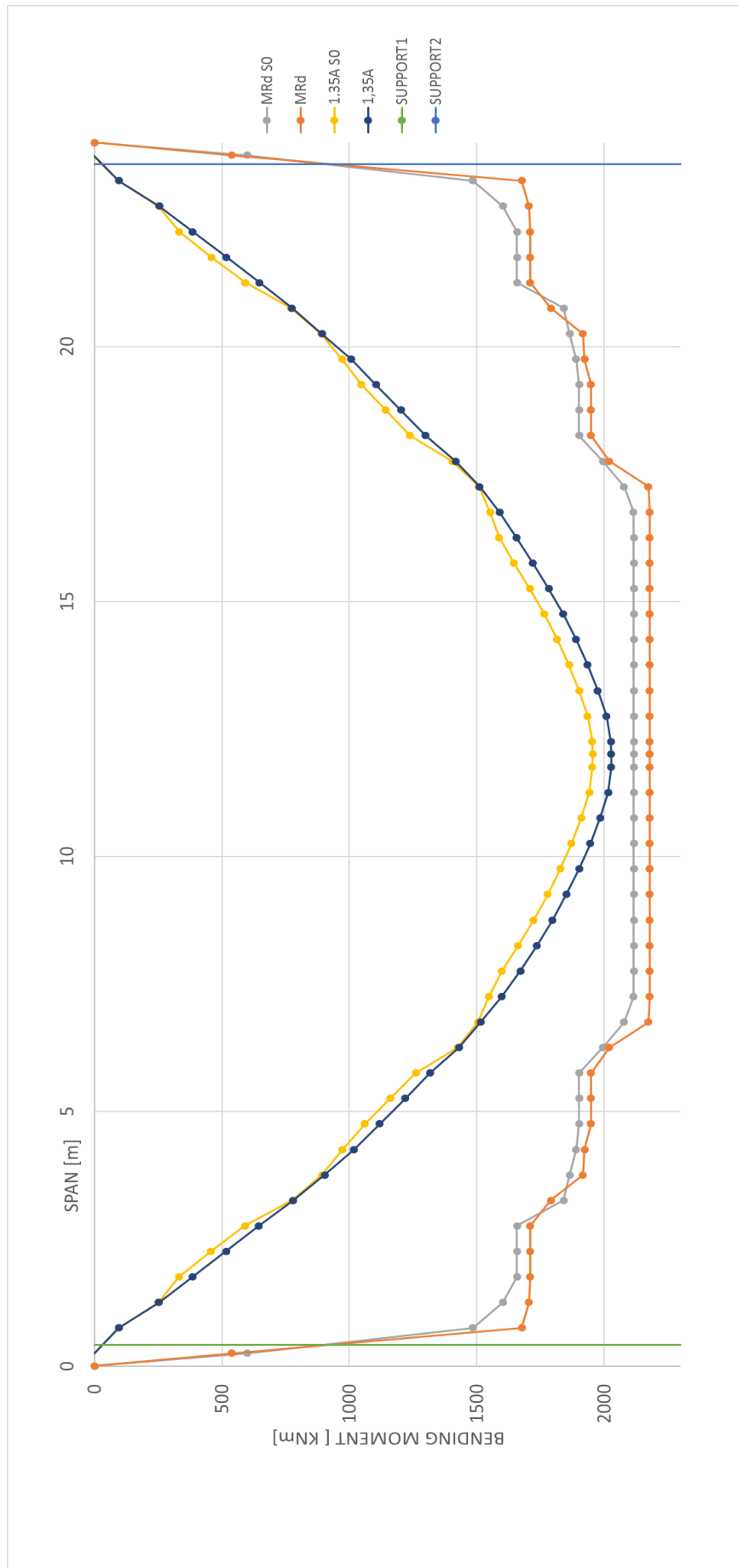
This scenario is totally different from the previous ones, because no tendons' cross section loss and bond loss is been hypnotized but the analysis is done on the intact element with a 20% loss of the prestress force.



Considering just a loss of the prestress force on the element which remains intact does not produce a sensitive reduction of the security coefficient; in fact, the reduction is negligible.

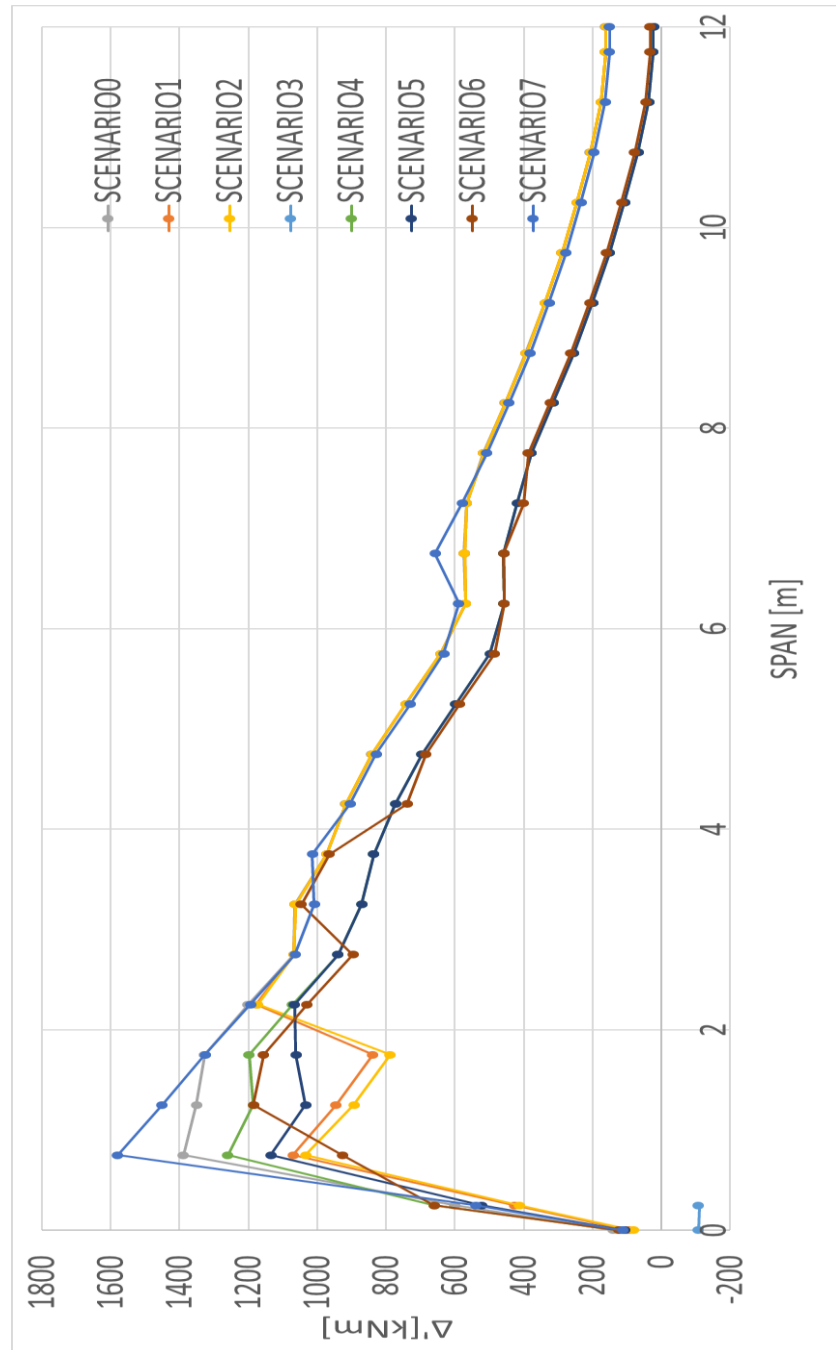


The difference Δ between the resistance and the actions does not change because a reduction of the prestress force brings a proportional increase of both the resistance and actions. This situation is clear comparing this scenario with SCENARIO0.



At this point, it can be said that the Δ is a measure of the security margin of the structure because it shows how much the actions are far from the resistance. Moreover, the Δ decreases with the increase of the corrosion state but it does not change much if it is considered just a prestress loss.

Theoretically, the critic parts are the ones near the support because it can be hypnotized that those are the first ones exposed to corrosion. Anyways, the Δ in those regions maintains high values in contrast of the midspan region.



CHAPTER 6: CONSIDERATIONS ABOUT THE REAL CORROSION STATE TRHOOUGH PICTURES

The present chapter desires to give a visual understanding of what has been said previously. The following pictures come from a visit of the site during the demolition activities.

The deck's external beams result to be the more stressed ones, as seen. Corrosion of the outermost I beam seems to be relevant so that the concrete cover is missing, as expected. In the picture the outermost beam results to have not experienced the cover spalling, but it must be highlighted that it is a U beam that have doubled the rigidity of a I beam.



Figure 49 Examples of the corroded outermost I beam

Many longitudinal cracks have been detected in the different elements. As shown in figure 48-49, the cracks are distant from the section edge an amount approximately equal to the concrete cover, so they coincide with the external tendons.



Figure 50 Longitudinal crack



Figure 51 Distance of a longitudinal crack from the edge

Up to this point everything results to follow the expectation about the corrosion propagation, in general.

The real unanticipated phenomenon is shown in the following picture, where it is an internal I beam to exhibit the greater corrosion.



Figure 52 Corrosion of an intermediate beam

This circumstance was revealed to be caused by many drainage channels broken. They are, in some points, completely missing. Because of this maintenance lack, a mix of rain, pollution agents, coming from the vehicles, and de-icing salts, used during the winter season, they were not drained but probably they remained stagnant inside the support.



Figure 53 Examples of the problems at the drainage channels detected.

In the following picture another clear example of what already said:



Figure 54 Clear corroded beams close to the support

Moreover, many beams of the bridge reveal a corrosion state so advanced that is legit to think that in those cases there is a complete support loss with considerable consequences as a total or partial prestress loss.



Figure 55 Supposed support loss because of strong corrosion state

CONCLUSIONS

The model proposed is composed by beam elements characterized through the moment-curvature diagram, in function, not just of the axial force, but even of a bending moment M^* . In fact, a variable axial force has been modeled along the transferring length and depending on the different reinforcement design along the beam's span. The axial force variation changes the constitutive law section by section, so, just the resistant part of the σ - ϵ diagram has been considered, that actually means to take just the residual material properties; moreover, in the anchorage zone the σ - ϵ diagram is limited to the amount of force that the tendons can actually transfer. The bending moment M^* depends by the axial force because it is the moment related to a null curvature in presence of a high axial force, just like in a common prestressed structure. Different M - χ diagrams are plotted into the FEM program, shifted of the M^* "factor" to make them pass throughout the axis origin, as required by the FEM program. The shift is a rigid shift along the ordinate axis, so the shifted curve donates the same curvature of the unshifted one, but for an acting bending moment equal to the actual bending moment plus M^* .

Corrosion scenarios have been modeled as a loss of the prestressing force, due to a reduction of the tendons cross section loss, which causes a reduction of the M - χ diagram. Furthermore, a reduction of the concrete-tendons bond, proportional to the cross-section loss, has been considered. In this work, the bond degradation provokes essentially a variation of the transfer length.

Results show a strong reduction of the security level of the bridge due to corrosion. Moreover, the corrosion attack that coincides with the analytical level results to be a limit configuration for the safety of the element because the actions, evaluated with the Eurocode partial coefficient, are almost equal to the resistance. Increasing the corrosion attack, the USL actions overpass the resistance of the system. The problem results to be that in many parts the bridge shows a greater corrosion percentage than the analytical one. So, it can be said that probably many beams of

the bridge do not explicate the Eurocode partial coefficient and so present serious security problems.

This work wants to be a starting point to determine a simple way to characterize a pretensioned prestressed beam. A certain improvement can be a better automation of the modelling process. In addition, could be interesting to use the model to define the behavior of hyperstatic structures, even with seismic loads, for example, because the negative bending moment can be controlled by the $M-\chi$ diagrams.

Surely, the hope is to access experimental tests to compare the numerical results. Above all, because, both nondestructive than full-scale failure tests of bridges, are important for improving understanding of bridges' behavior and refining evaluation methods. However, such experiments are challenging, often expensive, and thus rare.

BIBLIOGRAPHY

Andrade C., Rodriguez, J., CONTECVET – A validated users manual for assessing [Book]. - Madrid : Division of Building Materials, LTH, Lund University, 2001.

Bertolini L. Materiali da costruzione [Book]. - [s.l.] : Città Studi, 2006.

C. Alonso C. Andradel, j. Rodriguez, J.M. Diez Factors controlling cracking of concrete affected by reinforcement corrosion [Journal]. - [s.l.] : Materials and Structures, 1998. - 435-441 : Vol. 31.

D. Coronelli P. Gambarova Structural Assessment of Corroded Reinforced Concrete [Journal]. - [s.l.] : ASCE, 2004. - 130(8) : Vol. JOURNAL OF STRUCTURAL ENGINEERING.

D.Coronelli A.Castel, N.A.Vub, R.François Corroded post-tensioned beams with bonded tendons and wire failure [Journal] // Engineering Structures 31. - 2009. - p. 1687_1697.

D.Coronelli A.Castel, N.A.Vub, R.François Structural Response of Corroded, Unbonded Posttensioned Beams [Journal] // Structural Engineering. - 2011. - pp. 137(7): 761-771.

Fumin Li Xiaofei Shi, Fuping Jia Experimental Study on Anchoring Bond Behavior of Pre-tensioned Prestressed Concrete Beams with Corroded Steel Strands [Journal]. - Switzerland : Advanced Materials Research, 2011. - 304-307 : Vols. 243-249.

Fumin Li Yingshu Yuan Effects of corrosion on bond behavior between steel strand and concrete [Journal]. - [s.l.] : ELSEVIER, 2013. - 413-422 : Vol. Construction and Building Materials 38.

G. Parry Osborn Paul J. Barr, David A. Petty, Marvin W. Halling and Travis R. Brackus Residual Prestress Forces and Shear Capacity of Salvaged Prestressed Concrete Bridge Girders [Journal]. - [s.l.] : J. Bridge Eng, 2012. - Vols. 17(2): 302-309.

J. Rodriguez L.M. Ortega, J. Casal, J.M.Diez Assessing structural conditions of concrete structures with corroded reinforcements, [Conference] // 4th Int. Congress on concrete in the service of mankind. - Dundee UK : [s.n.], 1996.

J. Woodtli R. Kieselbach Damage due to hydrogen embrittlement and stress corrosion cracking [Journal]. - [s.l.] : Eng. Fail. Anal., 2000. - 427–450.

J. Woodtli R. Kieselbach, Damage due to hydrogen embrittlement and stress corrosion cracking [Journal]. - [s.l.] : Eng. Fail. Anal. , 2000. - 427–450 : Vol. 7.

J.T. Halsey R. Miller Destructive Testing of Two Fourty-Year-Old Prestressed Concrete Bridge Beams [Journal]. - [s.l.] : PCI JOURNAL, 1996.

Jianren Zhang Ju Yi, Xuhui Zhang, Lei Wang, Yafei Ma Bond performance between corroded strand and concrete [Conference] // 19th IABSE Congress. - Stockholm : [s.n.], 2016.

Lei Wang Xuhui Zhang, Jianren Zhang, Lizhao Dai, Yongming Liu Failure analysis of corroded PC beams under flexural load [Journal]. - [s.l.] : Engineering Failure Analysis, 2017. - 11-24 : Vol. 73.

Ngoc Anh Vu Arnaud Castel *, Raoul François Effect of stress corrosion cracking on stress-strain response of steel wires used [Journal]. - [s.l.] : Elsevier, 2009. - 51 : Vol. Corrosion Science.

Niklas Bagge Jonny Nilimaa, Lennart Elfgren In-situ methods to determine residual prestress forces in concrete bridges [Journal]. - [s.l.] : ELSEVIER, 2017. - 41-52 : Vol. Engineering Structures 135.

Ruijin Zhang Arnaud Castel b, Raoul François Concrete cover cracking with reinforcement corrosion of RC beam during chloride-induced corrosion process [Journal]. - [s.l.] : ELSEVIER, 2010. - 40 : Vol. Cement and Concrete Research.

Saetta A., Scotta, R., Vitaliani, R., Coupled environmental-mechanical damage model of rc structures [Journal]. - 1999. - Vol. Journal of Engineering Mechanics.

Stewart M.G. Mechanical behaviour of pitting corrosion of flexural and shear reinforcement and its effect on structural reliability of corroding RC beams [Journal]. - 2009. - 31 : Vol. Structural Safety.

Toribio J. The role of crack tip strain rate in hydrogen assisted cracking [Journal]. - [s.l.] : Corros. Sci., 1997. - 1687–1697 : Vol. 39 (9) .

Tuutti Kyösti Corrosion of steel in concrete [Book]. - Stockholm : CBI, 1982.

U. Angst B. Elsener, C.K. Larsen, Vennesland Critical chloride content in reinforced concrete – A review [Journal]. - [s.l.] : Cement and Concrete Research, 2009. - Vols. 1122-1138.

Y. Liu R. Weyers, Modeling the Time-to-Corrosion Cracking in chloride contaminated reinforced concrete structures [Journal]. - [s.l.] : ACI Materials Journal, 1998. - Vol. 95.

FIGURE INDEX

FIGURE 1 GALVANIC CELL.....	6
FIGURE 2 SCHEMATIC REPRESENTATION OF CORROSION MECHANISM.....	6
FIGURE 3 MAJOR METALS' POTENTIAL.....	8
FIGURE 4 EVOLUTION OF STEEL CORROSION IN CONCRETE (TUUTTI, 1982)	9
FIGURE 5 TYPES OF CORROSION OF REINFORCEMENT: (A) CARBONATION, (B) CHLORIDE ATTACK AND (C) STRESS CORROSION CRACKING.	11
FIGURE 6 EVOLUTION OF CARBONATION VELOCITY IN FUNCTION OF RH WITH NO WETTING (BERTOLINI, 2006).....	12
FIGURE 7 K EVOLUTION IN FUNCTION OF TIME (ABSCISSA IN YEARS) AND PENETRATION DEPTH (ORDINATE IN MM)	13
FIGURE 8 EXAMPLE OF PIT CORROSION.....	14
FIGURE 9 CRITICAL CHLORIDE CONTENT ACCORDING TO FIB "MODEL CODE FOR SERVICE LIFE DESIGN"	17
FIGURE 10 EXAMPLE OF SCC OF A ZTA IN AN INOX STEEL WHICH IS INCLINED TO IT BECAUSE OF NITROGEN.....	18
FIGURE 11 CORROSION LEVEL TREND IN FUNCTION OF THE CHLORIDES CONTENT, TIME AND TEMPERATURE.	20
FIGURE 12 CONSEQUENCES OF REINFORCEMENT CORROSION.....	22
FIGURE 13 EVOLUTION OF THE BAR CROSS SECTION BECAUSE OF CORROSION	22
FIGURE 14 CORROSION PATTERN EVOLUTION ACCORDING TO (RUIJIN ZHANG, 2010).....	23
FIGURE 15 CROSS SECTION LOSS BECAUSE OF BOTH HOMOGENEOUS CORROSION AND PITTING	24
FIGURE 16 SAME ATTACK PENETRATION ON TWO DIFFERENT DIAMETER REINFORCES.....	25
FIGURE 17 SECTION LOSS BECAUSE OF PITTING ACCORDING TO (STEWART, 2009).....	25
FIGURE 18 LINEAR RELATIONSHIP BETWEEN CRACK WIDTH GROWTH AND RADIUS LOSS ACCORDING TO (C. ALONSO, 1998)	29
FIGURE 19 BOND- SLIP DIAGRAMS BY (FUMIN LI, 2013): (1) NO CORROSION, (2) CORROSION CRACK OF 0.2MM (3) CORROSION CRACK OF 0.5MM (4) CORROSION CRACK OF 0.8MM	31
FIGURE 20 BOND REDISTRIBUTION BY (FUMIN LI, 2011)	31
FIGURE 21 BOND FORCE SHIFT	32
FIGURE 22 SATELLITE VIEW OF THE SITU FROM GOOGLE EARTH PRO	35
FIGURE 23 CORSO GROSSETO'S FLYOVER: DECK'S SECTION "A TYPE" RELATIVELY TO THE 24 M, 20 M, 19.60 M, 18 M, 16 M, AND 15.60 M SPANS	36
FIGURE 24 CORSO GROSSETO'S FLYOVER PLANIMETRY	37
FIGURE 25 TRANSVERSAL DECK'S SECTION AS REPORTED IN THE EXECUTIVE REPORT	39
FIGURE 26 CROSS SECTIONS GEOMETRY	40
FIGURE 27 DECK'S HORIZONTAL SECTION CLOSENESS TO THE SUPPORT	40
FIGURE 28 BORDER BEAM CROSS SECTION	44
FIGURE 29 INTERMEDIATE BEAM CROSS SECTION	46
FIGURE 30 TRANSVERSE BEAM CROSS SECTION	49
FIGURE 31 PRESTRESS FORCE TRANSFER IN PRE-TENSIONED ELEMENTS	51
FIGURE 32 STRESSES IN THE ANCHORAGE ZONE OF PRETENSIONED MEMBERS: (1) AT RELEASE TENDONS (2) AT ULS.....	54
FIGURE 33 CONCENTRATED LOAD DISPERSION.....	55
FIGURE 34 LOAD MODEL 1	56
FIGURE 35 COURBON METHOD: STATIC SCHEME OF TRANSVERSE BEAM	57
FIGURE 36 LOAD DISTRIBUTION FROM THE EXECUTIVE REPORT	59
FIGURE 37 ADINA MODEL	69
FIGURE 38 PRESTRESS FORCE ACTING AND RESISTING QUOTA	69
FIGURE 39 RESISTANT Σ-E DIAGRAM	70
FIGURE 40 TENDONS Σ-E DIAGRAM ALONG THE TRANSFER LENGTH BECAUSE OF ANCHORAGE.....	70
FIGURE 41 GENERIC SECTION SUBJECTED TO BOTH AXIAL FORCE AND BENDING MOMENT	71

FIGURE 42 INTERMEDIATE BEAM CROSS SECTION: (A) REAL, (B) APPROXIMATED AND (C) APPROXIMATED AND DIVIDED IN FIBERS.....	72
FIGURE 43 STRESSES ON A GENERAL SECTION.....	74
FIGURE 44 BEAM'S LONGITUDINAL DEVELOPMENT AND CROSS SECTIONS.....	75
FIGURE 45 TRANSLATION OF A GENERIC LINEAR M-X DIAGRAM BECAUSE OF AN AXIAL FORCE	76
FIGURE 46 EXAMPLE OF THE M-X CURVES	77
FIGURE 47 GENERIC LOADED ELEMENT	77
FIGURE 48 TIME FUNCTION	78
FIGURE 49 EXAMPLES OF THE CORRODED OUTERMOST I BEAM.....	109
FIGURE 50 LONGITUDINAL CRACK	110
FIGURE 51 DISTANCE OF A LONGITUDINAL CRACK FROM THE EDGE	110
FIGURE 52 CORROSION OF AN INTERMEDIATE BEAM	111
FIGURE 53 EXAMPLES OF THE PROBLEMS AT THE DRAINAGE CHANNELS DETECTED.....	112
FIGURE 54 CLEAR CORRODED BEAMS CLOSE TO THE SUPPORT	113
FIGURE 55 SUPPOSED SUPPORT LOSS BECAUSE OF STRONG CORROSION STATE	113